Endocannabinoid Signaling Collapse Mediates Stress-Induced Amygdalo-Cortical Strengthening

By

David J. Marcus

Dissertation

Submitted to the Faculty of the

Graduate School of Vanderbilt University

in partial fulfillment of the requirements

for the degree of

DOCTOR OF PHILOSOPHY

in

Neuroscience

January, 31, **2020**

Nashville, Tennessee

Approved

Sachin Patel, M.D., Ph.D.
Danny Winder, Ph.D.
Ariel Deutch, Ph.D.
Brad Greuter, Ph.D.

DEDICATION

Dedicated to my friends and family, who have (for the most part) kept me sane over the past five years. Whenever I feel beaten down my science, it is their company and reassurance that has kept me going.

ACKNOWLEDGMENTS

Sachin has been absolutely instrumental over the past five years in my development as a scientist. What astounds me the most about his mentorship is how dynamic it has been throughout my tenure in his lab. In the early days, I was presented with a host of new techniques with which I had no experience. Sachin was incredibly hands-on in the beginning, and integral to me learning a variety of new skills and concepts that I needed to succeed. However, as time has gone on, he seems to have intuitively realized that I need less hands-on guidance and have become significantly more independent as a researcher. It is to his credit that has been able to dramatically change his mentoring styles based on his intuition about his students' needs.

I would also be remiss if I did not mention the INCREDIBLE support system I have had throughout my life that have been integral to me getting where I am today. None of this would have been possible without a loving and supporting family that have kept me going during trying times. I am also heavily indebted to friends from many walks of life, who help to ground me and realize that there is more to the world than science. Lastly, I can not stress just important my lab mates have been both in stimulating me intellectually and in making my time in lab enjoyable, giving me yet another reason to be excited to come into lab every day. In all, although the doctorate is being granted to me, it should really be in part shared among the multitude of inspiring, loving, and encouraging people in my life who have made this goal possible for me.

TABLE OF CONTENTS

LIST OF FIGURES

CHAPTER I

Introduction

The burden of mental illness

Over the past ten years, many of the world's largest pharmaceutical and biotech companies, including Pfizer, Novartis, and Amgen, have either completely shut down or severely pruned their neuroscience drug development programs (Abbott, 2011; Miller, 2010). From an outside perspective, this seems an imprudent course of action. How, at a time when the global burden of neurological and psychiatric disorders continues to be highly resistant to current treatment options (Kessler et al., 2005b), do the world's leaders in drug discovery decide to pull the plug on their neurological disease drug pipeline altogether (Gourie-Devi, 2018; Vigo et al., 2016)? Even if we operate under the cynical assumption that a pharmaceutical company's primary motive is profit, one would presume that the sheer number of people suffering from neurological and psychiatric illnesses would represent a lucrative source of income. The answer, while multifaceted, can be most succinctly described by the fact that we simply do not understand the etiology or pathophysiology that underlies a substantial portion of the diseases afflicting the brain and nervous system. This paucity of mechanistic understanding precludes rational drug design of pharmaceutical treatments for these disorders. This rings especially true for mental illnesses (Cuthbert and Insel, 2013; Kessler et al., 2012; Vigo et al., 2016).

A prominent issue in tackling the global burden of mental illnesses, is oddly enough, semantic and categorical. Over the past hundred years, the definition and diagnosis of psychiatric disorders has been in a constant state of flux (International Advisory Group for the

Revision of and Behavioural, 2011; Steel et al., 2014; Vigo et al., 2016). Many of the disorders that exist today simply weren't diagnosed 100 years ago. This is further complicated by the fact that, traditionally, disorders of the central nervous system that lead to mental illness were categorized as either psychiatric or neurological. However, this distinction is rooted in tradition and professional areas of competence rather than being a reflection of biological substrates. For example, Schizophrenia, typically classified as a psychiatric disorder, is commonly associated with observable changes in brain structure that could easily place it under the purview of neurological rather than a psychiatric disorder (Vigo et al., 2016).

These categorical issues notwithstanding, a substantial effort has been placed on trying to get a true measure of the global prevalence and burden of mental disorders. The World Health Organization defines mental health as "a state of well-being in which every individual realized his or her own potential, can cope with the normal stresses of life, can work productively and fruitfully, and is able to make a contribution to his or her community." In this context, mental health disorders comprise a vast array of disorders afflicting the nervous system, and in all, nearly a third of individuals worldwide will experience one of these disorders in their lifetime (Ginn and Horder, 2012; Steel et al., 2014). Additionally, mental disorders constitute 32.4% of total years lived with disability worldwide, and 13.0% of disability-adjusted life-years (Vigo et al., 2016). This places mental illnesses just behind cardiovascular disease, as the second leading cause of global disability burden. Unlike many cardiovascular diseases, a large percentage of mental health disorders remain idiopathic, with no known common pathological feature to define them (Kotov et al., 2017).

A new outlook on anxiety disorders and pharmacotherapeutic treatments

Among mental health disorders, anxiety disorders represent the highest lifetime risk prevalence (Kessler et al., 2012). In the United States, over 28% of the population will experience an anxiety disorder during their life, leading to an estimated financial burden in excess of $44 billion dollars annually (Greenberg et al., 1999; Gross and Hen, 2004). Anxiety in and of itself is typified by subjectively dysphoric sense of dread in anticipation of or uncertainty about a future event, and results in enhanced vigilance despite the absence of an immediate threat. This is importantly distinguished from fear, which is the response to an immediate threat or environmental challenge, typically leading to autonomic arousal and invigoration of a 'fight or flight' response. Although anxiety may serve an adaptive and evolutionarily conserved role in human health and survival by promoting harm avoidance, it becomes pathological when it interferes with normal day-to-day functioning or leads to substantial personal or economic burdens (Bereza et al., 2009; Calhoon and Tye, 2015; Mondin et al., 2013).

The primary diagnostic rubric for mental disorders in the United States, the *Diagnostic and Statistical Manual of Mental Disorders, Fifth Edition* (DSM V), classifies pathological anxiety as belonging to three broad categories: stressor related, obsessive-compulsive and related disorders, and anxiety disorders (Battle, 2013). Despite the unique etiology, these disorders share common features of deleterious apprehension and enhanced vigilance that persist beyond appropriate periods. This shared feature has proved to be a useful diagnostic tool for categorizing pathological anxiety. Indeed, a primary goal of the DSM V was to create a shared language that could be used by psychiatrists to decrease inter-rater variability (Hyman, 2010). However, over the last decade, it has become increasingly clear that these categorical diagnoses of anxiety disorders do not reflect any underlying neurobiological systems, which stymies both

research into the etiology of these disorders as well as the development of novel therapeutics (Hyman, 2010).

To ameliorate the systemic issues of categorical diagnoses, the National Institute of Mental Health (NIMH) has championed an alternative to the DSM V: The Research Domain Criteria (RDoC) (Cuthbert and Insel, 2010). This new directive opines that the DSM's grouping of heterogeneous symptoms should be replaced by a trans-diagnostic approach that focuses on neurobiological mechanisms that underlie observable symptoms. With respect to anxiety disorders, the RDoC classifies anxiety disorders as falling under the broad domain of Negative Valence Systems. This category includes responses to aversive situations, such as anxiety, fear, and sustained threat. Importantly, these features "overlap with a key concept from the clinical psychology literature- negative affective bias" (Carlisi and Robinson, 2018). Negative affective bias is a key component of many psychiatric illnesses, and is especially eminent in anxiety disorders, in which a bias in thought and attention towards affectively negative information is thought to promote and uphold the anxious state (Craske et al., 2017; Grupe and Nitschke, 2011, 2013).

Given that we still have a poor understanding of the causative mechanisms driving anxiety disorders, it is of no surprise that current therapeutic strategies are moderately efficacious at best (Ravindran and Stein, 2010; Trivedi et al., 2006; Warden et al., 2007). One of the mainstays in the treatment of anxiety disorders since the early sixties has been the benzodiazepines. This class of compound was serendipitously discovered in the late fifties, and was quickly realized to elicit strong sedative, anti-convulsant, and muscle relaxant effects, while having a larger therapeutic window than barbiturates, which they largely replaced (Miller and Gold, 1990; Ravindran and Stein, 2010; Sternbach, 1978). Multiple randomized controlled trials

(RCT) have shown that benzodiazepines have clinical efficacy in the treatment of panic disorder (Ballenger et al., 1988), generalized anxiety disorder (Mitte et al., 2005), and social phobia (Munjack et al., 1990). However, serious concerns have been raised regarding both the acute adverse effects (e.g. oversedation and psychomotor impairment) and risk of overdose, as well as long term tolerance and dependence to benzodiazepines (King, 1992). This has led to waning interest in this class of compounds in the long-term management of anxiety disorders.

Over the last twenty years, selective serotonin reuptake inhibitors (SSRIs) have seen increasing use for long-term management of anxiety disorders. Initially indicated for treatment of major depressive disorder, multiple RCTs have indicated positive therapeutic effects for SSRIs in the treatment of panic disorder (Otto et al., 2001), generalized anxiety disorder (Ball et al., 2005), and social phobia (Blanco et al., 2003). However, as with benzodiazepines, there are a multitude of concerns about the safety profile and side effects of these compounds, including sexual dysfunction, suicidal ideation, and gastrointestinal disturbances (Olfson et al., 2006; Taylor et al., 2013). Additionally, given that these compounds only have a clinical efficacy of 40-60%, there remains a critical unmet need to develop novel therapeutic strategies to treat anxiety disorders (Trivedi et al., 2006; Warden et al., 2007).

Recent studies have suggested that modulators of endogenous cannabinoid (eCB) signaling could represent a novel therapeutic target for the treatment of anxiety and stress-related disorders (Lisboa et al., 2017; Patel et al., 2017). The rationale for such an approach stems from centuries of anecdotal reports and well as more recent clinical studies suggesting that cannabinoid agonists such as Δ^9-Tetrahydracannabinol (THC), the primary psychoactive constituent of marijuana, are capable of eliciting potent anxiolytic effects (Herodotus et al., 1936; Hyman and Sinha, 2009; Roitman et al., 2014; Sung et al., 2001). Although THC was isolated in

the mid 1960s (Mechoulam and Gaoni, 1965), it was not until almost three decades later that its cognate receptor in animals tissues was discovered (Matsuda et al., 1990). This was followed two years later by the identification of a second cannabinoid receptor (Munro et al., 1993), leading to their classification as the cannabinoid receptor 1 (CB1) and cannabinoid receptor 2 (CB2), respectively.

The endocannabinoid signaling system

The cloning and characterization of these receptors led to rapid identification of two endogenously produced brain constituents that bind CB1 and CB2, namely *N*-Arachidonoylethanolamide (AEA) (Devane et al., 1992) and 2-Arachidonoylglycerol (2-AG) (Mechoulam et al., 1995). However, it was in 2001 that the unique physiological role of these compounds was described. That year, multiple different groups independently reported that eCBs mediated retrograde signaling at central synapses (Kreitzer and Regehr, 2001; Maejima et al., 2001; Wilson and Nicoll, 2001). These experiments showed that activity-dependent mobilization of eCBs from the post-synaptic neuron led to transient depression of presynaptic neurotransmitter release. These results were groundbreaking, as they revealed a biochemical mechanism for how diffusible messengers mediate retrograde signaling in the central nervous system. Earlier work had demonstrated that direct depolarization of a neuron can elicit transient suppression of synaptic transmission (Llano et al., 1991). Given that this process, was dependent on postsynaptic calcium influx and elicited a reduction in neurotransmitter release probability, it was hypothesized that the phenomenon was mediated by a retrograde messenger (Pitler and Alger, 1992). In 2001, the groups of Kano and Nicoll conclusively showed that this process was mediated by the eCBs (Maejima et al., 2001; Wilson and Nicoll, 2001).

Given that the CB1 receptor is the primary cannabinoid receptor expressed in neurons, it was suggested that these physiological effects were driven through activation of presynaptic CB1 (Gong et al., 2006; Herkenham et al., 1991; Herkenham et al., 1990). The CB1 receptor is a 473 amino acid G protein-coupled receptor of the rhodopsin-like family. Expression of CB1 is highly heterogenous throughout the brain, and shows robust expression in the olfactory bulb, substantia nigra, globus pallidus, and cerebellum. Moderate expression is found in many forebrain regions, such as the cerebral cortex, amygdala, hypothalamus, and septum, while the thalamus and brain stem show low expression (Herkenham et al., 1991). As the CB1 receptor is primarily presynaptically located, there is a noted discrepancy between CB1 mRNA transcript localization and localization of the protein. For example, target regions of the dorsal striatum (which has high levels of CB1 mRNA) such as the globus pallidus and substantia nigra show high CB1 immunoreactivity, while showing low CB1 mRNA transcript levels (Matyas et al., 2006).

In neurons, the CB1 receptor signals primarily through $G_{i/o}$ transduction pathways. As such, CB1 activation inhibits adenylyl cyclase and decreases cAMP production (Pertwee, 1997). In addition to this canonical effect of $G_{i/o}$ signaling, CB1 activation also directly modulates the activity of numerous ion channels. In neurons or CB1 transfected cells, application of a CB1 agonist increases A-type (Hampson et al., 1995) and inward rectifier (Mackie et al., 1995) potassium channel currents, and inhibits N- and P/Q-type calcium channels (Twitchell et al., 1997). Given that these effects would be predicted to hyperpolarize and decrease the excitability of neurons, it follows that CB1 activation elicits a reduction in neurotransmitter release probability. Numerous neurotransmitter systems have been demonstrated to be modulated by CB1 signaling, including GABA (Szabo et al., 1998), glutamate (Levenes et al., 1998),

acetylcholine (Gifford and Ashby, 1996), dopamine (Cadogan et al., 1997), serotonin (Nakazi et al., 2000), and many others.

In the CNS, it has been demonstrated that AEA and 2-AG represent the primary ligands for the CB1 receptor, although other putative eCB ligands have been described (Hanus et al., 1993). Unlike conventional neurotransmitter systems such as glutamate in which neurotransmitters are packaged into vesicles that fuse with the plasma membrane to release their contents into the extracellular space, the eCBs are synthesized on demand from plasma membrane phospholipids in the post-synaptic neuron (Kano et al., 2009). Activity-dependent production of AEA has been demonstrated via high K^+ solution (Stella and Piomelli, 2001), used to induce neuronal depolarization, and high frequency stimulation(Di et al., 2005), among others. Early studies suggested a two-step enzymatic reaction for the biosynthesis of anandamide. The first step comprises an *sn*-1 transfer of an arachidonate group to the primary amine group of the membrane phospholipid, phosphatidylethanolamine. This reaction, catalyzed by *N*-acyltransferase, yields *N*-arachidonoyl phosphatidylethanolamine (Cadas et al., 1997). This reaction has been shown to be stimulated by Ca^{2+} influx and represents the putative rate-limiting step in AEA production. The second step is catalyzed by *N*-acylphosphatidylethanolamine-hydrolyzing phospholipase D (NAPE-PLD), yielding AEA and phosphatidic acid (Kano et al., 2009; Schmid et al., 1983). However, subsequent studies revealed that this represents just one of several biosynthetic pathways for AEA, with others necessitating lysoPLD (Sun et al., 2004), phospholipase C (PLC) and tyrosine phosphatase (Liu et al., 2008), and glycerophosphodiesterase 1 (Simon and Cravatt, 2008).

Similar to AEA, 2-AG synthesis can be stimulated via neuronal activation (Di et al., 2005; Stella et al., 1997). However, unlike AEA, it appears that the vast majority of 2-AG in the

CNS is produced via a single conserved biosynthetic pathway (Kano et al., 2009). This pathway first involves the PLCβ-dependent cleavage of an arachidonic acid-containing membrane phospholipid, such as phosphatidylinositol 4,5-bisphosphate. This reaction yields IP_3 and diacylglycerol, the latter of which is hydrolyzed by diacylglycerol lipase (DAGL) to yield 2-AG (Kondo et al., 1998; Lafourcade et al., 2007).

To terminate signaling, the eCBs can be degraded by either hydrolytic or oxidative pathways (Vandevoorde and Lambert, 2007). As opposed to the multiple pathways for AEA biosynthesis, its hydrolysis appears to by almost entirely mediated by one enzyme, fatty acid amide hydrolase (FAAH), which is primarily expressed post-synaptically. This enzyme hydrolizes AEA at the primary amine group, yielding arachidonic acid and ethanolamine (Cravatt et al., 1996). 2-AG on the other hand is primarily degraded by the presynaptic enzyme monoacylglycerol lipase (MAGL), which hydrolyzes 2-AG into arachidonic acid and glycerol (Dinh et al., 2002; Dinh et al., 2004). MAGL is responsible for ~85% of 2-AG hydrolysis, with the other 15% being contributed by the enzymes ABHD6 and ABHD12 (Blankman et al., 2007). Additionally, both AEA and 2-AG have been shown to be oxidatively degraded by the enzyme cyclooxygenase 2 and various lipooxygenase enzymes in the postsynaptic neuron (Vandevoorde and Lambert, 2007).

A central unresolved question in the eCB field regards the mechanism of eCB release and diffusion to its presynaptic targets. The eCBs are highly lipophilic molecules, synthesized directly within the phospholipid bilayer. Indeed, it seems highly energetically unfavorable for an integral membrane lipid to simply diffuse into the aqueous intracellular or extracellular fluid. Much work over the past decade has focused on how this process takes place. For AEA, multiple models for intracellular transport have been proposed. The first requires a transport

protein to facilitate diffusion into aqueous environments. Multiple proteins have been found to be involved in this process, most prominently several Fatty Acid Binding Proteins (FABP) (Fegley et al., 2004; Kaczocha et al., 2009). The second model proposes that AEA passes through the membrane by simple diffusion due to a strong concentration gradient set by intracellular degradation (Glaser et al., 2003). Lastly, a third model proposes that AEA "undergoes endocytosis through a caveolae-related uptake process" (Kano et al., 2009). In contrast, far less is understood regarding the mechanisms of 2-AG release. Recently, a study revealed that FABP5 is indispensable for retrograde 2-AG signaling in the dorsal raphe nucleus, revealing for the first time an extracellular protein involved in retrograde transport of 2-AG (Haj-Dahmane et al., 2018).

The first well-characterized form of eCB mediated retrograde signaling was almost simultaneously reported by three separate groups in 2001. This short term plasticity phenomenon, known as depolarization induced suppression of excitation (DSE) (Kreitzer and Regehr, 2001) or inhibition (DSI) (Maejima et al., 2001; Wilson and Nicoll, 2001) is characterized by a transient depression of EPSC or IPSC amplitude that typically lasts on the order of seconds to a few minutes. Both DSE and DSI had been previously reported as necessitating retrograde signaling, but was initially attributed to an unknown neurotransmitter (Pitler and Alger, 1992). Since the discovery that these phenomena were eCB dependent, substantial effort has been placed on identifying the underlying mechanism of eCB release. Most studies have shown that with respect to both DSE and DSI, a rise in postsynaptic Ca^{2+} is indispensable (Lenz and Alger, 1999; Ohno-Shosaku et al., 2001; Wilson and Nicoll, 2001). This increase in intracellular Ca^{2+} levels is primarily attributable to increased conductance through voltage-gated Ca^{2+} channels (Pitler and Alger, 1992), although eCB synthesis driven by

Ca^{2+} influx through N-Methyl D-Aspartate (NMDA) receptors (Ohno-Shosaku et al., 2007) or Ca^{2+} release from intracellular stores (Isokawa and Alger, 2006) has also been reported.

Although the necessity of Ca^{2+} for these forms of plasticity are well documented, it is still not fully understood how this ultimately results in increased eCB production. Initial studies demonstrating that inhibition of MAGL but not FAAH was capable of prolonging both of these phenomena strongly suggested that they are both mediated by 2-AG and not by AEA (Hashimotodani et al., 2007; Kim and Alger, 2004; Makara et al., 2005). More recent studies have further demonstrated that inhibition of DAGL with THL is able to fully block DSE or DSI in multiple preparations (Hashimotodani et al., 2007; Hashimotodani et al., 2008). Lastly, a recently generated line of mice in which the gene for DAGLα is functionally knocked out show almost completely attenuated DSE, strongly suggesting that this form of plasticity is solely mediated by 2-AG (Shonesy et al., 2014). However, it still remains unclear how Ca^{2+} influx is coupled to activation of DAGL and production of 2-AG. Additionally, an important facet of DSI in particular is that is obligatorily heterosynaptic. In order for native depolarization of a neuron to occur, excitatory input is needed. Thus in order for eCBs to shunt inhibitory input (e.g. DSI), the excitatory input induced depolarization will lead to production of eCBs that bind to CB1 on proximal GABAergic synapses. This heterosynaptic eCB synaptic plasticity has been demonstrated by multiple groups (Pitler and Alger, 1992; Wilson and Nicoll, 2001)

In addition to these Ca^{2+} dependent forms of eCB production, there are multiple G$_q$-coupled receptors (GqGPCR) that have been shown to be capable of driving short-term eCB plasticity (Kano et al., 2009). As mentioned previously, GqGPCR activation leads to stimulation of PLCβ activity which cleaves PIP$_2$ into IP$_3$ and DAG, the latter of which is the direct precursor to 2-AG. The two most well characterized classes of GqGPCRs that drive eCB

release are the metabotropic glutamate receptors (mGluR) (Galante and Diana, 2004; Neu et al., 2007) and muscarinic acetylcholine receptors (mAchR) (Kim et al., 2002; Ramikie et al., 2014). Similarly to DSE and DSI, this GqGPCR driven eCB release can be blocked with inhibitors of DAGL, strongly suggesting a prominent role for 2-AG in mediating this phenomenon as well (Hashimotodani et al., 2007; Hashimotodani et al., 2008). However, more recent studies have demonstrated 2-AG independent forms of GqGPCR driven eCB release, suggesting that AEA production may similarly be stimulated by GqGPCR activation (Kim and Alger, 2010; Ramikie et al., 2014).

More recent studies have begun to put increasing focus on the role of eCBs in mediating long-term forms of synaptic plasticity. Indeed, eCBs have been implicated in mediating various forms of long-term depression (Kreitzer and Malenka, 2005; Sjostrom et al., 2003), a canonical form of activity-dependent weakening of synaptic efficacy (Malenka and Bear, 2004). Interestingly, the induction of eCB-LTD is highly variable based on the stimulation paramaters and the brain region being examined, suggesting that there are multiple mechanistically distinct modes of eCB-LTD. More recent studies have even demonstrated astrocytic and microlical eCB signaling as a crucial regulators of synaptic plasticity, adding further complexity to the physiological role of eCBs (Franco et al., 2019; Navarrete and Araque, 2010; Navarrete et al., 2014).

The investigation of eCB signaling over the last two decades has led the development of numerous tool compounds to modulate various components of the eCB production, release, and degradation machinery (Ahn et al., 2009; Baggelaar et al., 2015) (Long et al., 2009; Simon and Cravatt, 2008). Given the decades of evidence suggesting that CB1 agonism is capable of eliciting an anxiolytic effect, many of these tools compounds have been screened in translational

models to determine whether potentiation of eCB signaling is similarly able to induce anxiolysis. Multiple studies have demonstrated that enhancing both AEA (Busquets-Garcia et al., 2011; Patel and Hillard, 2006) and 2-AG (Bedse et al., 2017; Busquets-Garcia et al., 2011) signaling is capable of reducing anxiety-like behavior in mice. Given these preclinical findings, similar compounds are now being considered for use in humans for the treatment of anxiety-related disorders. Despite the rapid advancement of these compounds through translational models, a critical question remains that has stymied further development: how are these drugs reducing anxiety? Recent studies have begun to shed light on this mechanism by demonstrating that potentiation of eCB/CB1 signaling in either the basolateral complex of the amygdala (BLA) (Ganon-Elazar and Akirav, 2009; Gray et al., 2015) or medial prefrontal cortex (Fogaca et al., 2012; Rubino et al., 2008a) is capable of reducing anxiety-like behavior. This suggests that these two regions could be important in the generation of anxiety-like states, and that decreasing their activity via potentiation of eCB/CB1 signaling could contribute to the anxiolytic effects of cannabinoids.

The role of the amygdala in anxiety and fear related behaviors

The BLA is a highly evolutionarily conserved subcortical limbic structure that possesses several cortical-like qualities, such as being composed primarily of glutamatergic projection neurons (Ehrlich et al., 2009; McDonald, 1998). The BLA is the lateral most component of the amygdaloid complex, which additionally comprises the central nucleus of the amygdala (CeA) and medial amygdala (MeA). The BLA itself can be further subdivided into the lateral (LA), basal (BA) and basomedial (BM) regions. The BLA receives dense input from the sensory thalamus and sensory cortices, which primarily target the LA (LeDoux et al., 1990b; McDonald,

1998). There is also abundant hippocampal(Bluett et al., 2017), prefrontocortical (Likhtik et al., 2014), and midline thalamic (Matyas et al., 2014) glutamatergic input, which predominantly targets the BA and BM subregions. Unlike hierarchically organized glutamatergic structures like the thalamus, the amygdala displays dense inter-nuclei connectivity, as both the LA and BA send dense excitatory projections to regions of the CeA. Additionally, the BA and BM serve as the primary glutamatergic output structures of the amygdala, sending dense excitatory projections to the mPFC (Felix-Ortiz et al., 2015), ventral hippocampus (Felix-Ortiz et al., 2013), and nucleus accumbens(Beyeler et al., 2018).

The first inkling as to the function of the BLA and the amygdala as a whole came from medial temporal lobe lesions, which resulted in emotional apathy and an inability to assign value to stimuli (Janak and Tye, 2015). More specific lesions of the area around the amygdala led to reduced aggression, fear, and defensive behaviors, and specific amygdalar lesions led to impairment in acquiring responses to shock predictive cues (Weiskrantz, 1956). These results were soon also reported in both rodents (LeDoux et al., 1990a) and humans (Anderson and Phelps, 2001), showing strong functional conversion across species, and suggesting a pivotal role for the amygdala in a type of associative learning which has been operationally described as 'fear conditioning.' Historically, a substantial amount of amygdala research has focused on this function of the BLA, which is studied in the laboratory using a Pavlovian learning task. In this paradigm, an animal is trained to associate an initially neutral conditioned stimulus (CS) with a paired aversive unconditioned stimulus (US). Over the course of the training, the subject learns to associate the CS with the US, and displays behavioral signs of fear upon CS presentation.

Over the last decade, the advent of optogenetics has allowed for unprecedented insight into the neural circuitry that drives fear related behaviors. The LA was an early focal point for

these studies, as it has direct access to sensory information relating to the both the CS and US. It was found that during Pavlovian conditioning, LA neurons develop and maintain excitatory responses to the CS that has been paired with the US (Quirk et al., 1995). These responses are proposed to be initiated by a potentiation of auditory sensory inputs, as CS-US pairings lead to enhanced measures of synaptic plasticity *in vivo* (Rogan et al., 1997) and in acute slice preparations(McKernan and Shinnick-Gallagher, 1997). This model proposes that "an initially weak afferent carrying sensory information about the CS and a strong afferent carrying US information converge on individual principal neurons in the LA and, through a Hebbian plasticity mechanism, lead to enhanced strength of the excitatory synapses carrying CS information" (Janak and Tye, 2015). Thus, following conditioning, the CS alone will be able to lead to activation of LA neurons, which in turn will drive freezing behavior through its outputs (discussed below). This has been demonstrated by optogenetic experiments showing that activation of LA cell bodies can substitute for the US (Johansen et al., 2010) while activation of auditory thalamus inputs to the LA can substitute for the CS (Nabavi et al., 2014).

The LA in turn projects directly to the CeA, which is a primary output nucleus of the amygdala and is composed primarily of GABAergic interneurons and GABAergic projection neurons. CeA lesions block the expression of conditioned fear, leading to the proposition that the LA relays information regarding the CS/US association to the CeA to drive conditioned fear responses (Kapp et al., 1979). Given the necessity of the CeA for Pavlovian conditioning, a substantial amount of work has examined how the CeA is involved in generating defensive behavioral outputs. There appear to be two mutually inhibitory cellular populations in the lateral CeA (CeL) that collectively regulate these behaviors, which have been labeled 'fear off' neurons, that express PKCδ (CeL$_{OFF}$), and 'fear on' neurons, that do not express PKCδ and primarily

express the neuropeptide somatostatin (CeL$_{ON}$)(Ciocchi et al., 2010; Haubensak et al., 2010). In addition to being mutually inhibitory, these neurons both project to the medial component of the CeA (CeM), which is the primary output nucleus of the CeA. The model proposes that conditioned fear responses occur following activation of CeL$_{ON}$ neurons that inhibit CeL$_{OFF}$ neurons, leading to disinhibition of CeM output, which drives freezing behavior (Ciocchi et al., 2010; Haubensak et al., 2010). Furthermore, more recent studies have demonstrated that the LA sends direct excitatory input to CeL$_{ON}$ neurons, and that this input is strengthened following fear conditioning, demonstrating that these neurons could drive the behavioral output of the learning induced Hebbian plasticity that occurs in the LA during fear conditioning (Li et al., 2013).

Amygdalo-cortical communication in fear and anxiety states

Despite these findings, it was quickly realized that although LA neurons are tone responsive during fear conditioning, their responses are transient and do not last the duration of the behavior, suggesting there must be additional circuitry involved in mediating the persistent freezing observed during tone presentation (Quirk et al., 1995). Interestingly, both the BA and the prelimbic component of the mPFC (PL) show persistent responding throughout the entire CS presentation (Amano et al., 2011; Burgos-Robles et al., 2009). These two regions communicate via dense reciprocal glutamatergic projections, and this communication appears to be essential for the expression of conditioned fear responses (Sotres-Bayon and Quirk, 2010). As such, inactivation of the PL impairs fear expression (Corcoran and Quirk, 2007), and inactivation of the BLA abolishes tone responses in the PL (Sotres-Bayon et al., 2012). Furthermore, CS responsive neurons in the BA project to the PL, and inhibition of these neurons diminishes

conditioned fear responses (Senn et al., 2014). Similarly, inhibition of PL projections to the BLA diminishes the expression of conditioned fear (Do-Monte et al., 2015).

It should be noted that the mPFC is a highly heterogenous structure, with a significant functional dichotomy along the dorsal-ventral axis (Riga et al., 2014). Indeed, the ventral mPFC, or infralimbic cortex (IL), appears to play an opposing role to the dorsal PL in regulating fear related behaviors. While the PL supports the expression of conditioned fear, the IL is necessary for fear extinction, a process in which the animal is trained to learn that the CS is no longer of predictive of the US, thereby creating a "new inhibitory memory that competes with the fear memory for control of behavior" (Duvarci and Pare, 2014; Myers and Davis, 2007). Similar to the PL after fear conditioning, IL neurons show increased activity after extinction training (Burgos-Robles et al., 2007), and inhibition of the IL impairs the acquisition of fear extinction (Sierra-Mercado et al., 2011). Additionally, activation of IL projections to the amygdala enhances extinction learning, in opposition to the effects of activation of PL projections (Adhikari et al., 2015). These results demonstrate a crucial role for cortico-amygdalar communication in the acquisition of Pavlovian fear conditioning.

Although substantial effort has been directed toward understanding the neural circuitry of fear related behaviors, far less is known regarding the circuitry involved in mediating anxious states. Here, an important distinction between fear and anxiety must be made. Fear is typically conceptualized as a behavioral or physiological response to a threatening stimulus in the immediate environment. Anxiety, on the other hand, is a negative affective state of heightened arousal that is prompted by distal or uncertain threats that are not present in the immediate environment. Interestingly, both the BLA and PL also appear to be implicated in driving anxiety-like behavior in rodents and upholding anxious states in humans. As such, activation of

either of these regions is anxiogenic (Calhoon and Tye, 2015; Suzuki et al., 2016). Although previous literature has primarily focused on fear conditioning, more recent experiments have suggested a broader role for the BLA in imbuing stimuli with emotional valence (either negative or positive) (Beyeler et al., 2018; Beyeler et al., 2016). The PL has similarly been shown to play an integral role in threat interpretation (Carlisi and Robinson, 2018). As such, direct optogenetic activation of BLA input to the PL is capable of eliciting anxiety-like behavior in the elevated-zero maze (EZM), a well-characterized assay for measuring rodent anxiety, while inhibition of this circuit increases open-arm time in the EZM, indicative of anxiolysis (Felix-Ortiz et al., 2015). As observed with fear conditioning, activation of IL inputs to the amygdala elicits the opposite effect, driving a robust anxiolytic phenotype(Adhikari et al., 2015).

Convergent data from human functional magnetic resonance imaging (fMRI) studies strongly support these preclinical findings. Behavioral responses to anxiety-provoking situations are associated with activity in dorsomedial PFC (dmPFC), the human homologue of the PL. This region is active during threat appraisal, and appears to be overactive in patients with pathological anxiety (Kalisch and Gerlicher, 2014). Conversely, patients with anxiety disorders display reduced activation of the ventromedial PFC (vmPFC), the human homologue of the rodent IL(Milad et al., 2009). Both of these findings support the notion that there is significant functional homology between the PL/dmPFC, and the IL/vmPFC, and that they play similar roles in regulating anxiety and fear states in rodents and in humans. They further demonstrate that increased activity in the dmPFC and reduced activity in the vmPFC are both associated with negative affective bias, a key clinical hallmark of anxiety disorders (Carlisi and Robinson, 2018; Machado and Bachevalier, 2008).

As in rodents, the amygdala plays an integral role in driving anxious states in humans. fMRI studies have reveled that exposure to threatening stimuli enhances amygdalar activity(Linnman et al., 2012). Furthermore, a similar pattern of anxiety-induced activity emerges in cortico-amygdalar circuits in humans as observed in rodents. During the processing of threatening stimuli, functional connectivity between the amygdala and dmPFC is significantly increased. Additionally, the strength of this connection is positively correlated with the subjects' subjective ratings of anxiety (Robinson et al., 2012). Activity in this circuit was also positively correlated with a negative bias in behavioral responding, suggesting an integral role for amygdala-dmPFC coupling in driving negative affective bias (Robinson et al., 2012). Supporting this, coupling within this circuit was also increased at baseline in patients suffering from anxiety disorders (Robinson et al., 2014). In humans, the vmPFC interacts with the amygdala in a similar fashion to IL-BLA interactions in rodents. That is, increased vmPFC activation was associated with decreased amygdalar activity (Vytal et al., 2014). Additionally, during extinction recall, positive vmPFC activity negatively predicted amygdalar activity, again showing functional homology to the rodent IL-BLA circuit (Linnman et al., 2012). These results suggest a crucial role for the dmPFC-amygdala circuit in driving negative affective bias and associated anxious states, an effect which is counteracted by activity in the ilPFC-amygdala circuit (Carlisi and Robinson, 2018).

In most experimental paradigms investigating anxiety, a stressor of some modality is used to provoke anxiety-like behavior. Stress exposure is well understood to be a primary risk factor for the development of numerous affective disorders, including generalized anxiety and post-traumatic stress disorder (Arnsten, 2015; McEwen, 2012; Sharma et al., 2016). There has thus been substantial effort put into understanding the neurophysiological effects of stress

exposure, and how these are ultimately related to the resultant behavioral pathologies. Both the BLA and the mPFC have been focal points for this research, as both play integral roles in driving anxiety-like behavior. Additionally, both of these regions have been shown to interface with the prototypical neuroendocrine stress response system: the hypothalamic-pituitary-adrenal (HPA) axis.

Stress adaptation and the hypothalamic-pituitary-adrenal axis

While the definition of stress can vary depending on context, as a biological variable it typically refers to the response of an organism to an environmental or interoceptive stimulus (i.e. a stressor) that threatens its homeostasis. The stressor then initiates an organismal reaction to the stimuli with the goal of restoring homeostasis. These varied biological processes have been collectively referred to as the 'stress response' (Ulrich-Lai and Herman, 2009) (Rodrigues et al., 2009). The mechanisms mediating the stress response are highly dependent on the modality of the stressor. For example, when an acute stressor is encountered, the autonomic nervous system provides the most immediate response. Through both its sympathetic and parasympathetic arms, it is able to provide rapid alterations in blood pressure and heart rate on the order of seconds (Ulrich-Lai and Herman, 2009).

The most well characterized stress response system in mammalian organisms is the hypothalamic-pituitary-adrenal (HPA) axis (Bhatnagar et al., 2004; Herman et al., 2003). This system represents the primary endocrine response to stress exposure, and typically operates on the time span of seconds to hours. Signals of homeostatic imbalance directly lead to activation of this system; ascending brainstem and spinal signals, carrying sensory, visceral, and autonomic information, directly project to the paraventricular nucleus of the hypothalamus (PVN). The

20

PVN is a primary site for integration of stress signals arriving from different sensory modalities (Herman et al., 2003; Sawchenko et al., 1996).

Following detection of stress signals, parvocellular neurons of the PVN secrete the neuroendocrine factor Corticotropin Releasing Hormone (CRH) (Antoni, 1986). This and other neuroendocrine hormones are released into the median eminence, which lacks a blood-brain barrier and represents an interface between the brain and the circulating endocrine system. CRH then binds to CRH receptors in the pituitary gland to promote release of the endocrine hormone, adrenocorticotrophin hormone (ACTH) into the blood stream (Antoni, 1986). Circulating ACTH subsequently binds to its cognate receptor in the zona fasciculata of the adrenal glands, which stimulates release of the stress hormone cortisol (or corticosterone in rodents) (Ulrich-Lai and Herman, 2009). The effects of glucocorticoids (such as cortisol), through binding to glucocorticoid receptors, are multifaceted and play a key role in mediating the stress response. These include increased energy mobilization (glycogenolysis), potentiation of vasoconstriction, and inhibition of innate immunity, among many others (McEwen and Stellar, 1993; Munck et al., 1984). These changes appear to be important for freeing energy stores for the initiation of behavioral and autonomic responses to stress (Herman et al., 2003). Importantly, the glucocorticoids play an autoregulatory negative feedback role by inhibiting CRH release from the PVN and ACTH release from the pituitary gland (Ulrich-Lai and Herman, 2009).

In addition to being regulated by circulating cortisol, the PVN receives dense innervation from a number of limbic brain regions that regulate its activity and subsequent release of CRH. The CeA sends direct projections to the PVN (Prewitt and Herman, 1998), and is directly activated by homeostatic stressors (Sawchenko et al., 1996). Furthermore, CeA lesions impair bradychardic responses to stress exposure (Roozendaal et al., 1990). While the CeA appears to

preferentially involved in regulating the autonomic stress response, the BLA is preferentially activated by psychological stressors (Dayas et al., 2001) (Cullinan et al., 1995). Lesions of the BLA significantly dampen HPA-axis response to chronic restraint stress (Bhatnagar et al., 2004). However, it should be noted that the BLA sends few direct projections to the PVN, and thus most likely influences its function through disynaptic connections to other brain regions like the bed nucleus of the stria terminalis (BNST) (Ulrich-Lai and Herman, 2009).

Conversely, the mPFC sends dense projections directly to the lateral hypothalamus and neurons in the peri-PVN zone that surrounds the PVN (Jankord and Herman, 2008). The direct cortico-hypothalmic projections originate primarily from the PL, and these projections have been found to play a pivotal role in inhibiting HPA axis responses to psychogenic stressors (Radley et al., 2006). Inhibition of the PL has thus been shown to enhance the autonomic responses to stress exposure (Akana et al., 2001). In contrast, the IL appears positively regulate HPA axis function and is involved in initiating neuroendocrine responses to stressors (Radley et al., 2006). Activation of the IL can directly invigorate autonomic stress responses, while inhibition of this region can ameliorate stress-induced depression-like behavior (Slattery et al., 2011).

Stress and amygdalo-cortical communication

In addition to directly modulating the neuroendocrine stress response, both the physiology and functioning of the mPFC and the BLA are profoundly affected by stress exposure. Indeed, numerous genetic and transcriptomic changes are observed in BLA neurons following stress exposure(Ponomarev et al., 2010). Among the stress-induced genetic changes in the BLA, downregulation of $GABA_A$-R receptor subunits has been consistently demonstrated (Hsu et al., 2003; Karssen et al., 2007; Segman et al., 2005). These, and other molecular

changes, lead broadly to enhanced excitability of BLA principal neurons, and are correlated with increased indices of anxiety (Truitt et al., 2007). These data support both optogenetic and pharmacological experiments demonstrating increasing the activity of BLA principal neurons induces anxiogenesis (Calhoon and Tye, 2015; Tovote et al., 2015). In addition to these genetic and physiological changes, both acute and chronic stressors also induce dramatic morphological changes in BLA principal neurons. Acute stress has been demonstrated to increase spine density on BLA dendrites, while chronic stress leads to significant expansion of the dendritic arbor of BLA neurons (McEwen and Morrison, 2013).

The mPFC similarly undergoes a dramatic array of biochemical and molecular changes in response to acute and chronic stressors(McEwen and Morrison, 2013). The mPFC is well positioned to modulate both the endocrine and emotional responses to stress through its projections to the lateral hypothalamus and the amygdala (Gabbott et al., 2005). In contrast to the BLA, a wide body of literature has suggested that stress exposure impairs prefrontocortical function through multiple mechanisms.   Physiologically, stress induced catecholamine release in the mPFC has been shown to weaken synaptic efficacy (Arnsten et al., 2012; Vijayraghavan et al., 2007), and the magnitude of stress induced cognitive impairment correlates with prefrontocortical levels of catecholamines (Murphy et al., 1996). In addition to these acute functional changes, chronic stress induces long lasting changes in mPFC neuron morphology. Chronic stress has been repeatedly demonstrated to lead to dendritic retraction and spine elimination in mPFC pyramidal neurons in a glucocorticoid dependent manner (Cerqueira et al., 2007; Cook and Wellman, 2004). This is contrasted to the BLA, where chronic stress elicits dendritic outgrowth, which accentuates the imbalance of amygdalo-cortical functioning. This amygdalo-cortical imbalance hypothesis has been corroborated by recent findings demonstrating

the stress exposure enhances amygdalar output to the mPFC (Lowery-Gionta et al., 2018). Interestingly, mPFC neurons that project to the BLA do not show the expected dendritic retraction and spine elimination, suggesting that while cortical circuits involved in cognition (e.g. cortico-cortical circuits) are weakened by stress exposure, cortical circuits involved in emotional processing (e.g. cortico-amygalar) are preserved or strengthened (Shansky et al., 2009).

Prefrontocortical endocannabinoids as a stress-buffering system

Recently there has been significant interest in the eCB signaling system in the context of stress adaptation. Systemic administration of drugs that potentiate eCB signaling have been shown to ameliorate the negative affective states induced by stress, while interfering with eCB signaling can enhance these effects (McLaughlin et al., 2014) (Patel et al., 2004) (Worley et al., 2018). There is recent converging evidence that eCBs are able to directly influence HPA axis activation, as mice CB1 knockout mice have significantly increased levels of stress-induced corticosterone release and display similar anxiety-like phenotypes to stressed mice (Hill et al., 2010). Additionally, these mice display similar cytoarchitectural abnormalities to mice that have undergone chronic stress exposure, including dendritic retraction in the mPFC (Hill et al., 2011a). These converging data suggest that eCBs in the mPFC could play a crucial role in regulating the physiological and behavioral responses to stress.

Stress itself appears to potently modulate eCB signaling within the mPFC. Following acute uncontrollable stress exposure, there is a rapid drop in AEA levels within the mPFC (McLaughlin et al., 2012). As in other brain regions, this has been primarily attributed to an increased FAAH activity and thus enhanced degradation of AEA. Interestingly, an opposing pattern emerges with regards to stress-induced modulation of prefrontocortical 2-AG signaling.

Acute restraint stress induced a delayed increase in 2-AG content within the mPFC, that emerges ~60 minutes following exposure to the stressor (Hill et al., 2011b). This stress-induced increase in 2-AG levels appears to be dependent on corticosterone binding to glucocorticoid receptors locally within the mPFC. If this stress-induced increase in 2-AG signaling is blocked, the timecourse of corticosterone secretion is significantly prolonged (Hill et al., 2011b). These data suggest that AEA and 2-AG may play pivotal, but functionally distinct roles in prefrontocortical control of the endocrine and behavioral responses to stress. A prevailing hypothesis is that " a stress-induced reduction in AEA tone disengages tonic suppression of the HPA axis and facilitates mobilization of corticosterone, which when released activated glucocorticoid receptors and results in a delayed increase in 2-AG mediated CB1 receptor signaling in the prelimbic cortex, thereby contributing the HPA negative feedback during the recovery phase following cessation of the stressor" (McLaughlin et al., 2014).

There appears however to be significant heterogeneity as to the effect of different stress regimens on prefrontocortical eCBs. For example, exposure to a chronic habituating homotypic stress elicits an increase in mPFC 2-AG content on day 10 of the stressor but not on day 1 (Rademacher et al., 2008). As observed with acute exposure, AEA levels remain diminished throughout the stress regimen (Rademacher et al., 2008). These data further support a pivotal role for prefrontocortical 2-AG signaling in stress adaptation and habituation, and suggest that impairment of AEA signaling diminishes prefrontocortical control over the HPA axis. In contrast, a different pattern emerges during exposure to a non-habituating chronic stressor. For example, chronic unpredictable stress exposure produces a significant reduction in prefrontocortical AEA levels, but no detectable change in 2-AG levels at any time point (Hill et al., 2008). Unlike the eCBs, CB1 expression does not seem to be particularly selective to the

regimen of stress applied. Both chronic habituating (Zoppi et al., 2011) and non-habituating stressors have been shown to increase CB1 mRNA expression (Bortolato et al., 2007) and binding site density (Hill et al., 2008) in the mPFC.

In addition to being directly involved in modulating the neuroendocrine stress response, prefrontocortical eCB signaling has been highly implicated in regulating the emotional and behavioral responses to stress exposure. For example, inhibiting AEA hydrolysis in the PL (thereby boosting levels) is able to significantly reduce stress-induced corticosterone release (McLaughlin et al., 2014), attenuate behavioral responses to environmental threat (Aliczki et al., 2016), and reduce anxiety-like behaviors (Rubino et al., 2008b). Conversely, diminishing AEA signaling by overexpressing FAAH in the mPFC elicits a robust anxiogenic phenotype. Similar studies have demonstrated that directly antagonizing CB1 locally within the mPFC leads to prolonged corticosterone secretion following stress and increased passive coping responses to stress exposure (McLaughlin et al., 2013). The opposite effects have been demonstrated with CB1 agonists, where their administration into the mPFC is able to reduce anxiety (Rubino et al., 2008b) and increase active coping responses to stress (Bambico et al., 2007).

Recent efforts to rescue stress-induced anxiety-like behavior by overexpressing the CB1 receptor in the mPFC have not proven particularly fruitful (Klugmann et al., 2011). It was theorized that because CB1 agonism in the mPFC is anxiolytic, that CB1 overexpression would elicit similar behavioral effects. However, this effect is not particularly surprising, given the fact that CB1 is a presynaptically expressed receptor, which would lead to overexpression in distal projection targets of the mPFC, rather than in the mPFC itself. A recent study has further shed light on the behavioral effects of cannabinoids, by demonstrating that the anxiolytic effect of CB1 agonists is driven by activation of CB1 on forebrain glutamatergic axon terminals (Rey et

al., 2012).   This finding, combined with the anxiolytic effect of prefrontocortical eCB administration, suggests that the anxiolytic properties of cannabinoids could be due to shunting of excitatory input to the mPFC.

However, there are multiple sources of glutamatergic input to the mPFC, including the BLA (Felix-Ortiz et al., 2015), mediodorsal thalamus (Schmitt et al., 2017), paraventricular thalamus (Matyas et al., 2014), and ventral hippocampus (Marek et al., 2018). The question is, which excitatory inputs to the mPFC are eCBs shunting to elicit their anxiolytic effect? As previously mentioned, direct activation of BLA inputs to the mPFC is anxiogenic (Felix-Ortiz et al., 2015). Furthermore, restraint stress exposure enhances BLA excitatory input to the mPFC and induces anxiety like behavior (Lowery-Gionta et al., 2018). Given that stress caused an increase in presynaptic release probability, these data led us to investigate whether stress-induced anxiety like behavior is caused by impaired eCB regulation of excitatory input from the BLA to the mPFC.

CHAPTER II

Endocannabinoid Signaling Collapse Mediates Stress-Induced Amygdalo-Cortical Strengthening

David J. Marcus[1,2], Gaurav Bedse[1], Andrew Gaulden[1], James D. Ryan[3,4], Veronika Kondev[1,2], Nathan D. Winters[1,2], Luis Rosas-Vidal[1], Megan Altemus[1], Eric Delpire[5], Francis S. Lee[3,4], Ken Mackie[6,7], and Sachin Patel[1,2,8]*

[1]Department of Psychiatry and Behavioral Sciences, Vanderbilt University Medical Center, Nashville, TN 37232
[2]The Vanderbilt Brain Institute, Vanderbilt University, Nashville, TN 37232
[3]Department of Psychiatry, Weill Cornell Medicine, New York, NY 10065
[4]Sackler Institute for Developmental Psychobiology, Weill Cornell Medicine, New York, NY 10065
[5]Department of Anesthesiology, Vanderbilt University Medical Center, Nashville TN 37232
[6]Gill Center for Biomolecular Science, Indiana University, Bloomington, IN 47405
[7]Department of Psychological and Brain Sciences, Indiana University, Bloomington, IN 47405
[8]Department of Molecular Physiology & Biophysics, Vanderbilt University Medical Center, Nashville, TN 37232

*Lead Contact:
Sachin Patel, MD, PhD
Professor of Psychiatry and Behavioral Sciences,
Molecular Physiology & Biophysics, and
Pharmacology
2213 Garland Avenue
Medical Research Building IV, Rm 8425B
Vanderbilt University Medical Center
Nashville, TN 37232
Email: sachin.patel@vanderbilt.edu
Phone: (615) 936-7768
Fax: (615) 322-1462

Summary

Functional coupling between the amygdala and the dorsomedial prefrontal cortex (dmPFC) has been implicated in the generation of negative affective states under stressful conditions in both humans and rodents; however, the synaptic and molecular mechanisms by which stress increases amygdala-dmPFC synaptic strength and generates anxiety-like behaviors are not well understood. Here we show that the mouse basolateral amygdala (BLA)-prelimbic prefrontal cortex (plPFC) circuit is functionally engaged by acute stress exposure and that activation of this pathway can recapitulate the anxiogenic effects of stress. Furthermore, we demonstrate that acute stress exposure leads to a lasting increase in synaptic strength within a reciprocal BLA-plPFC-BLA subcircuit. Importantly, we identify 2-arachidonoylglycerol (2-AG)-mediated endocannabinoid signaling as a key mechanism limiting glutamate release at BLA-plPFC synapses and the functional collapse of multimodal 2-AG signaling as a molecular mechanism leading to persistent circuit-specific synaptic strengthening and anxiety-like behaviors after stress exposure. These data suggest circuit-specific impairment in 2-AG signaling could facilitate functional coupling between the BLA and plPFC and the translation of environmental stress to affective pathology.

Keywords

2-Arachidonoylglycerol; glutamate; prefrontal cortex; anxiety; cannabis; cannabinoid; amygdala

Introduction

Stress exposure is a major risk factor for the development and exacerbation of major mental illnesses including major depression, anxiety disorders, and substance use disorders (Arnsten, 2015; McEwen, 2012; Sharma et al., 2016). Furthermore, exposure to severe stress is required for the development of posttraumatic stress disorder (PTSD) (Fenster et al., 2018; Gillespie et al., 2009; Henigsberg et al., 2019; Kessler et al., 2005a; Mark et al., 2018). In this context, understanding the molecular, cellular and circuit-level mechanisms by which stress exposure is translated into distinct psychopathological behavioral, emotional, and cognitive domains could have broad translational implications. Moreover, elucidating conserved molecular mechanisms linking stress to affective psychopathology could reveal novel therapeutic approaches to mitigate the adverse effects of stress on mental health. Although identification of a number of stress-regulatory neuromodulatory signaling systems has revealed potentially novel therapeutic targets for affective disorders, endogenous cannabinoid (eCB) signaling represents a leading drug-development candidate (2017; Hill et al., 2018; Hill and Patel, 2013; Lowe et al., 2018; Patel et al., 2017).

eCB signaling systems have been heavily implicated in stress-response physiology and pharmacological augmentation of eCB signaling has been suggested to represent a novel approach for the treatment of stress and trauma-related psychiatric disorders (Hill et al., 2018; Patel et al., 2017). At the synaptic level, 2-arachidonoylglycerol (2-AG)-mediated eCB signaling is a broadly expressed inhibitory retrograde signaling system. Specifically, 2-AG is canonically produced by postsynaptic neurons in an activity-dependent manner by diacylglycerol-lipase alpha (DAGLα) and activates presynaptic CB1 receptors to reduce neurotransmitter release probability (Kano et al., 2009; Stella et al., 1997; Wilson and Nicoll, 2001). 2-AG is degraded by

monoacylglycerol lipase (MAGL) expressed within presynaptic terminals and glial cells (Dinh et al., 2004). Recent studies have implicated 2-AG signaling as a critical stress modulatory system and revealed 2-AG augmentation as a novel approach for the treatment of stress-related psychiatric disorders (Lisboa et al., 2017; Lutz et al., 2015). For example, 2-AG deficiency is associated with increased anxiety, impaired fear extinction, and increased susceptibility to stress-induced anxiety (Bluett et al., 2017; Cavener et al., 2018; Shonesy et al., 2014). Conversely, 2-AG augmentation promotes stress resilience and prevents stress-induced anxiety (Bedse et al., 2017; Bluett et al., 2017; Bosch-Bouju et al., 2016; McLaughlin et al., 2014; Patel et al., 2009; Qin et al., 2015; Sciolino et al., 2011; Sumislawski et al., 2011). Despite these data, the precise cellular and circuit-level mechanisms by which 2-AG interacts with environmental stress to affect emotional behavior are not well understood.

Studies over the past decade have elucidated distinct brain circuits connecting emotional and cognitive control centers in the modulation of stress responsivity, anxiety, and emotional regulation (Apps and Strata, 2015; McEwen et al., 2015; Tovote et al., 2015; Tye, 2018). For example, top-down inhibition of amygdala function by the ventromedial prefrontal cortex (vmPFC) has emerged as an evolutionarily conserved mechanism counteracting the effects of stress and reducing anxiety (Adhikari et al., 2015; Sierra-Mercado et al., 2011). Indeed, activity within the vmPFC and amygdala are inversely correlated and impaired vmPFC activity is associated with increased symptom severity in PTSD (Henigsberg et al., 2019; Milad et al., 2009). In contrast to these well-established findings, more recent studies have revealed that dmPFC and amygdala activity are positively correlated and that increased activity within these regions is associated with anxiety in humans (Carlisi and Robinson, 2018; Cremers et al., 2010; Kim et al., 2011; Milad et al., 2009; Robinson et al., 2014). Consistent with these findings,

rodent studies have demonstrated that activation of basolateral amygdala (BLA) inputs to the prelimbic PFC (plPFC), a rodent homologue of the human dmPFC, generates anxiety-like behaviors and biases behavior toward fear responses in the face of uncertainty (Burgos-Robles et al., 2017; Felix-Ortiz et al., 2015; Senn et al., 2014). Recent studies have also demonstrated that BLA-plPFC glutamatergic synapses undergo presynaptic strengthening after stress exposure (Lowery-Gionta et al., 2018). Taken together, these data suggest enhanced amygdala-dmPFC (BLA-plPFC in rodents) coupling could represent a conserved circuit mechanism that translates stress exposure into anxiety-like emotional states. However, the molecular mechanisms subserving stress-induced strengthening of BLA-plPFC circuits and generation of anxiety-like behaviors after stress exposure are not well understood.

Here we elucidate an eCB mechanism linking stress exposure to BLA-plPFC subcircuit-specific synaptic strengthening and its causal relation to the resultant anxiety-like behavior. Our data reveal physiological activation of a BLA-plPFC circuit in response to foot-shock stress and that increased activity in this pathway is sufficient to generate anxiety-like behavioral responses. We next demonstrate increased synaptic strengthening in a specific BLA-plPFC-BLA reciprocal glutamatergic circuit after acute stress exposure, and that this circuit-specific strengthening is associated with collapse of retrograde 2-AG signaling at BLA-plPFC glutamatergic synapses. Importantly, pharmacological augmentation of 2-AG levels reverses stress-induced anxiety-like behaviors and circuit-specific synaptic strengthening *ex vivo*, while molecular genetic approaches revealed BLA-plPFC 2-AG-CB1 signaling deficiency promotes the translation of environmental stress to anxiety-like behaviors. These data provide insight into the molecular mechanisms by which stress exposure can influence amygdala-cortical circuit function and

emotional behavior and could shed light on the pathophysiological mechanisms underlying stress-related neuropsychiatric disorders.

Results

The BLA-plPFC circuit is stress responsive and anxiogenic

Multiple lines of research have implicated both the BLA and the dmPFC (plPFC in rodents) as critical nodal structures involved in the pathophysiology of stress-related affective disorders (Carlisi and Robinson, 2018; Kalisch and Gerlicher, 2014; Milad et al., 2009; Ongur and Price, 2000; Preuss, 1995; Robinson et al., 2014). The rodent plPFC has extensive reciprocal glutamatergic connections with the BLA that are modulated by stress exposure and capable of generating anxiety-like responses (Felix-Ortiz et al., 2015; Johnson et al., 2018; Lowery-Gionta et al., 2018; Vertes, 2004). In order to investigate the molecular mechanisms regulating BLA-plPFC connectivity and plasticity, we first sought to verify that this circuit is engaged by exposure to stressful stimuli **(Figure 1a)**. Using *in vivo* fiber photometry, we observed that exposure to unpredictable foot-shock stress significantly increased presynaptic calcium influx in BLA axon terminals innervating plPFC, time-locked to shock onset (**Figure 1b,c**). We next used *in vivo* single cell calcium imaging via head mounted epifluorescent microscope to examine plPFC neuronal responses to foot-shock exposure. The bulk calcium signal in the entire field of view was increased in response to shock exposure **(Figure 1d,e)**, with subsequent single cell analysis revealing three distinct populations of neurons: stress excitatory (44.40%), stress inhibitory (38.43%) and stress non-responsive (17.16%) **(Figure 1f,g)**. Overall, the peak excitatory response was greater in absolute magnitude than the peak inhibitory (excitatory: $|z| = 3.83$, inhibitory: $|z| = 2.62$, p=0.0073 by two-tailed t test) and resultant average
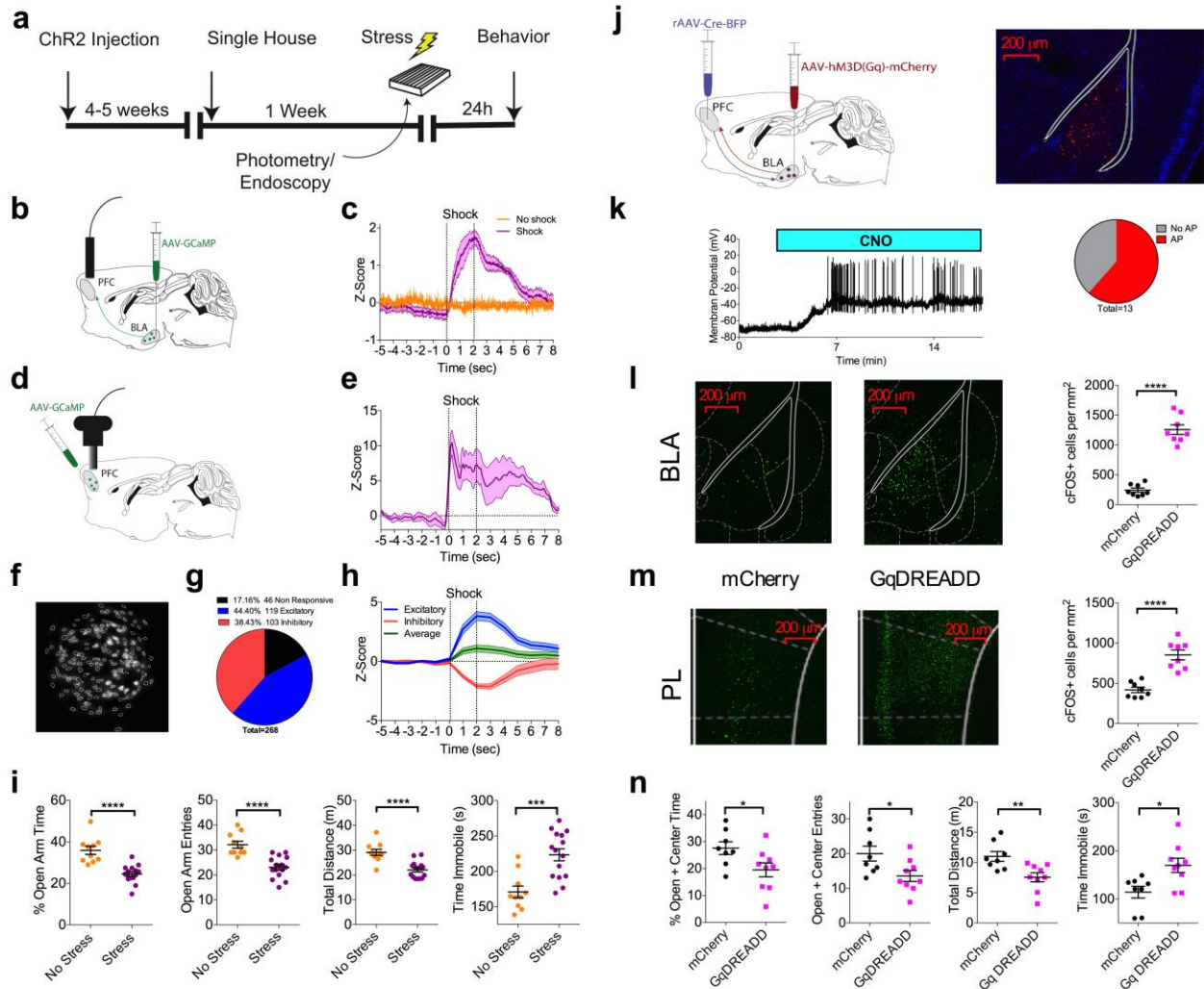
Figure 1. Stress exposure activates an anxiogenic BLA-plPFC circuit

(a) Schematic and timeline for stress exposure and behavioral analysis
(b) Schematic for *in vivo* fiber photometry recordings of BLA projections to the plPFC
(c) Z-score of ΔF/F signal recorded from GCaMP6s expressing BLA terminals in the plPFC in response to a 2 second 0.5 mA foot shock. Traces represent mean of 4-5 mice, with each mouse trace derived from the average of 20 shock trials (Stress N=5, control N=4).
(d) Schematic for *in vivo* miniendoscopy-based calcium imaging of plPFC neurons
(e) Z-score of bulk ΔF/F recorded from total GCaMP7f signal in the field of view in response to a 0.5 mA 2 second foot shock. Trace represents mean of 4 mice, with each mouse trace derived from the average of 20 shock trials (N=4).
(f) Miniendoscopic maximal projection image of calcium signal and extracted cell contours from representative mouse.
(g) Proportion of GCaMP7f expressing plPFC neurons displaying excitatory, inhibitory, or no responses to foot-shock (n=268 cells from N=4 mice).

(h) Z-score of excitatory (n=119), inhibitory (n=103), and averaged excitatory and inhibitory responses (n=222), across 1 second bins. Peak excitatory z-score=3.83, peak inhibitory z-score=-2.14, peak average=1.09.

(i) Effects of foot-shock stress on anxiety-like behavior in the elevated-zero maze (No Stress: N=10, Stress: N=15). Stress exposure decreased % open-arm time (p<0.0001), decreased open-arm entries (p<0.0001), decreased total distance (p<0.0001), and increased immobility time (p=0.0003).

(j) Schematic diagram of intersectional viral approach for hM3Dq (GqDREADD) expression in the BLA-plPFC circuit

(k) Example trace and proportion of BLA neurons that displayed CNO-induced action potential firing (n=13, N=4)

(l) Representative images and quantification of cFOS expression in BLA neurons following *in vivo* administration of 10 mg/kg CNO (mCherry: N=8, GqDREADD: N=8). mCherry vs. GqDREADD p<0.0001.

(m) Representative images and quantification of cFOS expression in plPFC neurons following *in vivo* administration of 10 mg/kg CNO (mCherry: N=8, GqDREADD: N=8). mCherry vs. GqDREADD p<0.0001.

(n) Effects of Clozapine N-Oxide (5 mg/kg) on anxiety-like behavior in the elevated-plus maze (GqDREADD: N=9, mCherry N=8). Mice expressing the GqDREADD in BLA neurons projecting to the plPFC had decreased % open and center time (p=0.0378), decreased open and center entries (p=0.0268), decreased total distance (p=0.0067), and increased immobility time (p=0.0119) compared to mCherry expressing controls.

All error bars represent ± SEM. "n" represents number of neurons, "N" represents number of mice. P values reported from two-tailed unpaired t-test (h,k,l,m)

signal was excitatory (Z=1.09; **Figure 1h**), suggesting that stress-induced excitation of plPFC neurons predominates over inhibition. These data indicate that stress exposure engages the BLA-plPFC circuit and leads into enhanced activity plPFC neurons.

Stress exposure is a ubiquitous risk factor for the development of anxiety disorders and stress exposure in rodents can model many psychopathological domains relevant to affective disorders. Indeed, 24 hours following foot-shock stress exposure, we observed an increase in anxiety-like behavior in the elevated-zero maze (EZM) (**Figure 1i**). Given that stress exposure enhanced activity within the BLA-plPFC circuit and induced anxiety-like behavior, we examined whether a 'stress-like' state could be recapitulated through direct activation of the BLA-plPFC circuit. To test this, we used an intersectional chemogenetic approach to specifically enhance the

excitability of BLA neurons that project to the plPFC (**Figure 1j**). We first examined whether this chemogenetic strategy was capable of inducing action potential firing in BLA-plPFC projection neurons.   We used whole-cell current clamp electrophysiological recordings of BLA pyramidal neurons while washing on the GqDREADD agonist, clozapine-n-oxide (CNO). We found that CNO caused significant neuronal depolarization and induced action potential firing in 8/13 neurons we recorded from **(Figure 1k)**. *In vivo* administration of CNO induced robust cFOS expression in both the BLA **(Figure 1l)** and the mPFC **(Figure 1m)** in GqDREADD-expressing mice relative to mCherry-expressing controls, demonstrating that this approach not only leads to *in vivo* activation of BLA neurons, but also plPFC neurons that receive excitatory input from the BLA. Furthermore, although stress led to neuronal activation in the plPFC (**Figure 1d,e**), stress did not lead to a further increase in cFOS expression in the BLA (N=6, p=0.6418) or plPFC (N=6, p=0.0855) after GqDREADD activation of BLA-plPFC neurons, suggesting that stress and GqDREADD activation recruit overlapping BLA-plPFC neural circuits (data not shown).   In the elevated-plus maze (EPM), chemogenetic activation of this circuit significantly enhanced anxiety-like behavior (**Figure 1n**), consistent with previous reports demonstrating an anxiogenic role of the BLA-plPFC circuit (Felix-Ortiz et al., 2015). These data indicate the BLA-plPFC circuit is stress responsive and its activation is anxiogenic in mice, suggesting that stress-induced anxiety like behavior could be mediated through activation of the BLA-plPFC circuit.

Stress exposure potentiates excitatory signaling in a BLA-plPFC reciprocal circuit

Our data thus far suggest enhanced BLA-plPFC circuit activity may be a relevant substrate for the translation of environmental stressors into anxiety-like behaviors.   Although

stress-induced strengthening of BLA-PFC glutamatergic projections has been demonstrated in mice (Lowery-Gionta et al., 2018), the molecular mechanisms subserving this enhanced coupling remains elusive. To examine stress-induced synaptic adaptations within the BLA-plPFC circuit, we used a combination of anterograde ChR2-assisted projection-targeting and retrograde tracing approaches, followed by *ex-vivo* brain slice electrophysiology (**Figure 2a-b**). Four to six weeks after co-injection of AAV5-CaMKII-ChR2-eYFP (ChR2) and retrograde rAAV2-CAG-td-tomato (rAAV) into the BLA, mice were sacrificed for *ex vivo* electrophysiological studies. BLA-originating, optically-evoked excitatory post-synaptic currents (oEPSCs) were recorded from rAAV-positive and rAAV-negative pyramidal neurons in both L2/3 and L5 in the plPFC. Our electrophysiological approach (see Methods) allowed for detection of BLA-originating monosynaptic glutamatergic inputs to plPFC that were sensitive to CNQX and TTX but insensitive to picrotoxin (**Figure S1a-c**). Consistent with previous studies, we found BLA inputs made stronger synaptic connections onto rAAV-positive reciprocally projecting, than rAAV-negative, plPFC neurons (**Figure S1d-i**) (Little and Carter, 2013), further validating our circuit-specific electrophysiological approach.

24 hours after foot-shock stress exposure, we observed an increase in BLA-originating oEPSC amplitude and a decrease in the paired-pulse ratio (PPR) specifically in rAAV-positive reciprocally projecting L2/3 plPFC neurons (**Figure 2c-e**), suggesting increased glutamate release probability within a reciprocal BLA-plPFC-BLA circuit. This enhanced excitatory drive within the reciprocal BLA-plPFC-BLA circuit was also accompanied by an increase in the probability of synaptically-driven action potential firing in rAAV-positive L2/3 neurons, and a small but significant increase in the intrinsic excitability of L2/3 rAAV-positive neurons (**Figure 2f-g**). We also observed an increase in the frequency, but not amplitude, of optogenetically-
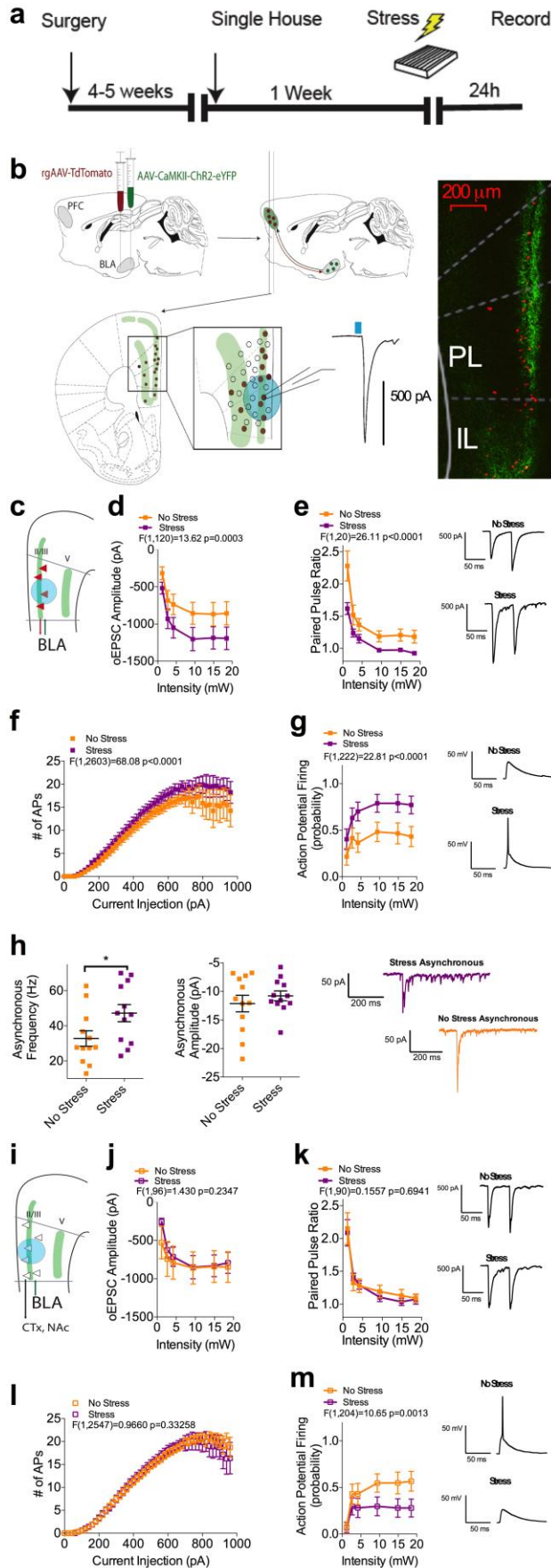
Figure 2: Stress exposure enhances glutamatergic signaling in the BLA L2/3-plPFC reciprocal circuit

(a) Experimental timeline.

(b) Schematic for stereotaxic delivery of AAV5-CaMKII-ChR2(H147R)-eYFP and rAAV2-CAG-tdTomato into the BLA and recordings of oEPSCs from retrogradely labeled plPFC neurons.

(c) Schematic for voltage-clamp recordings of oEPSCs from L2/3 rAAV-positive neurons.

(d) Optically-evoked input/output curve from L2/3 rAAV-positive neurons from non-stressed (n=11; N=4) and stressed (n=11; N=4 mice) mice. Stress exposure enhances excitatory input to L2/3 rAAV- positive neurons.

(e) Effects of stress on Paired Pulse Ratio (PPR) at BLA-L2/3 rAAV-positive synapses (No Stress: n=11, N=4, Stress: n=10, N=4). Stress exposure decreases PPR at BLA-L2/3 rAAV-positive synapses.

(f) Intrinsic excitability of L2/3 rAAV-positive neurons following stress exposure (No Stress: n=37, N=12; Stress: n=33, N=14). Stress exposure increases intrinsic excitability in L2/3 rAAV-positive neurons.

(g) Optically-evoked spiking in L2/3 rAAV-positive neurons in non-stressed (n=20, N=7) and stressed mice (n=19, N=7). Stress exposure increases optically-evoked spiking in L2/3 rAAV-positive neurons.

(h) Effects of stress on asynchronous EPSC frequency (No Stress: n=12, N=4; Stress: n=12, N=5; p=0.0394) and amplitude (NS, p=0.4311) at BLA-L2/3 rAAV-positive synapses.

(i) Schematic for voltage-clamp recordings of oEPSCs from L2/3 rAAV-negative neurons.

(j) Optically-evoked input/output curve from L2/3 rAAV-negative neurons from non-stressed (n=9, N=4) and stressed (n=9, N=4) mice. Stress exposure does not enhance

excitatory input to L2/3 rAAV-negative neurons.

(k) Effects of stress on PPR at BLA-L2/3 rAAV-negative synapses (No Stress: n=8, N=4; Stress: n=9, N=4). Stress exposure does not alter PPR at BLA-L2/3 rAAV-negative synapses.

(l) Intrinsic excitability of L2/3 rAAV-negative neurons following stress exposure (No Stress n=35, N=11; Stress n=28, N=10). Stress exposure does not alter intrinsic excitability of L2/3 rAAV-negative neurons.

(m) Optically-evoked spiking in L2/3 rAAV-negative neurons in non-stressed (n=17, N=7) and stressed mice (n=19, N=7). Stress exposure decreases optically-evoked spiking in L2/3 rAAV-negative neurons.

All error bars represent ± SEM. "n" represents number of neurons, "N" represents number of mice. P values reported from two-tailed unpaired t-test (h). F and P values for two-way ANOVA shown in relevant panels.

elicited asynchronous EPSCs (o-aEPSCs) onto L2/3 rAAV-positive neurons, confirming an increase in presynaptic release probability at BLA-plPFC synapses 24h after stress exposure (**Figure 2h**). In contrast to the effects observed in reciprocally projecting L2/3 neurons, there was no significant change in excitatory input (**Figure 2j**), PPR (**Figure 2k**), or somatically driven AP firing (**Figure 2l**) in L2/3 rAAV-negative neurons. The only change observed in L2/3 rAAV-negative neurons was a small but significant decrease in optogenetically elicited action potential firing (**Figure 2m**). This result was unexpected, considering we observed neither a stress induced change in excitatory input nor excitability of these neurons. Although our data show that presynaptic input from the BLA to L2/3 rAAV-negative neurons is unchanged, the change in synaptically driven spiking suggests that there could be broader changes in how plPFC neurons integrate and respond to excitatory input following stress, such as decreased synaptic integration or dendritic summation, which has been documented in mPFC neurons (Arnsten, 2009, 2015; Arnsten et al., 2012).

No stress-induced changes were found in L5 rAAV-positive or negative neurons (**Figure S2 a-h**), suggesting both sub-circuit (BLA-plPFC reciprocal vs. non-reciprocal circuits) and

laminar-specific synaptic strengthening occurs after acute stress exposure. Additionally, no stress-induced changes in either resting membrane potential or input resistance were found in any population of neurons (**Figure S2i-t**). Lastly, to determine the specificity of stress-induced synaptic strengthening in the plPFC, we examined whether projections from the mediodorsal thalamus (MDT), another brain region with strong reciprocal glutamatergic connectivity with the plPFC, were modulated by stress exposure (Matyas et al., 2014; Vertes, 2004). We observed that stress did not cause persistent alterations at MDT to L2/3 or to L6 synapses, suggesting that there is selective enhancement of excitatory signaling in the BLA-L2/3 plPFC-BLA reciprocal circuit (**Figure S2u-dd).**

Similar synaptic effects to those observed in male mice exposed to foot-shock were observed in male mice that were exposed to the predator odor 2-methyl-thiazoline (2MT) and in foot-shock exposed female mice, suggesting that stress induced enhancement of presynaptic glutamate release at BLA-plPFC-BLA synapses is not modality- or sex-specific (**Figure S3a-c,e,f**). To determine whether the stress induced presynaptic strengthening at BLA-L2/3 plPFC-BLA synapses was dependent on stressor intensity, we tested whether 0.1 or 0.25 mA foot-shocks were able to induce similar synaptic changes to those observed after 0.5 mA shocks. Fiber photometry approaches revealed an increase in BLA-plPFC terminal activity at 0.25 but not 0.1 mA shock intensity (**Figure S3h-j**). Similarly, 24 hours later, we observed a trend towards increased oEPSC amplitude and significantly reduced PPR in the 0.25 mA shock group but not the 0.1 mA shock group, suggesting stress induced BLA-plPFC activation and persistent strengthening both scale dynamically with the intensity of the stressor (**Figure S3k,l**). Lastly, to determine the duration of these synaptic modifications observed after acute stress, we also performed electrophysiological recordings at 3 and 10 days following exposure to 20 0.5 mA

foot-shocks. At three days post-stress, oEPSC amplitudes remained higher and PPR remained reduced, while these values were normalized 10 days post-stress, indicating that these stress-induced synaptic alterations are persistent but not permanent (**Figure S3n,o**).

Endocannabinoid signaling broadly inhibits glutamatergic input from the BLA to the plPFC

Given that the observed increase in BLA-plPFC glutamatergic transmission appears to be mediated largely through enhanced presynaptic release, we next sought to determine the mechanism driving this effect. The retrograde acting eCBs, primarily 2-AG and anandamide (AEA), are known to be key negative modulators of presynaptic neurotransmitter release that exert their effects through binding to presynaptic CB1 receptors (Kano et al., 2009; Wilson and Nicoll, 2001). Importantly, eCBs are known to be regulated by stress and inhibit presynaptic glutamate transmission in the PFC raising the possibility that functional impairment in this neuromodulatory system could contribute to increased presynaptic drive at BLA-plPFC synapses after stress exposure (Katona and Freund, 2012; Lafourcade et al., 2007; Manduca et al., 2017; McLaughlin et al., 2014). To begin to test this hypothesis, we first demonstrated, using the optogenetic circuit-mapping approach described above (see **Figure 2b**), that the cannabinoid receptor agonist CP55,940 robustly depressed BLA-evoked oEPSC amplitude in rAAV-positive and rAAV-negative layer 2/3 plPFC neurons, indicating that BLA projections to the plPFC are broadly regulated by CB1 signaling (**Figure 3a-b,e-f**). To determine whether eCBs regulate BLA-plPFC glutamatergic transmission, we analyzed depolarization-induced suppression of excitation (DSE), a well characterized form of 2-AG mediated short-term synaptic depression, in which brief post-synaptic depolarization leads to 2-AG production and inhibition of
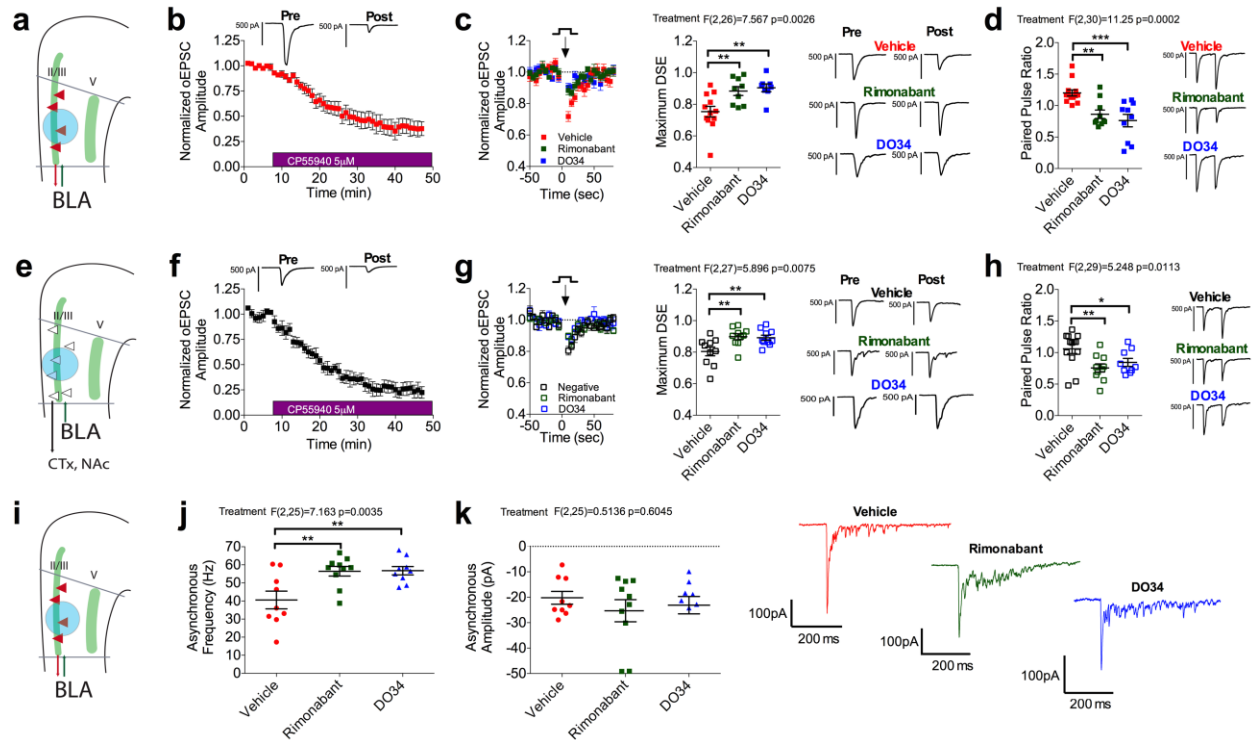
Figure 3: Phasic and tonic 2-AG signaling broadly regulate BLA-plPFC L2/3 glutamatergic synapses

(a) Schematic for voltage-clamp recordings of oEPSCs from L2/3 rAAV-positive neurons.

(b) Effect of 5 μM CP55,940 on oEPSC amplitude at BLA-L2/3 rAAV-positive synapses (n=6, N=3).

(c) Depolarization-induced suppression of excitation (DSE) at BLA-L2/3 rAAV-positive synapses (n=12, N=6) is blocked by 10 μM rimonabant (n=9, N=5; p=0.0049) and 2.5 μM DO34 (n=8, N=4; p=0.0039;).

(d) PPR at BLA-L2/3 rAAV-positive synapses (n=13, N=6) is reduced by 10 μM rimonabant (n=10, N=6; p=0.0034) and 2.5 μM DO34 (n=10, N=4; p=0.0002).

(e) Schematic for voltage-clamp recordings of oEPSCs from L2/3 rAAV-negative neurons.

(f) Effect of CP55,940 on oEPSC amplitude at BLA-L2/3 rAAV-negative synapses (n=5, N=4).

(g) DSE at BLA-L2/3 rAAV-negative synapses (n=10, N=5) is blocked by rimonabant (n=10, N=4; p=0.0095) and DO34 (n=10, N=4; p=0.0095).

(h) PPR at BLA-L2/3 negative synapses (n=13, N=5) is reduced by rimonabant (n=10, N=5; p=0.0084) and DO34 (n=9, N=4; p=0.0409).

(i) Schematic for voltage-clamp recordings of asynchronous EPSCs from L2/3 rAAV-positive neurons

(j) Asynchronous EPSC frequency at BLA-L2/3 rAAV-positive synapses (n=9, N=2) is increased by rimonabant (n=10, N=2; p=0.0058) and DO34 (n=9, N=2; p=0.0058).

(k) Asynchronous EPSC amplitude at BLA-L2/3 rAAV-positive synapses (n=9, N=2) is not altered by rimonabant (n=10, N=2; p=0.5392) or DO34 (n=9, N=2; p=0.5785).

All error bars represent ± SEM. "n" represents number of neurons, "N" represents number of mice. All post-hoc p values derived from one-way ANOVA with Holm-Sidak multiple comparisons (c,d,g,h,j,k). F and P values for ANOVA shown in relevant panels.

glutamatergic release through binding to presynaptic CB1 receptors (Kano et al., 2009; Wilson and Nicoll, 2001). We found that DSE, induced by 10 second post-synaptic depolarization to +30mV, was expressed at both L2/3 rAAV-positive and negative neurons, and could be blocked by rimonabant, a CB1 inverse agonist, or DO34, an inhibitor of the rate-limiting enzyme in 2-AG biosynthesis, diacylglycerol lipase (DAGL) (**Figure 3c,g**). Interestingly, these two compounds alone induced a dramatic reduction in the PPR at BLA-L2/3 plPFC rAAV-positive and negative synapses, suggesting tonic inhibition of glutamate release at BLA-plPFC synapses by 2-AG signaling (**Figure 3d,h**). Similar results were found in L5 rAAV-positive and negative neurons, although DSE could not be elicited efficiently in L5 rAAV-negative neurons suggesting there is cell-type specificity to eCB regulation of the BLA-plPFC circuit (**Figure S4a-h**). To ensure that the effect of rimonabant on PPR was actually due to blockade of tonic eCB signaling and not its inverse agonist properties, we also repeated this experiment with the neutral CB1 antagonist NESS0327 (NESS). Both NESS and rimonabant blocked DSE, reduced the PPR, and led to greater oEPSC amplitude, suggesting that they both function via blockade of tonic eCB signaling (**Figure S5j-k,l,m,p,q**). Given that tonic eCB signaling has generally been ascribed to AEA, rather than 2-AG, release in other brain regions, we augmented our PPR experiments via measurement of the frequency and amplitude of o-aEPSCs (Kim and Alger, 2010). These experiments revealed that rimonabant and DO34 both increased the frequency, but not amplitude, of optogenetically-elicited asynchronous EPSCs confirming tonic 2-AG signaling at these synapses (**Figure 3i-k**). These data provide the first evidence of broadly expressed multimodal tonic and phasic 2-AG-mediated regulation of presynaptic neurotransmitter release at

43

BLA-plPFC synapses. To examine the input-specificity of eCB signaling in the plPFC, we performed the same key experiments while examining MDT projections to the plPFC. The MDT is known to have low CB1 expression (Herkenham et al., 1990), and as such, we observed little CP55,940-induced depression of oEPSC amplitude and no DSE, suggesting there is circuit-level specificity to eCB regulation of excitatory transmission in the plPFC (**Figure S4i-k**).

Stress impairs 2-AG-mediated inhibition of the BLA-plPFC reciprocal glutamatergic circuits

Following the observation that stress increased presynaptic release probability within the BLA-plPFC reciprocal circuit and that BLA inputs to the plPFC are highly regulated by 2-AG signaling, we next sought to determine whether stress-induced synaptic strengthening within this circuit was mediated via dynamic remodeling of BLA-plPFC 2-AG signaling. Using mass spectrometry, we first observed that stress exposure decreased bulk 2-AG levels in the mPFC 24h later, consistent with previous studies in other brain regions (Qin et al., 2015) (**Figure 4a**). Furthermore, bulk levels of arachidonic acid (AA), a primary degradative product of 2-AG hydrolysis, were also significantly reduced in the mPFC of stressed mice (**Figure 4b**). These data suggest that stress exposure could downregulate 2-AG synthesis in the mPFC, as levels of both 2-AG and AA are similarly reduced following stress exposure; in support of this, inhibition of 2-AG hydrolysis with the monoacylglycerol lipase (MAGL) inhibitor JZL184 *increased* 2-AG and *reduced* AA (**Figure 4a-b**). Importantly, elevating 2-AG levels with JZL184 reversed, while depleting 2-AG levels with DO34 exacerbated, stress-induced increases in anxiety-like behavior in the EZM, supporting the notion that impaired 2-AG signaling contributes to stress-induced anxiety (**Figure 4c**). Lastly, the anxiolytic effect of JZL184 was dependent on CB1 receptor
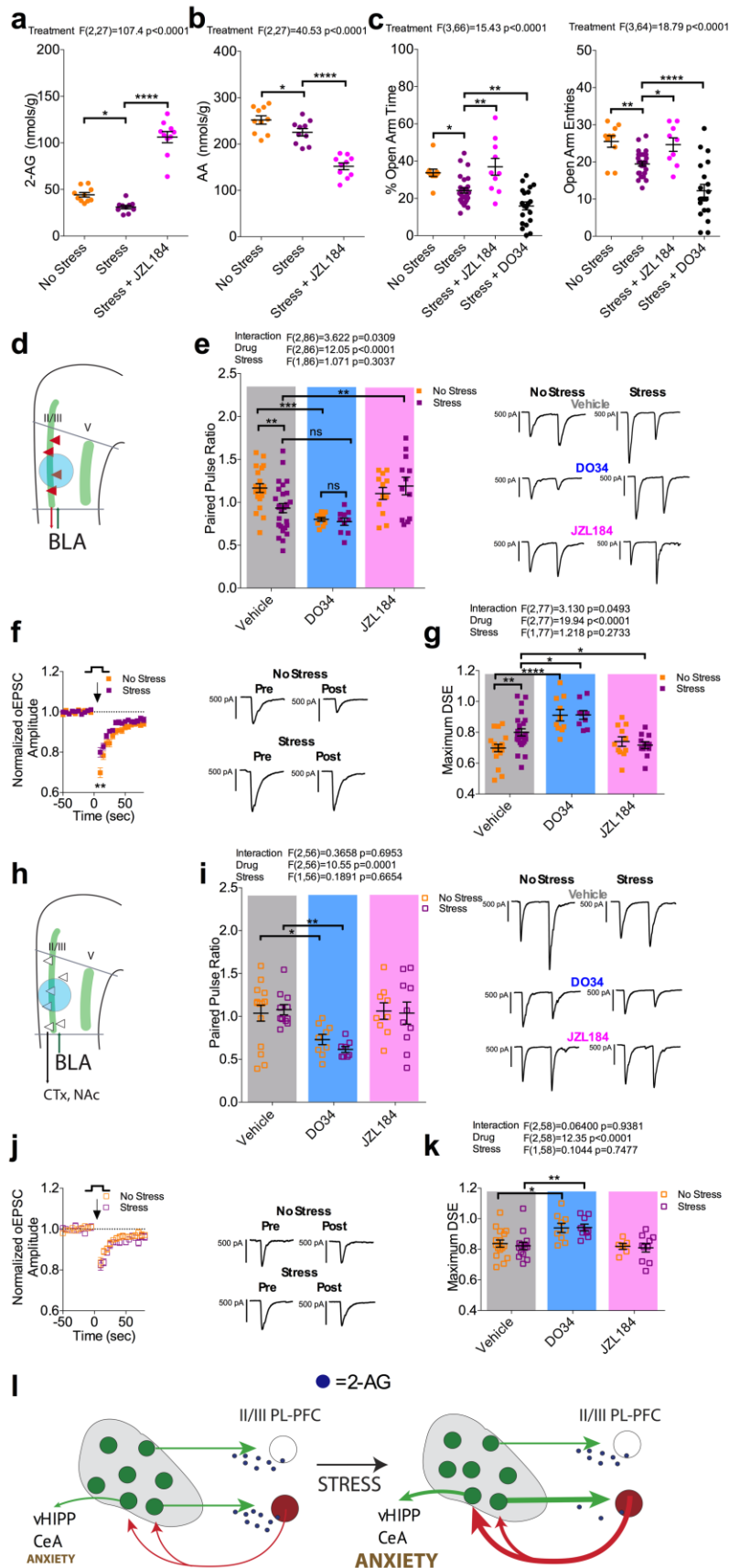
Figure 4: Stress impairs 2-AG signaling within the BLA L2/3-plPFC reciprocal circuit

(a) Effect of stress and JZL184 on mPFC 2-AG levels. Stress exposure decreased mPFC 2-AG levels (No Stress: N=10, Stress: N=10; p=0.0233). Treatment with 15 mg/kg JZL184 (N=10) increased mPFC 2-AG levels in stressed mice (p<0.0001).

(b) Effect of stress and JZL184 on mPFC AA levels. Stress exposure decreased mPFC levels of AA (No Stress: N=10, Stress: N=10, p=0.0290). Treatment with 15 mg/kg JZL-184 (N=10) reduced mPFC AA levels in stressed mice (p<0.0001).

(c) Effect of stress on anxiety like behavior in the EZM. Stress exposure decreased % time spent in the open-arms (p=0.0110) and open-arm entries (p=0.0099; No Stress: N=10, Stress: N=10). 15 mg/kg JZL184 (N=10) reversed the stress induced decrease in % open-arm time (p=0.0012) and open-arm entries (p=0.0278). 50 mg/kg DO34 exacerbated the stress induced decrease in % open-arm time (p=0.0077) and open-arm entries (p<0.0001).

(d) Schematic for voltage-clamp recordings of oEPSCs from L2/3 rAAV-positive neurons.

(e) Effect of stress, 2.5 μM DO34, and 1 μM JZL on PPR at L2/3 rAAV-positive synapses. Stress exposure decreased PPR (No Stress: n=21 N=8, Stress: n=27, N=11; p=0.0053). DO34

45

decreased PPR in non-stressed mice (n=10, N=4; p=0.0008) but not in stressed mice (n=10, N=4; p=0.0904). JZL184 reversed the stress induced decrease PPR (n=13, N=4; p=0.0075) but did not affect PPR in non-stressed mice (n=12, N=4; p=0.4778).

(f) Effect of stress on DSE at BLA-L2/3 rAAV-positive synapses.

(g) Effect of stress, DO34, and JZL184 on maximum DSE at BLA-L2/3 rAAV-positive synapses. Stress exposure impaired DSE (No Stress: n=18, N=7, Stress: n=24, N=11; p=0.0072). DO34 blocked DSE in both non-stressed (n=10 N=4; p<0.0001) and stressed (n=9 N=4; p=0.0129) mice. JZL184 selectively reversed the stress-induced impairment of DSE (n=11 N=4; p=0.0312).

(h) Schematic for voltage-clamp recordings of oEPSCs from L2/3 rAAV-negative neurons.

(i) Effect of stress, DO34, and JZL184 on PPR at BLA-L2/3-rAAV-negative synapses. Stress exposure did not alter PPR (No Stress: n=15 N=8, Stress: n=11 N=7; p=0.9249). DO34 significantly decreased PPR in both non-stressed (n=9 N=4; p=0.0451) and stressed (n=8, N=4; p=0.0035) mice.

(j) Effect of stress on DSE at BLA-L2/3 rAAV-negative synapses.

(k) Effect of stress, DO34, and JZL184 on maximum DSE at BLA-L2/3 rAAV-negative synapses. Stress exposure did not alter DSE (No Stress: n=16 N=8, Stress: n=14 N=7; p=0.9476). DO34 blocked DSE in both non-stressed (n=9 N=4; p=0.0155) and stressed (n=9 N=4; p=0.0035) mice.

(l) Stress impairs 2-AG regulation of the BLA-L2/3 plPFC-BLA synapses, leading to strengthening of BLA-L2/3 reciprocal circuits involved in generating anxiety-like responses via activation of BLA output neurons to the ventral hippocampus for example.

All error bars represent ± SEM. "n" represents number of neurons, "N" represents number of mice. All post-hoc p values derived from one-way ANOVA (a,b,c) or two-way ANOVA (e,g,i,k) with Holm-Sidak multiple comparisons. F and P values for ANOVA shown in relevant panels.

availability, as no anxiolytic effect was observed when JZL184 was co-administered with the CB1 inverse agonist rimonabant after stress exposure (**Figure S5c**).

We next tested the hypothesis that stress-induced strengthening of the BLA-plPFC reciprocal circuit was mediated by acute collapse of 2-AG-mediated inhibition of BLA-plPFC glutamatergic transmission. Using the aforementioned approach to physiologically interrogate the BLA-plPFC reciprocal circuit, we found once again that stress increased presynaptic release probability selectively onto L2/3 rAAV-positive neurons, as indicated by a decrease in the PPR 24 hours after stress exposure (**Figure 4d-e**). Interestingly, while bath application of DO34 reduced PPR in non-stressed mice, this effect was occluded in stressed animals. Furthermore,

DO34 application occluded further stress-induced reduction in PPR. Conversely, pharmacological augmentation of 2-AG signaling via bath application of JZL184 was able to selectively rescue this stress-induced decrease in PPR at BLA-L2/3 rAAV-positive synapses (**Figure 4e**), and this effect was blocked by co-application of the CB1 receptor inverse agonist, rimonabant, indicating a CB1 receptor-dependent effect of JZL184 (**Figure S5a**). Lastly, a similar pattern was observed with regard to phasic 2-AG signaling, as stress reduced DSE magnitude in L2/3 rAAV-positive neurons, an effect rescued by incubation with JZL184 (**Figure 4f-g**), and which was dependent upon stressor intensity and recovered by three days after stress exposure (**Figure S3m,p**). As observed with the PPR, the effect of JZL184 on DSE could be blocked by rimonabant pre-application (**Figure S5b**). No stress-induced changes were observed in L2/3 rAAV-negative neurons (**Figure 4h-k**) or L5 neurons (**data not shown**). These data suggest stress-induced collapse of phasic and tonic 2-AG signaling at BLA-plPFC synapses could contribute to stress-induced BLA-plPFC circuit strengthening and subsequent expression of anxiety-like behaviors via activation of BLA output to anxiety-generating structures such as the ventral hippocampus (**Figure 4l**). Interestingly, female mice did not show a stress-induced reduction in DSE magnitude, indicating that stress effects of modulating tonic vs. phasic 2-AG signaling could differ between sexes (**Figure S3d**). However, DSE was impaired by predator odor exposure, indicating that 2-AG signaling collapse is not stressor modality-specific (**Figure S3g**).

To further demonstrate functional collapse of 2-AG-CB1 regulation of excitatory input from the BLA, we performed an experiment to determine whether stress occludes the ability of the neutral CB1 antagonist NESS or CB1 inverse agonist rimonabant to enhance presynaptic release and occlude stress-induced PPR reductions. As noted above, we found that in the non-

stressed group, both NESS and rimonabant increased oEPSC amplitude and decreased the PPR, suggesting that blockade of CB1 enhances presynaptic glutamate release from the BLA, presumably via inhibition of tonic 2-AG-mediated suppression of BLA-plPFC glutamate release (see **Figure S5l,m,p,q**). However, following stress, neither compound was able in increase oEPSC amplitude, demonstrating an occlusion of their pharmacological effects by stress, likely due to a stress induced reduction in tonic 2-AG-CB1 signaling (**Figure S5n,r**). Stress exposure also completely occluded the ability of NESS to reduce the PPR, but only elicited a partial occlusion with rimonabant, which was still able to slightly reduce the PPR following stress (**Figure S5o,s**). This effect is most likely due to either a more potent blockade of CB1 by rimonabant, or its inverse agonist properties. However, the complete occlusion observed with the neutral CB1 antagonist NESS demonstrates tonic constraint of glutamatergic input from the BLA via 2-AG-CB1 signaling, and that stress-induced presynaptic strengthening at BLA-L2/3 plPFC-BLA synapses is due to impaired 2-AG-CB1 regulation of glutamatergic input from the BLA.

Lastly, our mass spectrometry data indicated that AEA levels are similarly decreased in the mPFC following stress exposure (**Figure S5d**). This hints at the possibility that stress could also impair AEA regulation of the BLA-plPFC circuit. However, incubation with an inhibitor of AEA degradation, PF3845, affected neither basal PPR nor rescued the stress induced decrease in PPR or DSE magnitude, suggesting that AEA does not strongly regulate BLA-plPFC glutamatergic transmission (**Figure S5e-g**). Furthermore, stress exposure did not affect CB1 agonist-induced synaptic depression at BLA-L2/3 plPFC synapses, suggesting stress impairs 2-AG production rather than affecting CB1 receptor sensitivity (**Figure S5h,i**).

Prelimbic DAGLα deletion increases BLA-plPFC strength and anxiety-like behavior

Our data thus far suggest that 2-AG plays a crucial role in limiting excitatory input from the BLA to the plPFC and that stress exposure compromises the efficacy of this signaling in a circuit-specific manner, contributing to synaptic strengthening after stress. These data suggest 2-AG signaling deficiency within the plPFC could contribute to stress-induced anxiety behaviors via enabling enhanced BLA-plPFC glutamatergic coupling after stress. To address this hypothesis experimentally, we took advantage of a line of mice in which exon nine of the gene for DAGLα is flanked by loxP sites (Bluett et al., 2017). Specifically, if stress impairs 2-AG signaling at BLA-plPFC synapses to facilitate circuit strengthening and anxiety generation, then selective deletion of DAGLα from the plPFC should recapitulate stress-induced circuit strengthening and increase anxiety-like behavioral responses. We first demonstrated that stereotaxic injection of AAV-Cre into the plPFC of DAGLα$^{f/f}$ mice resulted in selective reduction in DAGLα protein in the plPFC but not the adjacent infralimbic PFC (ilPFC) (**Figure 5a**). Using the plPFC-specific knockout combined with the aforementioned injections of ChR2 and rAAV2-tdTomato into the BLA, we found significantly impaired DSE and a robust decrease in PPR at BLA-plPFC glutamatergic synapses, recapitulating the synaptic phenotype observed after stress exposure (**Figure 5b-d**). Consistent with this stress-like synaptic phenotype, plPFC-specific DAGLα deletion elicited an anxiety-like behavioral phenotype that was similar to the anxiogenic effects observed after stress exposure **(Figure 5e)**. This behavioral profile persisted following exposure to stress examined in a separate cohort of mice, suggesting a crucial role for plPFC 2-AG signaling in regulating anxiety-like behavior **(Figure 5f)**. These data suggest that impaired plPFC 2-AG signaling results in a stress-like synaptic phenotype at BLA-plPFC glutamatergic synapses and is sufficient to induce anxiety-like behavior, recapitulating the
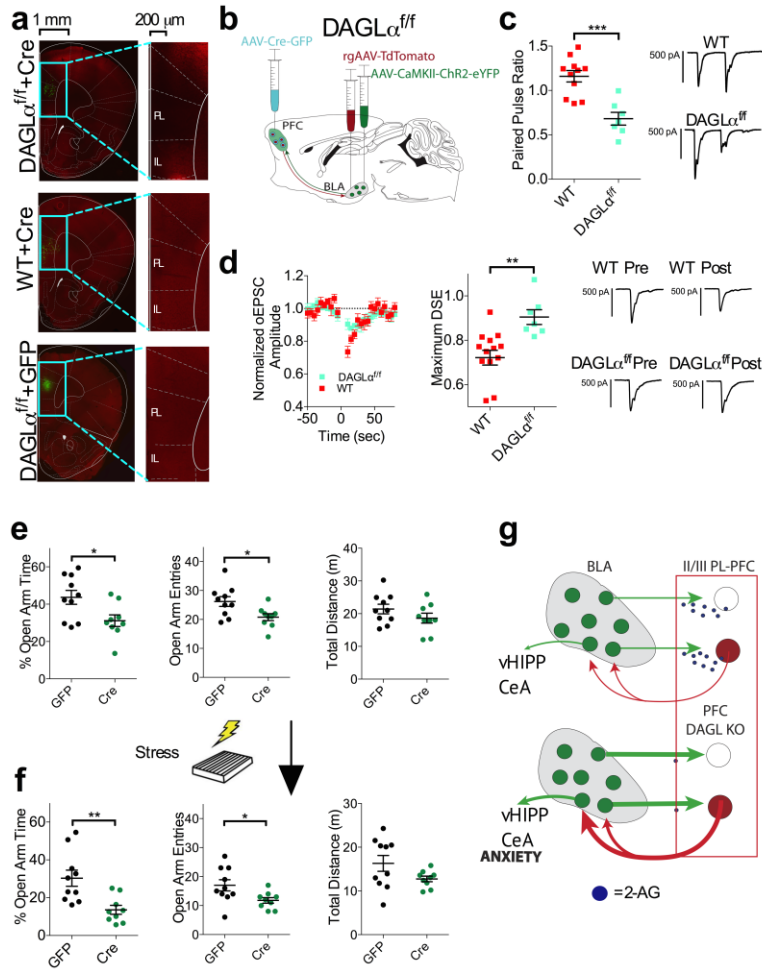
Figure 5: plPFC-specific DAGLα deletion phenocopies synaptic and behavioral effects of stress

(a) Immunohistochemical validation of plPFC conditional knockout of DAGLα. AAV-Cre injection into the plPFC (top and middle panel; green) resulted in decreased DAGLα expression (red) in the plPFC of DAGLα[f/f] mice but not WT mice. AAV-GFP injection into the plPFC of DAGLα[f/f] mice (bottom panel; green) did not affect DAGLα expression.

(b) Schematic approach for electrophysiological examination of BLA-plPFC circuit after plPFC-specific DAGLα deletion.

(c) Effect of plPFC DAGLα deletion on PPR. Deletion of DAGLα from the plPFC reduced PPR at BLA-L2/3 plPFC rAAV-positive synapses (WT: n=11 N=5, DAGLα[f/f]: n=7 N=3; p=0.0002).

(d) Effect of plPFC DAGLα deletion on DSE. Deletion of DAGLα from the plPFC impaired DSE at BLA- L2/3 plPFC rAAV-positive synapses (WT: n=14 N=6, DAGLα[f/f]: n=7, N=3; p=0.0026). Effect of plPFC DAGLα deletion on anxiety-like behavior in the EZM assay. Mice with plPFC DAGLα deletion (n=9) show decreased % open-arm time (p=0.0213), decreased open-arm entries (p=0.0197), and similar distance traveled (p=0.2006) compared to GFP injected controls (N=10).

(e) Effect of plPFC DAGLα deletion on anxiety-like behavior in the EZM assay 24 hours following stress exposure. Mice with plPFC DAGLα deletion (N=9) show decreased % open-arm time (p=0.0039), decreased open-arm entries (p=0.0322), and similar distance traveled (p=0.0941) compared to GFP injected control (N=10) following stress exposure.

(f) Deletion of DAGLα from plPFC neurons induces a stress-like synaptic phenotype and results in increased anxiety-like behavior.

All error bars represent ± SEM. "n" represents number of neurons, "N" represents number of mice. P values reported from two-tailed unpaired t-test (c,d,e,f).

effects of stress exposure (**Figure 5g**). Taken together our data support the hypothesis that stress-induced impairment in 2-AG signaling at BLA-plPFC synapses could represent an important mechanism translating the effects of stress into anxiety-like behavior.

BLA-plPFC circuit-specific CB1 deletion regulates stress-induced anxiety

Our previous data demonstrating BLA-plPFC 2-AG signaling collapse after stress, combined with our plPFC-specific DAGLα deletion experiments strongly suggests a role for BLA-plPFC 2-AG signaling impairment in the translation of environmental stress into anxiety-like behavioral responses. However, plPFC-specific DAGLα deletion could exert behavioral effects via impairment in 2-AG signaling at other limbic glutamatergic inputs or local GABAergic terminals. To further solidify the role of 2-AG-CB1 signaling specifically at BLA-plPFC synapses in the regulation of stress-induced anxiety, we utilized an INTRSECT approach to selectively delete the CB1 receptor from BLA neurons projecting to the plPFC (Fenno et al., 2017). Using a mouse in which the single coding exon for the CB1 receptor is flanked by loxP sites (**Figure S6a-e**), we injected a retrograde virus that drives the expression of Flp recombinase and td-Tomato into the plPFC and a virus that drives expression of Cre recombinase in a Flp-dependent manner into the BLA. Injection of both of these viruses into CB1$^{f/f}$ mice would be predicted to delete the CB1 receptor specifically from plPFC-projecting BLA neurons (**Figure 6a,e**). If 2-AG signaling collapse at BLA-plPFC synapses contributes to circuit-specific strengthening and stress-induced anxiety, then selective deletion of CB1 from BLA terminals innervating the plPFC should recapitulate the synaptic phenotype induced by stress and affect anxiety-like behaviors. To explicitly test these hypotheses in turn, we first combined this intersectional viral approach with a Cre-dependent ChR2 injected into the BLA and recorded
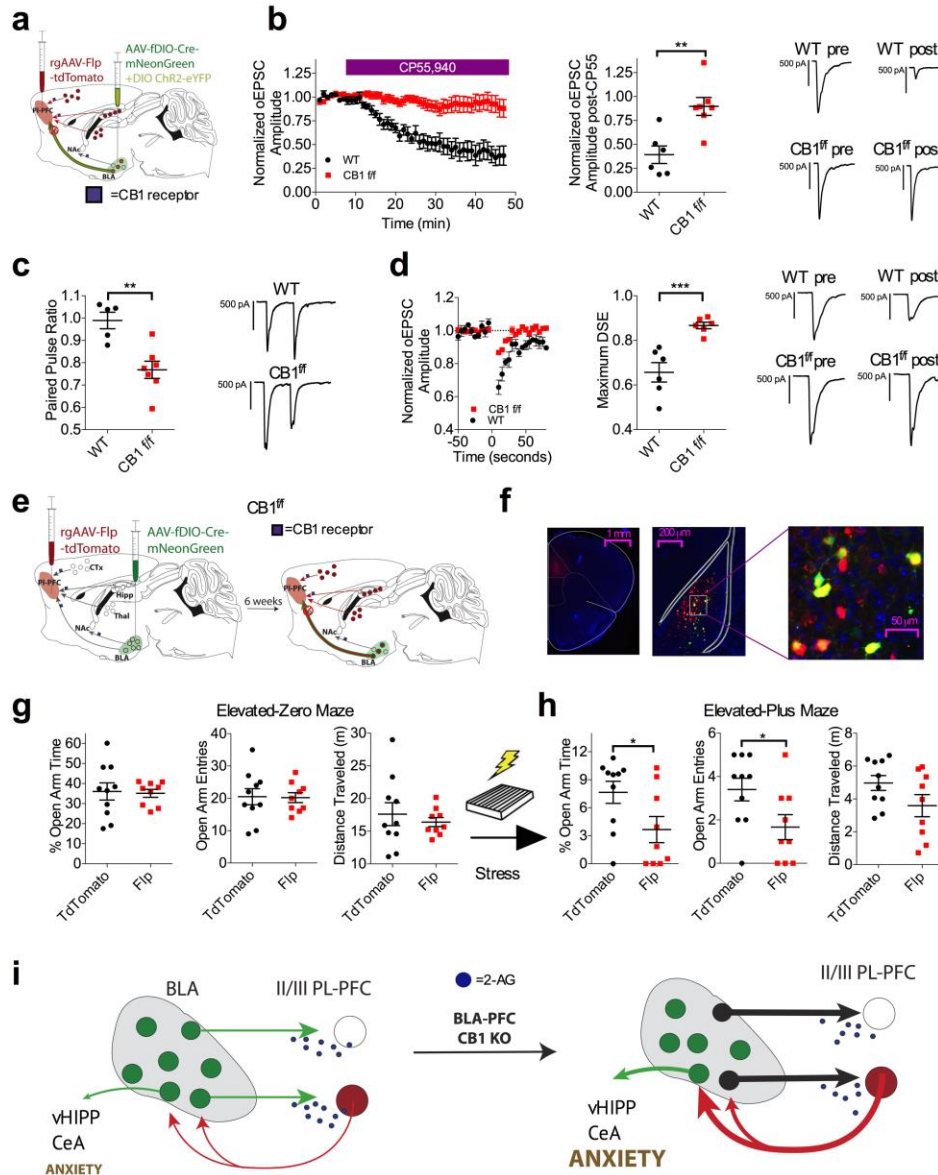
Figure 6: BLA-plPFC-specific CB1 deletion phenocopies stress-induced synaptic strengthening and exacerbates stress-induced anxiety

    (a) Schematic for physiological validation of the INTRSECT approach for deletion of the CB1 receptor from plPFC projecting BLA neurons.

    (b) Effect of 5 μM CP55,940 on oEPSC amplitude at BLA-L2/3 plPFC synapses. CP55,940-induced depression of oEPSC amplitude is dramatically attenuated in CB1$^{f/f}$ INTRSECT mice (n=7, N=3) compared to WT control INRSECT mice (n=6, N=2; p=0.0028)

    (c) Effect of BLA-plPFC CB1 deletion on PPR at BLA-L2/3 plPFC synapses. PPR in CB1$^{f/f}$ INTRSECT mice (n=7 N=3) is decreased compared to WT INTRSECT mice (n=5 N=2; p=0.0026).

    (d) Effect of BLA-plPFC CB1 deletion of DSE at BLA-L2/3 plPFC synapses. DSE at BLA-plPFC synapses in CB1$^{f/f}$ INTRSECT mice (n=6 N=3) is significantly impaired compared to WT INTRSECT mice (n=6 N=2; p=0.0010).

(e) Schematic of INTRSECT approach for deletion of the CB1 receptor from plPFC projecting BLA neurons for behavioral characterization.

(f) Representative images showing injection site of rAAV2-EF1-Flp-tdTomato into the plPFC and AAV5-fDIO-Cre-mNeonGreen into the BLA, showing co-expression of rAAV-positive neurons (red) and Cre-positive neurons (green) in the BLA.

(g) Effect of BLA-plPFC CB1 deletion on anxiety-like behavior in the EZM assay. No significant changes in basal anxiety-like behavior were observed in rAAV2-EF1-Flp-tdTomato (FLP) injected CB1$^{f/f}$ mice compared to CB1$^{f/f}$ mice injected with a control retrograde virus, rAAV-CAG-tdTomato.

(h) Effect of BLA-plPFC CB1 deletion on anxiety-like behavior in the EPM assay following stress exposure. Flp injected CB1$^{f/f}$ mice (N=9) show significantly decreased % open-arm time (p=0.0421) and decreased open-arm entries (p=0.0391), without changes in total distance travelled compared to control virus-injected littermates (N=10).

(i) Deletion of CB1 from BLA projections to the plPFC induces a stress-like synaptic phenotype and exacerbates the anxiogenic effects of stress exposure.

All error bars represent ± SEM. "n" represents number of neurons, "N" represents number of mice. P values reported from two-tailed unpaired t-test (b,c,d,g,h).

oEPSCs in the plPFC six to eight weeks following viral injection. We showed that this approach leads to almost complete functional removal of CB1 from BLA neurons projecting to the plPFC, as oEPSCs are completely insensitive to the CB1 agonist CP55,940 compared to wild-type mice injected with the same viral combinations (**Figure 6b**). The circuit-selectivity of this manipulation was verified in a separate cohort of CB1$^{f/f}$ mice where we used the same intersectional CB1 deletion and a non-Cre-dependent ChR2 injected into the BLA to allow for ChR2 expression within all BLA neurons regardless of projection target. Using this approach, we found CB1 expression completely intact at BLA-nucleus accumbens inputs as CP55,940-induced synaptic depression was identical to WT mice (**Figure S6f-h**), confirming achievement of circuit-specific CB1 deletion using this intersectional viral strategy.

Using this validated intersectional approach, similar to plPFC DAGLα deletion, we found that BLA-plPFC-specific CB1 deletion resulted in a synaptic phenotype comparable to that observed after stress exposure. Specifically, DSE is substantially attenuated and the PPR is

significantly reduced in the CB1[f/f] mice relative to WT control mice (**Figure 6c-d**). Taken together, our data indicate that selective genetic elimination of 2-AG-CB1 signaling within the BLA-plPFC circuit, either via plPFC-specific deletion of DAGLα or via selective deletion of CB1 from BLA-plPFC inputs, recapitulates synaptic strengthening observed after acute stress exposure. To next determine the behavioral consequences of BLA-plPFC specific CB1 deletion we examined anxiety-like behavior at baseline and after stress exposure (**Figure 6e-f**). Prior to stress exposure, BLA-plPFC-specific CB1-deletion did affect anxiety-like behavior in the EZM assay compared to control virus (plPFC rAAV-td-Tomato combined with fDIO-Cre-mNeonGreen in the BLA) injected CB1[f/f] littermates (**Figure 6g**). However, deletion of CB1 from the BLA-plPFC pathway dramatically enhanced anxiety-like behavior 24 hours after foot-shock stress exposure in the EPM in the same cohort of mice (**Figure 6h**). Together, these data indicate that selective deletion of CB1 from BLA-plPFC projections induces a stress-like synaptic profile similar to that observed after plPFC-specific DAGLα supporting our global hypothesis that stress-induced strengthening of BLA-plPFC circuits is mediated in part by circuit-specific impairment in 2-AG-CB1 signaling (**Figure 6i**). That BLA-plPFC specific CB1 deletion did not affect basal anxiety suggests that either compensatory mechanisms or 2-AG signaling at other glutamatergic or GABAergic synapses, are able to maintain allostasis under non-stressed conditions. However, after stress exposure, the importance of CB1 signaling in this circuit is unmasked, possibly due to failure of such compensatory mechanisms or due to enhanced recruitment of activity within activity within the BLA-plPFC circuit.

Discussion

Elucidating the molecular, synaptic, and circuit-level mechanisms by which the brain reacts and adapts to stress could reveal pathophysiological mechanisms of, and reveal novel treatment approaches for, affective and stress-related psychiatric disorders. Here we demonstrate circuit-specific 2-AG signaling collapse at BLA-plPFC synapses links environmental stress exposure to anxiety-like behavior. Specifically, we found that stress caused a selective strengthening of glutamatergic transmission within a reciprocal BLA-plPFC-BLA circuit, which was driven by collapse of multimodal retrograde 2-AG-mediated eCB signaling. Importantly, experimentally-induced circuit-specific impairment in BLA-plPFC 2-AG signaling phenocopied both stress-induced circuit strengthening and anxiety-like behavior. These studies support the critical role of the BLA-plPFC circuit in the generation of anxiety-like states and reveal new synaptic and molecular mechanisms subserving stress-induced circuit strengthening and behavioral adaptation.

The amygdala and the dmPFC are crucial components of the negative valence system in humans and their functional connectivity is integral to threat reactivity (Carlisi and Robinson, 2018; Kalisch and Gerlicher, 2014; Robinson et al., 2014). Using fiber-photometry and miniendoscopy, we found that the homologous circuit in rodents is potently engaged by unpredictable foot-shock exposure and this stressor induces a relatively persistent (~24-72h) and selective increase in presynaptic excitatory strength from the BLA specifically onto plPFC L2/3 neurons that send reciprocal projections back to the BLA. These data are consistent with the notion that the BLA and plPFC comprise an "aversive amplification circuit" associated with elevated threat processing during stress (Robinson 2014), and previous data indicating that BLA-plPFC circuit activation is capable of generating anxiety-like behavioral responses in mice

(Felix-Ortiz et al., 2015; Lowery-Gionta et al., 2018). Although previous studies have investigated the functional role of BLA input to the plPFC in the context of anxiety-like behaviors, few studies have examined its role in stress adaptation and obtained both input and output selectivity in this neural circuit, as detailed here. Specifically, we demonstrate that the stress-induced physiological alterations occur in both an input and output selective manner; no changes were observed in thalamocortical glutamatergic transmission, and BLA input was specifically strengthened only onto reciprocally projecting neurons. Importantly, BLA-projecting plPFC neurons, in addition to synapsing onto reciprocally projecting BLA-plPFC neurons, also strongly synapse onto open-loop BLA projection neurons innervating the hippocampus and CeA (McGarry and Carter, 2017), providing a potential mechanism where by the BLA-plPFC-BLA reciprocal circuit gains access to limbic output structures to generate behavioral responses to stress. Supporting this hypothesis, optogenetic activation of BLA-ventral hippocampal projections increases anxiety and induces social avoidance in mice (Felix-Ortiz et al., 2013). Taken together, these data suggest that aberrant activity and/or plasticity in this circuit could contribute to the pathogenesis of stress-related and affective disorders and that increased BLA-dmPFC connectivity/signaling represents a conserved translationally relevant mechanism linking environmental stress to its behavioral, emotional, and cognitive consequences.

Although there is a prominent role of prefrontocortical eCB signaling in regulating presynaptic glutamate release and anxiety-like behaviors (Lafourcade et al., 2007; Lisboa et al., 2014; Lutz et al., 2015; Manduca et al., 2017; Puente et al., 2011; Rubino et al., 2008b), whether this modulation is ubiquitous or circuit-specific is not known. Our data indicate that CB1 receptors and retrograde 2-AG signaling are present at BLA-plPFC but not MDT-plPFC synapses, suggesting that 2-AG regulates plPFC glutamatergic transmission in a circuit-specific

manner. Interestingly, our data indicate that 2-AG modulates BLA-plPFC glutamatergic transmission in both phasic and tonic modes. Specifically, although prototypical phasic 2-AG signaling in the form of DSE is present at BLA-plPFC synapses and blocked by inhibitors of CB1 receptors and DAGL, both inhibitors also decrease the PPR and increase the frequency of BLA-elicited asynchronous EPSCs, revealing tonic inhibition of BLA-plPFC glutamatergic transmission by 2-AG-CB1 signaling. Here, an important distinction arises related to tonic 2-AG (or tonic eCB signaling) vs. tonic CB1 signaling. Indeed it is well-known that the CB1 receptor exhibits constitutive activity (Coutts and Pertwee, 1997; Lange and Kruse, 2004; Sim-Selley et al., 2001), and some recent studies have identified constitutive CB1 activity as a mechanism limiting GABA release at central synapses (Lee et al., 2015). However, much of the early work examining putative tonic eCB signaling utilized compounds known to be inverse agonists at the CB1 receptor, such as rimonabant or AM251 (Hentges et al., 2005; Pan et al., 1998), thus clouding the interpretation of whether the observed effects were due to orthosteric CB1 blockade of eCB signaling, or inverse agonism of CB1. However, the advent of inhibitors of eCB breakdown allowed for more rigorous investigation of the tonic action of both AEA and 2-AG (Ahn et al., 2009; Long et al., 2009), with much of the early work suggesting that AEA was the primary eCB responsible for setting the eCB tone, while implicating 2-AG in point-to-point or phasic eCB signaling (Hashimotodani et al., 2008; Kim and Alger, 2010). However, more recent studies have suggested that 2-AG could also play a pivotal role as a mediator of the eCB tone (Anderson et al., 2015; Haj-Dahmane et al., 2018; Lee et al., 2015; Ramikie et al., 2014). A caveat to these studies is that they either exogenously boost 2-AG levels to supra-physiological levels (e.g. with JZL184) leading to 2-AG spillover, or they utilize the non-selective lipase (tetrahydrolipstatin) or PLC (U73122) inhibitors to demonstrate tonic 2-AG signaling. Thus, by

using a neutral CB1 antagonist (NESS), BLA-plPFC-specific CB1 deletion, and both a selective DAGL inhibitor and a conditional DAGLα knockout, our data strongly indicate that 2-AG exerts both tonic and phasic circuit-specific presynaptic inhibition of BLA-plPFC glutamatergic transmission.

Given that that BLA projections to the plPFC are multimodally inhibited by 2-AG signaling and that some forms of stress impair eCB signaling (Bluett et al., 2017; Hill et al., 2009; McLaughlin et al., 2012; Patel et al., 2004; Rademacher et al., 2008; Wamsteeker et al., 2010), we next determined whether 2-AG signaling collapse could drive the stress-induced strengthening of BLA-plPFC glutamatergic synapses. In support of this hypothesis, we found impairment in both tonic and phasic 2-AG modulation of BLA to L2/3 plPFC reciprocally-projecting neuron synapses. This impairment was occluded by DAGL and CB1 inhibition and could be reversed by pharmacological inhibition of MAGL, which increases 2-AG levels, but not by inhibition of FAAH, which selectively increases AEA levels. Paralleling these data, systemic MAGL inhibition reduced, while DAGL inhibition increased, stress-induced anxiety-like behaviors. Given these findings, in tandem with our data demonstrating that activation of the BLA-plPFC circuit is sufficient to induce anxiety-like behavior, we suggest 2-AG-CB1 signaling collapse within the BLA-plPFC-BLA reciprocal circuit could represent a mechanistic link between stress exposure, BLA-plPFC synaptic strengthening, and stress-induced anxiety-like behaviors.

Previous studies have shown that prolonged stress exposure can compromise eCB signaling via reductions in CB1 receptor signaling and/or expression (Hill et al., 2005; Hillard, 2014; Patel et al., 2009; Wamsteeker et al., 2010). However, our acute stress manipulations did not affect CB1 receptor function at BLA-plPFC synapses. Therefore, the most likely mechanisms

subserving 2-AG signaling collapse after acute stress is a reduction in 2-AG signaling availability, which could occur via reduced 2-AG synthesis or enhanced degradation. Our data support an impairment in 2-AG synthesis over changes in degradation, as both 2-AG and free AA levels were reduced and only the maximal magnitude (but not recovery) of DSE was reduced in the PFC ~24h after stress exposure. If increased 2-AG degradation were the primary driver of reduced 2-AG signaling, one would expect elevated levels of AA and a faster DSE decay (Pan et al., 2009; Zhong et al., 2014), neither of which were observed. However, additional mechanisms such as impaired 2-AG transport, or combinatorial effects of multiple mechanisms, cannot currently be excluded. It is also unclear from the present results what the initiating factors for 2-AG signaling collapse are. Although we hypothesize that the increase in excitatory input from the BLA, and potentially other brain regions, during the stressor serves as the trigger that leads to a persistent reduction in 2-AG signaling capacity in reciprocally projecting L2/3 plPFC neurons, this remains to be tested experimentally and the subsequent molecular cascades resulting in impaired 2-AG signaling remain to be established. In addition, our single-cell calcium imaging and cFOS data suggest broad plPFC neuronal activation after stress exposure, suggesting there must exist mechanisms to guide the postsynaptic specificity of stress-induced 2-AG signaling impairment to BLA-plPFC-BLA reciprocal circuit, which likewise remain to be elucidated.

The BLA is highly heterogeneous and its distinct roles in the processing of positive and negative valence have been dissected and defined by projection target, gene expression, and electrophysiological characteristics (Beyeler et al., 2018; Kim et al., 2016; Kyriazi et al., 2018; Namburi et al., 2016). Interestingly, putative 'negative valence' and 'positive valence' BLA neurons, as defined by genetic markers, show distinct projections to the mPFC (Kim et al., 2016). Specifically, 'negative valence' BLA neurons project most strongly to superficial cortical

layers of the plPFC, while 'positive valence' BLA neurons project most strongly to deeper cortical layers of the ilPFC and to a lesser degree the plPFC. These data suggest the BLA-L2/3 plPFC-BLA reciprocal circuit is a critical component of a negative valence system and that reciprocal activity in this circuit is involved in driving anxious states. Our data indicating that stress selectively increases coupling between the BLA and reciprocally projecting superficial layer plPFC neurons further supports this notion and suggests eCB signaling collapse could contribute to stress-induced negative valence sub-circuit-specific strengthening and behavioral adaptations to stress exposure.

To investigate whether BLA-plPFC 2-AG signaling collapse is causally related to circuit strengthening and behavioral adaptations to stress, we used two different genetic strategies to impair BLA-plPFC 2-AG-mediated eCB signaling. We hypothesized that, because stress exposure reduces mPFC 2-AG levels and leads to anxiety-like behavior, then direct depletion of plPFC 2-AG, via plPFC-specific DAGLα deletion, would recapitulate stress-induced BLA-plPFC circuit strengthening and increase anxiety-like behavior. Consistent with this hypothesis, we found that plPFC DAGLα deletion increased release probability at BLA-plPFC synapses, impaired DSE, and elicited a corresponding increase in anxiety-like behavior, mimicking the effects of stress at the synaptic and behavioral level. Interestingly, a different behavioral pattern was observed following deletion of the CB1 receptor selectively from BLA neurons projecting to the plPFC. Although this circuit-specific manipulation again phenocopied stress-induced synaptic strengthening, the deletion had a minimal effect on basal anxiety, but increased anxiety-like behavior following stress exposure. A possible explanation for lack of robust behavioral effects of BLA-plPFC CB1 deletion under basal conditions is that 2-AG-CB1 signaling plays a minimal role in regulating the activity of the quiescent circuit. However, following stress-

60

induced activation of the BLA-plPFC circuit, attenuation of 2-AG-CB1 negative feedback signaling impairs the ability of L2/3 plPFC neurons to reduce excitatory input from the BLA, leading to an exacerbation of stress-induced anxiety-like behaviors. The differential effects of plPFC DAGLα deletion and BLA-plPFC-specific CB1 deletion in terms of effect on basal anxiety could also be explained by the fact that plPFC DAGLα deletion impairs 2-AG signaling at all synapses (including other limbic inputs not examined here) resulting in a more robust behavioral phenotype. Future studies should be aimed at elucidating the role of additional afferent and local eCB-sensitive circuits in the regulation of stress adaptation and anxiety-like behavior. Taken together, these data suggest that 2-AG-CB1 signaling plays a crucial role in gating stress-induced activation of the BLA-plPFC circuit and that functional collapse of 2-AG signaling at BLA-plPFC synapses may be important for translation of stress exposure into anxiety-like behavior.

Here we explored the neurobiological substrate by which stress exposure is translated into anxiety-like behavior and identified collapse of 2-AG-CB1 signaling within a reciprocally connected BLA-plPFC-BLA circuit as a molecular mechanism subserving stress-induced circuit strengthening and generation of anxiety-like behavior. These data suggest that the enhancing 2-AG-CB1 signaling, via MAGL inhibition for example, could represent an attractive therapeutic target for the treatment of stress-induced psychiatric disorders (Chanda et al., 2019; Lisboa et al., 2017; Patel et al., 2017). Furthermore, our data suggest that functional connectivity in the BLA-dmPFC circuit could represent a useful intermediate circuit-based biomarker bridging preclinical studies to MAGL inhibitor efficacy trials and could facilitate optimal patient selection for future clinical studies.

Author Contributions

DM conducted electrophysiological studies and contributed to experimental design, data analysis, and interpretation of results; DM, AG and GB conducted behavioral and biochemical studies in laboratory of SP. JR conducted photometry experiments in laboratory of FSL. ED generated CB1 floxed mice. VK, MA, and NW assisted with electrophysiological studies. LRV conducted the miniendoscopic recordings. KM supplied the DAGLα antibody. SP and DM are responsible for study conception, experimental design, and data interpretation. DM and SP wrote the manuscript with input from all authors.

Declaration of Interests

SP has received research support from H. Lundbeck A/S within the past 3 years and has received consultation fees from Psy Therapeutics, Sophren Therapeutics, and Atlas Ventures in the past 3 years.

Methods

Mouse Studies

Animals. All experiments were approved by the Vanderbilt University Institutional Animal Care and Use Committees and were conducted in accordance with the National Institute of Health guidelines for the Care and Use of Laboratory Animals. 8-14 week-old male and female C57BL/6J mice obtained from Jackson Labs were used for electrophysiological and behavioral experiments. 8-14 week-old DAGLα$^{f/f}$ and WT controls were used for electrophysiological and behavioral experiments in figure 5. 10-18-week old CB1$^{f/f}$ and WT controls were used for electrophysiological and behavioral experiments in figure 6. Mice were housed in a temperature and humidity-controlled housing facility under a 12h light/dark cycle with *ad libitum* access to food. All behavioral and physiological experiments were run on littermate-matched stressed or non-stressed mice that had been singly housed ≥1 week. DAGLα$^{f/f}$ and CB1$^{f/f}$ mice bred in house on a homozygous x homozygous breeding scheme, and littermate-matched controls were used for all behavioral experiments.

Littermate-matched mice were randomly assigned to treatment (e.g. stress vs. no stress or virus vs. control virus) for all behavioral and electrophysiological experiments performed, excluding the physiological validation for the DAGLα$^{f/f}$ and CB1$^{f/f}$ knockouts. For behavioral cohorts, we used a homozygous/homozygous-breeding scheme, as preliminary reports from our lab and others that suggest that the CB1$^{f/f}$ mice have a basal phenotype in various behavioral assays that differentiates them from their wild-type littermates. Therefore, we used a homozygous/homozygous breeding scheme to generate only CB1$^{f/f}$ homozygotes, so that both the experimental and control groups had the same genetic background. However, this breeding scheme precluded our ability to perform physiological validation on littermate-matched controls,

due to the fact that Cre expression would always lead to CB1 deletion in addition to allowing for expression of DIO ChR2. Therefore, we used non-littermate matched WT controls for physiological validation to determine whether the CB1 receptor or DAGLα was functionally deleted in the experimental group.

Generation of CB1$^{f/f}$ mice. To produce a conditional knockout mouse of the cannabinoid receptor 1 (cnr1 gene), we created a targeting construct centered around exon 2, the single coding exon of the gene (**Figure S7**). A first loxP site was inserted 141 bp upstream of the exon, whereas a DNA fragment containing a neomycin-resistance gene cassette flanked by frt and loxP sites was inserted 622 bp downstream of exon 2. Relatively large arms of recombination: 6.5 kb (5' end) and 3.1 kb (3' end) were then added to the construct (**Figure S7**). The cnr1 construct was electroporated into 129/SvEvTac embryonic stem cells and 540 neomycin resistant clones were picked and analyzed by Southern blot analysis. Genomic DNA was digested with *Mfe*I, run on agarose gel, and transferred to nitrocellulose membranes to identify a 16 kb control fragment (wild-type allele) and a 7 kb mutant fragment (targeted allele) by Southern blot analysis. Out of the 540 clones, three clones were identified containing the mutant allele (**Figure S7**). Presence of the three loxP sites in ES cell clone 3H3 was verified by PCR and sequencing. The ES cell clone was injected into C57BL6 blastocysts which were implanted into pseudo-pregnant females to produce cnr1 chimeric mice. Three chimeras were produced from the 3H3 clone and one of these chimeras went germline and produced 9 pups, five of which carried the 3 loxP allele. After 2 backcrossing into C57BL6/J mice, the neomycin-resistance gene cassette was successfully removed by breeding a 3 loxP male mouse with two females carrying a FlpE allele (**Figure S7**). Functionality of the remaining 2 loxP sites was demonstrated by crossing a male carrying an

E2a-CRE allele with two females carrying a cnr1 2 loxP allele. Seven out of 16 pups carried the E2a-CRE allele and out of them, four pups demonstrated successful elimination of exon 2 (**Figure S7**). The cnr1 line was then backcrossed to C57BL/6J mice for an additional 5-6 generations prior to breeding to homozygosity.

Generation of DAGL$^{f/f}$ mice. See (Bluett et al., 2017).

Viruses. For chemogenetic manipulation of the BLA-plPFC circuit, we used rAAV2-Syn1-eBFP-Cre (200nL) in the plPFC and AAV5-hSyn-DIO-hM3d(Gq)-mCherry (500nL)(Addgene, Cambridge MA) in the BLA. For electrophysiological interrogation of the BLA-plPFC circuit, we used AAV5-CaMKII-ChR2(H134R)-eYFP (UPenn Vector Core, Philadelphia, PA) and rAAV2-CAG-tdTomato (Addgene). We combined these viruses in a 2:1 ratio and injected a total volume of 250nL into the BLA. For plPFC deletion of DAGLα, we used AAV5-CMV-Cre-eGFP (200nL)(Addgene). For deletion of the CB1 receptor from BLA cells projecting to the plPFC, we designed a custom Flp recombinase dependent Cre virus, AAV5-CMV-fDIO-Cre-P2A-mNeonGreen(500nL into bilateral BLA)(Catalogue# VB180530-1030aad, VectorBuilder, Shenandoah, TX) and used a commercially available retrograde Flp virus, rAAV2-EF1α-mCherry-IRES-Flp (200nL into bilateral plPFC). For electrophysiological validation of this approach, we injected a 600nL combination of custom fDIO-Cre virus with AAV5-EF1α-DIO-ChR2(H134R)-eYFP in a 3:1 ratio. Finally, for *in vivo* fiber photometry experiment, we used AAV1.Syn.GCaMP6s.WPRE.SV40 (Penn Vector Core) which was bilaterally injected into the BLA at a volume of 200nL.

Surgeries. Mice were initially anesthetized with 5% isoflurane and then transferred to the stereotax (Kopf Instruments, Tujunga, CA) and kept under 2% isoflurane anesthesia. The hair over the incision cite was trimmed and the skin was prepped with alcohol and iodine scrub. The skull was exposed via a midline sagittal incision and treated with the local anesthetic, benzocaine (Medline Industries, Brentwood, TN). For all surgeries, we used a motorized digital software (NeuroStar; Stoelting Co., Wood Dale, IL) to guide a 10μL microinjection syringe (Hamilton Co., Reno, NV) driven by a Micropump Controller (World Precision Instruments, Sarasota, FL). Virus was delivered bilaterally into the plPFC (AP:+2.42, ML:±0.35, DV: 2.09), BLA (AP: -1.25, ML: ±3.30, DV: 5.10), or MDT: (AP:-1.1, ML.: ±0.59, DV: 3.4). Following completion of each surgery, 10mg/kg ketoprofen (AlliVet, St. Hialeah, FL) was administered as an analgesic, and post-operative treatment with ketoprofen was administered 24 and 48 hours after the surgery.

Ex Vivo **Electrophysiology.** Coronal brain slices were prepared at 250μM on a vibrating Leica VT1000S microtome using standard procedures. Mice were anesthetized using isoflurane, and transcardially perfused with ice-cold and oxygenated cutting solution consisting of (in mM): 93 N-Methyl-D-glucamine (NMDG), 2.5 KCL, 20 HEPES, 10 MgSO4□7H20, 1.2 NaH2PO4, 0.5 CaCl2□2H20, 25 glucose, 3 Na+-pyruvate, 5 Na+-ascorbate, and 5 N-acetylcysteine. Following collection of coronal sections, the brain slices were transferred to a 34°C chamber containing oxygenated cutting solution for a 10-minute recovery period. Slices were then transferred to a holding chamber consisting of (in mM) 92 NaCl, 2.5 KCl, 20 HEPES, 2 MgSO4□7H20, 1.2 NaH2PO4, 30NaHCO3, 2 CaCl2□2H20, 25 glucose, 3 Na-pyruvate, 5 Na-ascorbate, 5 N-acetylcysteine and were allowed to recover for ≥30 min. For recording, slices were placed in a

perfusion chamber (Warner Instruments RC-27L) and perfused with oxygenated artificial cerebrospinal fluid (ACSF; 31-33°C) consisting of (in mM): 113 NaCl, 2.5 KCl, 1.2 MgSO4☐7H20, 2.5 CaCl2☐6H20, 1 NaH2PO4, 26 NaHCO3, 20 glucose, 3 Na+-pyruvate, 1 Na+-ascorbate, at a flow rate of 2-3ml/min. All drugs were stored in DMSO stocks and then included in ACSF containing 1:2000 (w/v) Bovine Serum Albumin (Fisher Scientific) and ≤1:2000 (v/v) DMSO.

Fluorescently labeled neurons in the mPFC were identified using a series 120Q X-cite lamp at 40X magnification with an immersion objective with differential interference contrast microscopy (DIC). The plPFC was visually distinguished from the ilPFC by packing density of L2/3 neurons and termination of BLA projections to L2/3. L2/3 plPFC neurons were differentiated from L5 neurons by packing density and a change in the laminar distribution of BLA projections, where a prominent gap in BLA projections is observed between L2/3 and deep layer 5. For investigation of thalamo-cortical circuitry (Figures S4 and S6), L6 was identified by expression of strong reciprocal thalamo-cortical projections (i.e. eYFP expressing axon terminals from the MDT and rAAV positive reciprocally projecting plPFC neurons). plPFC neurons were voltage clamped in whole-cell configuration using borosilicate glass pipettes (2-4 MΩ) filled with internal solution containing (in mM): 125 K+-gluconate, 4 NaCl, 10 HEPES, 4 MgATP, 0.3 Na-GTP, and 10 Na-phosphocreatine (pH 7.30-7.35). For all experiments other than those shown in Figure S2, neurons were clamped at -70mV and 50µM picrotoxin (Cayman Chemical, Ann Arbor, Michigan) was included in the patch pipette. Following break-in to the cell, we waited ≥3 minutes to allow for exchange of internal solution and stabilization of membrane properties. Neurons with an access resistance of >20MΩ or that exhibited greater than a 20% change in access resistance during the recording were not included in our data sets.

***Ex vivo* optogenetics.** For electrophysiological interrogation of the BLA-plPFC circuit, mice were bilaterally injected with 250 nL of AAV5-CaMKIIα-ChR2(H134R)-eYFP and rAAV2-CAG-tdTomato in a 2:1 ratio into the BLA or MDT. 3-5 weeks of viral expression was allowed prior to sacrificing the mice. ≥1 week prior to electrophysiological analysis, littermate-matched mice were singly housed. 24 hours before electrophysiological analysis, littermate-matched mice were randomly assigned to receive either 20 randomly interspersed 0.5 mA shocks over a 10-minute period or no shocks.

For optogenetic recordings of input/output curves, we used a Thorlabs LEDD1B T-Cube driver and obtained separate recordings of 470nm wavelength oEPSCs at 200, 400, 600, 800, 1000, and 1200 mA of LED intensity. The same stimulation paradigm was used for current clamp input/output curves. Current clamp recordings of somatic current injection induced AP firing were obtained by initially injecting enough current to hold the neuron at -70mV and then applying sequential depolarizing steps that increase by 20pA. PPR recordings of oEPSCs were obtained in voltage-clamp with an inter-stimulus interval of 50ms. PPR is reported as a ratio between the amplitude of the second oEPSC divided by the first. In **Figure 2**, PPR values are shown across the entire range of stimulus intensities. PPR effects are not dependent on the stimulus intensity; therefore, in subsequent figures, PPR values are shown at the maximum stimulus intensity. For optogenetically elicited AP firing, three 2ms light stimulations were given at each intensity, and the probability was calculated as the % of neurons firing APs (e.g. spiking on 2 of 3 stimulations =0.67). Recordings of DSE were obtained following at 10 second voltage step to +30mV. A baseline of 10 oEPSCs were taken prior to the depolarizing step, and all data is plotted as an oEPSC amplitude normalized to the baseline period. A light exposure

time of 2ms was used for all optogenetic experiments. For recordings of asynchronous neurotransmitter release, the CaCl2☐6H20 in the ACSF was replaced with SrCl2☐6H20. Asynchronous release events were analyzed in a 500ms window following optogenetic stimulation. A Clampfit template was made by selecting individual asynchronous release events and averaging them. The template was then used to analyze asynchronous events.

Fiber Photometry. Adult male C57BL/6N mice (8-12 weeks of age) were used for all fiber photometry experiments. Mice were placed on a stereotaxic frame and unilateral holes drilled over PL (A/P = +2.0 mm, M/L = ± 0.3 mm) and BLA (A/P = -1.75 mm, M/L = ±3.3 mm). A 10 µL Nanofil syringe (World Precision Instruments) fitted with a 33-gauge beveled needle and connected to an infusion pump was used to microinject 200nl of AAV1.Syn.GCaMP6s.WPRE.SV40 (Penn Vector Core) into the BLA (D/V = -4.6 mm) at a rate of 50 nl/min. A 400 μm diameter optical fiber (Doric) was implanted into the PL (D/V = -1.6 mm) and secured to the skull with Metabond (Parkell). Two to four weeks after surgery, mice underwent the acute shock exposure protocol with concurrent recording of GCaMP6s signal. The fiber photometry rig was based on a previously described design (Cui et al., 2013; Gunaydin et al., 2014); briefly, to induce GCaMP6s fluorescence, 470 nm wavelength light emitted from an LED (Thorlabs) was passed first through a filter (Semrock, FF02-472/30) and then connected to the fiber implant with a 0.48 NA fiber optic patch cord (Doric). Activity-dependent GCaMP6s fluorescent signal was then transmitted through the fiber optic patch cord and separated from the excitation light with a dichroic (Semrock, FF495-Di03) and then passed through a single band filter (Semrock, FF01-535/50) and focused on a photodetector (Newport, Model 2151) until finally being recorded by a real-time processor (Tucker Davis Technologies). A pulse from the

behavioral set-up (Video Freeze) was used to time lock fluorescent signal recordings with shock presentations. To confirm fiber placement and GCaMP6s expression, mice were perfused, and brains were sectioned for histological verification of injection sites and fiber optic placement using Stereo Investigator software (MBF Bioscience) with a fluorescent microscope (Nikon Eclipse 80i). Fiber photometry data was analyzed in MATLAB (MathWorks), where $\Delta F/F$ was calculated to normalize fluorescent signal data from each mouse and z-scored to account for between-subject variability in signal magnitude. To control for photobleaching, median fluorescence during a rolling window of 80 seconds (40 seconds before and 40 seconds after every given data point) was calculated and subtracted from each data point across the recording session.

Miniendoscopy: For *in vivo* single cell calcium imaging, mice were injected with AAV expressing GCaMP7f into the plPFC at 2 different levels (1.6 and 1.9 DV, 300 nL per injection). Following or prior to injection a 0.5 mm diameter tract was created over PL with a blunt needle connected to a vacuum line stereotaxically driven to DV 1.55. Thereafter, a 0.5 mm diameter GRIN lens (Inscopix, Palo Alto, CA) was introduced into the tract and slowly lowered into position (1.8 DV). Animals were allowed to recover for at least 2 weeks and a baseplate was installed over the lens in order to dock the miniaturized microscope at an empirically optimized working distance. Mice were habituated to the microscope for at least 2 days. On test day, mice were exposed to 20 shocks as previously described, the recording system (nVista, Inscopix, Palo Alto, CA) was synchronized to the fear conditioning software (FreezeFrame, actimetrics) via a TTL pulse. Data was acquired at a frame rate of 10 Hz. Laser power, gain, and lens focus were

empirically adjusted to maximize the quality of the recordings. Data was acquired continuously throughout the duration of the session.

Recordings were spatially downsampled by a factor of 2, bandpass filtered, and motion corrected using Inscopix Data Processing software V1.2. Individual calcium traces were extracted using Constrained Nonnegative Matrix Factorization for miniendoscopic data (CNMFE)(Zhou et al., 2018). For CNMFE, we used the following parameters: min corr= 0.9, min pnr= 20, gSiz= 20, gSig= 10. For our analysis we used the raw extracted values rather than the denoised values. Individual extracted traces and corresponding identified neurons were visually confirmed and traces that corresponded to artifacts rather than neurons were excluded. For bulk fluorescence analysis, the total fluorescence for the full field of view was extracted from recordings prior to band pass filtering. Both total fluorescence signals and individual traces were analyzed using a custom Matlab code. The stimulus response period was defined as the 10 seconds preceding shock onset and the 10 seconds following tone onset. For bulk fluorescence signal, the total fluorescence was averaged across the 20 stimulus response periods. Similarly, for single cell analysis, each individual trace was averaged across the 20 stimulus trials and binned into 1 second bins. To normalize the data, z-scores were calculated using the 10 second pre-shock period as the baseline. Traces exceeding a z-score value of 1.645 or -1.645 (p<0.05, two-tails) for any of the following 3 1-second bins were considered excitatory shock-responsive or inhibitory shock-responsive, respectively.

Lipid analysis. Mice underwent cervical dislocation immediately followed by decapitation. The brain was quickly removed and placed in a brain matrix. 2 mm thick coronal sections containing the target brain regions were frozen on a metal block in dry ice. Dissections were performed on

the frozen tissue using a 2 mm diameter metal micropunch. Samples were stored at −80 °C until extraction.

Lipids were extracted from brain tissue by sonication in 1 ml of acetonitrile (ACN). The samples were sonicated at 60% power for 1 min while incubated in an ice bath to prevent sample heating (the sonicator was a Hielscher UP100H ultrasonic device – 100W, 30kHz). The ACN contained the following internal standards: 2-AG-d5 (1 nmol), AEA-d4 (2 pmol), AA-d8 (2 nmol), OG-d5 (0.25 nmol) and OEA-d4 (25 pmol) was included for selected samples. The sonicated homogenate was stored at −20°C overnight and then centrifuged at 4°C for 5 min at 3,000 rcf. The supernatant was dried under nitrogen. Samples were re-suspended in 200 μl of methanol:water (50:50), followed by brief centrifugation to pellet any solid material. The cleared samples were transferred to autosampler vials and analyzed via LC-MS/MS as described in Bedse et 2017 (Biol Psychiatry. 2017 Oct 1;82(7):488-499).

Foot-shock stress. Foot-shock stress occurred 24 h before behavioral testing and consisted of twenty unpredictable 0.5 mA foot-shocks within 10 min using a MED Associates fear-conditioning chamber (St. Albans, VT, USA). 24 h after foot-shock stress mice were tested in elevated zero maze or elevated plus maze test.

Elevated-zero maze. The elevated-zero maze (EZM, San Diego Instruments, San Diego, California, USA) is an annular white platform and divided four equal quadrants. It consisted of two open arms and two closed arms. The outer and inner diameters of the EZM were 60.9 cm and 50.8 cm, respectively. The apparatus was elevated 60.9 cm from the floor. Light levels in the open arms were approximately 200 lux, while the closed arms were <100 lux. Mice were placed

in the closed arm of the maze and allowed to explore for 5 min. ANY-maze (Stoelting, Wood Dale, Illinois, USA) video-tracking software was used to monitor and analyze behaviors during the test.

Elevated-plus maze. The elevated plus maze was custom built (Vanderbilt Machine Shop, Nashville, TN) and consists of two pairs of open and closed arms which intersect in an open center platform. The total length of each set of arms is 27", and the closed arms are bordered with 6" walls. The maze platform is elevated to 15.5". Mice were placed in the maze center, facing the entrance to the closed arm away from the experimenter. Light was set to a lux value of 150-200 for the open arms. Mice were allowed to roam for five minutes, and movement was measured with ANY-maze software (Stoelting Co., Wood Dale, IL).

INTRSECT behavior. Littermate-matched homozygous CB1$^{f/f}$ mice were bilaterally injected with 500nL AAV5-CMV-fDIO-Cre-mNeonGreen into the BLA and 200µL rAAV2-EF1α-mCherry-IRES-Flp or mCherry control virus (rAAV2-EF1α-mCherry) into the plPFC. 6 weeks after stereotaxic surgery, mice were singly housed and allowed to acclimate for > 1 week. Prior to testing, mice were transported from a housing room to a nearby experimental room. We then allowed at least 10 minutes for mice to habituate to the experimental room. Mice were then run through EZM and Light/Dark box test (data not shown) on non-sequential days. One day following the last behavioral test, mice were exposed to the aforementioned 20 foot-shock stress protocol, and 24 hours later, run through the EPM test. For both the EZM and EPM, open arm light levels were set to 150 lux, and anxiety-like behaviors were analyzed by examining open

arm entries and % open arm time using ANY-Maze software (Stoelting Co., Wood Dale, IL). The experimenter was blinded to the experimental group of the mice.

Chemogenetic behavior. Littermate-matched WT C57 mice were bilaterally injected with rAAV2-pmSyn1-EBFP-Cre in the plPFC, and AAV5-hSyn-DIO-hM3D(Gq)-mCherry or AAV5-hSyn-DIO-mCherry control virus in the BLA. A minimum of six weeks was allowed for virus expression. Thirty minutes prior to testing, mice were given I.P. administration of Clozapine N-Oxide (CNO) (MilliporeSigma, St. Louis, MO) at 5mg/kg. Mice were transported from a housing room to a nearby experimental room. We then allowed at least 10 minutes for mice to habituate to the experimental room. The EPM assay was run as described above.

Immunohistochemistry and Imaging. Mice were anesthetized using isoflurane and transcardially perfused with ice-cold phosphate buffered saline (PBS) followed by 4% paraformaldehyde (PFA) solution in PBS. Brains were dissected and stored overnight in 4% PFA and transferred to a 30% sucrose solution for four days. 40μm brain sections were taken using a Leica CM3050 S cryostat (Leica Microsystem, Weitzlar, Germany). Brain sections were then washed in Tris-Buffered Saline (TBS) 3X for 10 minutes. Slices were then directly mounted on glass slides and VectaShield mounting medium (Vector Laboratories, Burlingame, CA) was applied before coverslipping. Images were taken using an Axio Imager M2 epifluorescent microscope. Whole slice images were acquired using a 5x objective while zoomed in images of the BLA or plPFC were acquired using a 10 or 20x objective. Brightness and contrast were adjusted using Adobe CS4 software for presentation in figures.

cFOS Cell Counting.   Four to six weeks after intracranial viral injection surgery, both GqDREADD and mCherry mice were given an IP injection of 10mg/kg CNO-HCl dissolved in saline.   Two hours after IP injection, mice were perfused as previously described.   40 μm sections were cut, and immediately washed in TBS 3X for 10 minutes. Slices were then washed in a blocking buffer 1x TBS containing 4% horse serum and 0.2% Triton X-100 (Fisher Scientific)(TBS+). Slices were then placed into 1.5 mL Eppendorf tubes containing the blocking buffer and 1:500 Rabbit-α-cFOS antibody (abcam) and covered and put on a nutator overnight. The following day, slices were washed 3X in TBS+, and then put into Eppendorf tubes containing TBS+ and 1:1000 Alexa Fluor 488 Donkey-α-Rabbit and allowed to incubate for two hours. Slices were subsequently washed and mounted as previously described.

For imaging, a set exposure time of 400 ms for the GFP channel was used to ensure that there was no bias in the image acquisition process. Scale bars were included on each image to allow for subsequent processing. Raw 10x images were then opened with ImageJ, and the scale was set using the aforementioned scale bar. Images were then thresholded, and the region of interest was drawn using the Image J software with the Allen Brain Atlas being used to ensure the correct region was selected. Image J particle counting software was then used to analyze the number of cFOS cells in the region of interest. This number was then divided by the area of the region of interest to get the number of cFOS cells per square mm.

Quantification and Statistical Analysis

Electrophysiology

Electrophysiological data was initially analyzed using ClampFit 10.5 software (Molecular Devices, San Jose, California). Data sets were organized in Microsoft Excel and then transferred

to GraphPad Prism 6.0 for generation of graphs and statistical analyses. All statistical tests are reported in the figure legends. For analysis of two groups, an unpaired Student's t-test was used, with error bars indicating the mean ± SEM. For analysis of three more groups, a one-way ANOVA with Holm-Sidak post-hoc correction was used, with error bars indicating the mean ± SEM. For analysis of two or more groups across two or more treatments or time points, a two-way ANOVA with Holm-Sidak post-hoc correction was used, with error bars indicating the mean ± SEM. For all data sets, significance was defined by a p value of <0.05. The Grubbs outlier test was run on each data set individually and outliers were excluded from our data. Mice were excluded from physiological experiments if there was improper targeting of the BLA or plPFC or if there was no viral expression in plPFC terminals. Neurons were excluded from physiological experiments for four reasons. 1: if the holding current dropped below -200 pA at any time during the recording. 2: if the access resistance was > 20 MΩ. 3: if the access resistance fluctuated by more than 20% throughout the recording. 4: There was no optogenetically-evoked response. Paired-pulse ratios were only taken from neurons in which both the first and the second oEPSC had an amplitude ≥ 50pA.

Behavior

All behavior was analyzed via ANY-maze (Stoelting, Wood Dale, Illinois, USA) software. All statistical tests are reported in the figure legends. For analysis of two groups, an unpaired Student's t-test was used, with error bars indicating the mean ± SEM. For analysis of three more groups, a one-way ANOVA with Holm-Sidak post-hoc correction was used, with error bars indicating the mean ± SEM. For analysis of two or more groups across two or more treatments or time points, a two-way ANOVA with Holm-Sidak post-hoc correction was used, with error

bars indicating the mean ± SEM. For all data sets, significance was defined by a p value of <0.05. The Grubbs outlier test was run on each data set individually and outliers were excluded from our data. Mice were excluded from behavioral experiments if any of the viral injections were misplaced or if there was no viral expression. Furthermore, mice were excluded if there was a technical issue during the behavioral experiment (e.g. mouse fell out the EZM/EPM or there was a malfunction on the behavioral hardware or software).
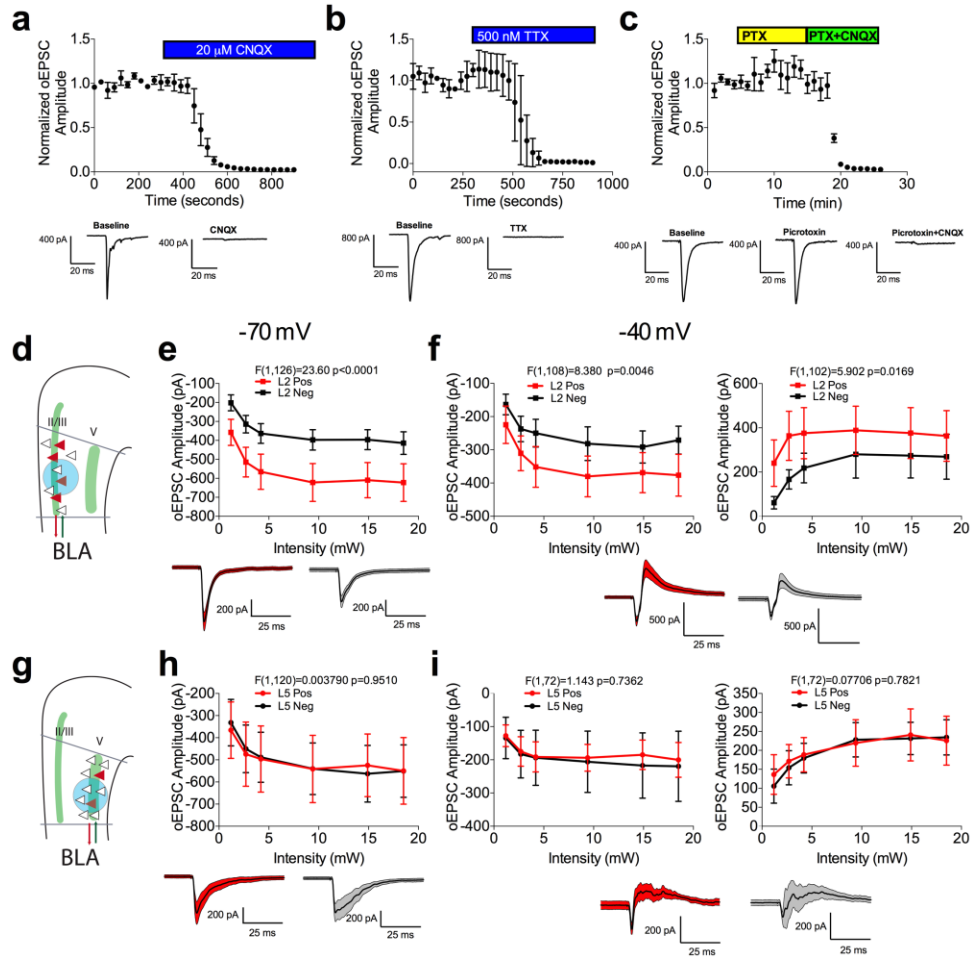
Figure S1: Stimulation of BLA terminals in the plPFC elicits a monosynaptic excitatory and disynaptic inhibitory current

(a) Effect of the AMPAR antagonist CNQX (20 µM) on oEPSC amplitude at BLA-plPFC synapses. Bath application of CNQX abolished oEPSCs (n=3, N=2).

(b) Effect of the Voltage Gated Sodium Channel Blocker Tetrodotoxin (TTX)(500nM) on oEPSC amplitude at BLA-plPFC synapses. Bath application of TTX abolished oEPSCs (n=3, N=2).

(c) Effect of the $GABA_A R$ channel blocker picrotoxin (PTX)(50 µM) on oEPSC amplitude at BLA-plPFC synapses. Bath application of PTX did not affect oEPSCs, while subsequent addition of CNQX abolished oEPSCs (n=3, N=2).

(d) Schematic for voltage-clamp recordings of oEPSCs from L2/3 rAAV-positive and negative neurons at -70mV (left) and -40mV (right).

(e) Optically evoked input/output curve from L2/3 rAAV-positive and negative neurons at -70mV. The BLA sends stronger excitatory input to reciprocally projecting L2/3 neurons (n=11, N=5) than non-reciprocally projecting neurons L2/3 neurons (n=12, N=5)

78

(f) Optically evoked input/output curve from L2/3 rAAV-positive and negative neurons at -40mV. Stimulation of BLA terminals in the plPFC elicits a monosynaptic excitatory and disynaptic inhibitory current, presumably through feed-forward inhibition. Both excitatory and inhibitory responses are larger in L2/3 rAAV-positive neurons (n=10,N=5) compared to rAAV negative neurons at -40mV (n=9,N=5).

(g) Schematic for voltage-clamp recordings of oEPSCs from L2/3 rAAV positive and negative neurons at -70mV (left) and -40mV (right).

(h) Optically evoked input/output curve from L5 rAAV-positive and negative neurons at -70mV. No difference in excitatory input to L5 rAAV-positive (n=11,N=5) compared to negative neurons (n=11,N=5) were observed.

(i) Optically evoked input/output curve from L5 rAAV-positive and negative neurons at -40mV. Stimulation of BLA terminals in the plPFC elicited a monosynaptic excitatory and disynaptic inhibitory current. No difference in excitatory or inhibitory response in L5 rAAV-positive (n=7, N=5) compared to rAAV-negative neurons at -40mV were observed (n=7, N=5).

All error bars represent ± SEM. "n" represents number of neurons, "N" represents number of mice. F and P values from 2-way ANOVA shown in relevant panels.
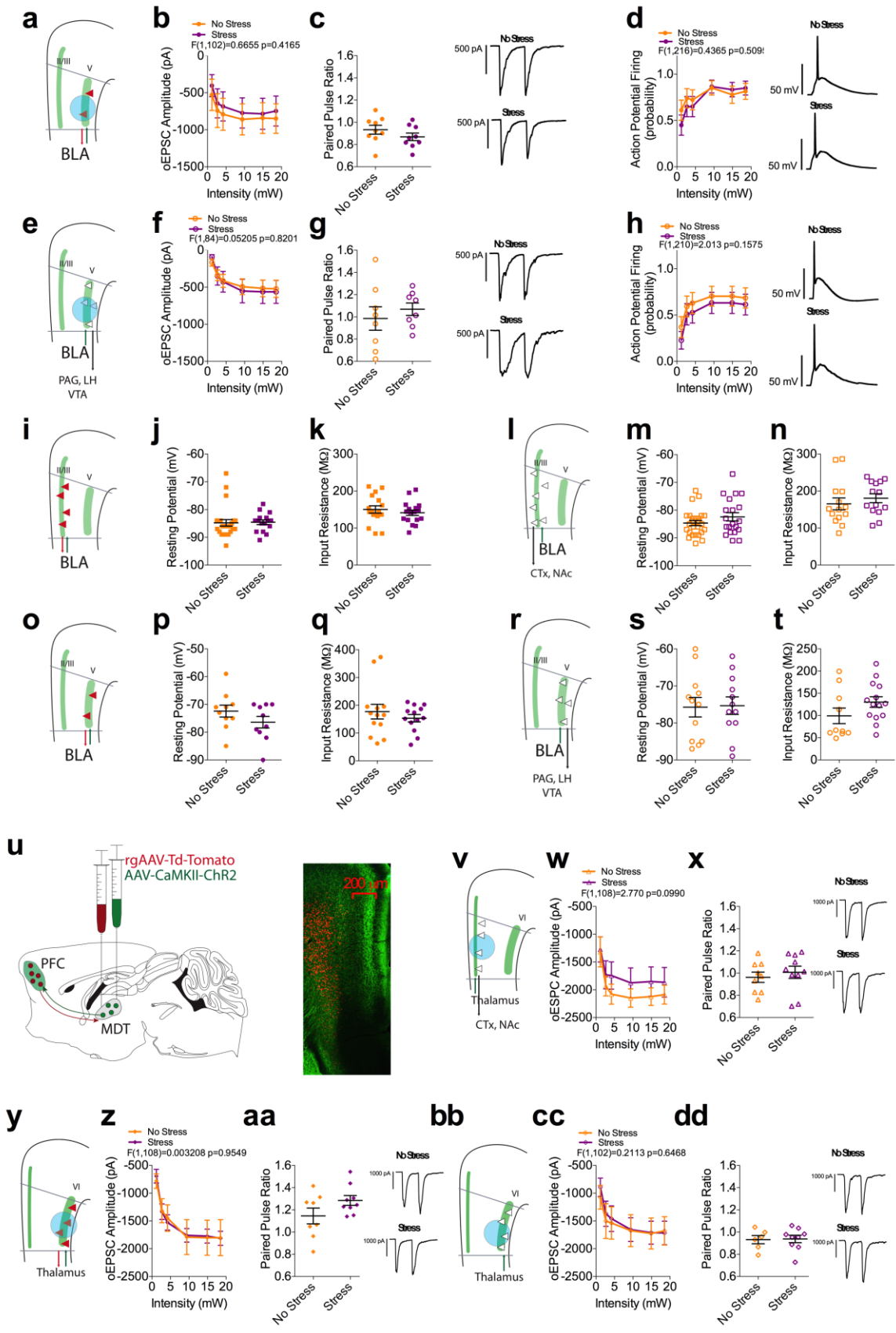
Figure S2: Stress does not alter excitatory input from the BLA to plPFC L5 neurons

    (a) Schematic for voltage clamp-recordings of oEPSCs from L5 rAAV-positive neurons at -70mV.

    (b) Optically evoked input/output curve from L5 rAAV-positive neurons from non-stressed (n=9, N=4) and stressed mice (n=10, N=4). Stress does not alter excitatory input from the BLA to plPFC L5 rAAV-positive neurons.

    (c) Effect of stress on paired pulse ratio (PPR) at BLA-L5 rAAV-positive synapses (No Stress n=10, N=4; Stress n=9, N=4). Stress exposure does not alter PPR at BLA-L5 rAAV positive synapses (p=0.2413).

    (d) Optically evoked spiking in L5 rAAV-positive neurons in non-stressed (n=18, N=8) and stressed mice (n=20, N=8). Stress exposure does not alter optically induced spiking in L5 rAAV positive neurons.

    (e) Schematic for voltage clamp-recordings of oEPSCs from L5 rAAV-negative neurons at -70mV.

    (f) Optically evoked input/output curve from L5 rAAV-negative neurons from non-stressed (n=8, N=4) and non-stressed (n=8, N=5) mice. Stress does not alter excitatory input onto L5 rAAV-negative neurons.

    (g) Effect of stress on PPR at BLA-L5 rAAV-negative synapses (No Stress: n=8, N=5; Stress: n=8, N=4). Stress exposure does not alter PPR at BLA-L5 rAAV-negative synapses (p=0.4958).

    (h) Optically evoked spiking in L5 rAAV-negative neurons in non-stressed (n=18, N=8) and stressed mice (n=19, N=7). Stress exposure does not alter optically induced spiking in L5 rAAV-negative neurons.

    (i) Schematic for current-clamp recordings from L2 rAAV-positive neurons

    (j) Resting membrane potential (RMP) of L2 rAVV-positive neurons from non-stressed (n=24, N=10) and stressed (n=20, N=8) mice. Stress does not alter RMP in L2 rAAV positive neurons (p=0.8866).

    (k) Input resistance (IR) of L2 rAAV-positive neurons from non-stressed (n=16, N=6) and stressed (n=17, N=5) mice. Stress does not alter IR in L2 rAAV-positive neurons (p=0.4725).

    (l) Schematic for current-clamp recordings from L2 rAAV-negative neurons

    (m) RMP of L2 rAAV-negative neurons from non-stressed (n=26, N=8) and stressed (n=23, n=7) mice. Stress does not alter RMP in L2 rAAV negative neurons (p=0.1852)

    (n) IR of L2 rAAV-negative neurons from non-stressed (n=14, N=6) and stressed (n=15, N=6) mice. Stress does not alter IR in L2 rAAV negative neurons (p=0.4494).

    (o) Schematic for current clamp-recordings from L5 rAAV-positive neurons at -70mV.

    (p) RMP from L5 rAAV-positive neurons from non-stressed (n=10, N=5) and stressed (n=10, N=3). Stress does not alter RMP in L5 rAAV-positive neurons (p=0.2014).

    (q) IR from L5 rAAV-positive neurons from non-stressed (n=12, N=6) and stressed (n=13, N=4) mice. Stress does not alter IR in L5 rAAV-positive neurons (p=0.4312).

    (r) Schematic for current-clamp recordings of oEPSCs from L5 rAAV-negative neurons

    (s) RMP from L5 rAAV-positive neurons from non-stressed (n=12, N=5) and stressed (n=12, N=5). Stress does not alter RMP in L5 rAAV-negative neurons (p=0.9073).

    (t) IR from L5 rAAV-negative neurons from non-stressed (n=10, N=6) and stressed (n=14, N=5) mice. Stress does not alter IR in L5 rAAV-negative neurons (p=0.1415).

(u) Schematic for stereotaxic delivery of AAV5-CaMKII-ChR2(H147R)-eYFP and rAAV2-CAG-tdTomato into the MDT

(v) Schematic for voltage clamp-recordings of oEPSCs from L6 rAAV positive neurons at -70mV.

(w) Optically evoked input/output curve from L6 rAAV positive neurons from non-stressed (n=10, N=) and stressed mice (n=10, N=3). Stress does not alter excitatory input L6 rAAV-positive neurons.

(x) Effect of stress on PPR at MDT-L6 rAAV- positive synapses (No Stress: n=8, N=3; Stress: n=9 N=3). Stress exposure does not alter PPR at MDT-L6 rAAV positive synapses (p=0.1075).

(y) Schematic for voltage clamp recordings of oEPSCs from L6 rAAV negative neurons at -70mV.

(z) Optically evoked input output curve from L6 rAAV negative neurons from non-stressed (n=9, N=3) and stressed mice (n=10, N=3). Stress does not alter excitatory input from the MDT to L6 rAAV negative neurons.

(aa) Effect of stress on PPR at MDT-L6 rAAV-negative synapses (No Stress n=6, N=3; Stress: n=9, N=3). Stress exposure does not alter PPR at MDT-L6 rAAV negative synapses (p=0.9048).

(bb) Schematic for voltage clamp recordings of oEPSCs from L2/3 rAAV negative neurons at -70mV.

(cc) Optically evoked input output curve from L2/3 rAAV-negative neurons from non-stressed (n=9, N=3) and stressed (n=11, N=3) mice. Stress does not alter excitatory input to L2 rAAV-negative neurons.

(dd) Effect of stress on PPR at MDT-L2/3 rAAV-negative synapses (No Stress: n=9, N=3; Stress: n=10 N=3). Stress exposure does not alter PPR at MDT-L2/3 rAAV-negative synapses (p=0.5496).

All error bars represent ± SEM. "n" represents number of neurons, "N" represents number of mice. P values reported from two-tailed unpaired t-test (c,g,j,k,m,n,p,q,s,t,x,aa,dd). F and P values from ANOVA shown in relevant panels.
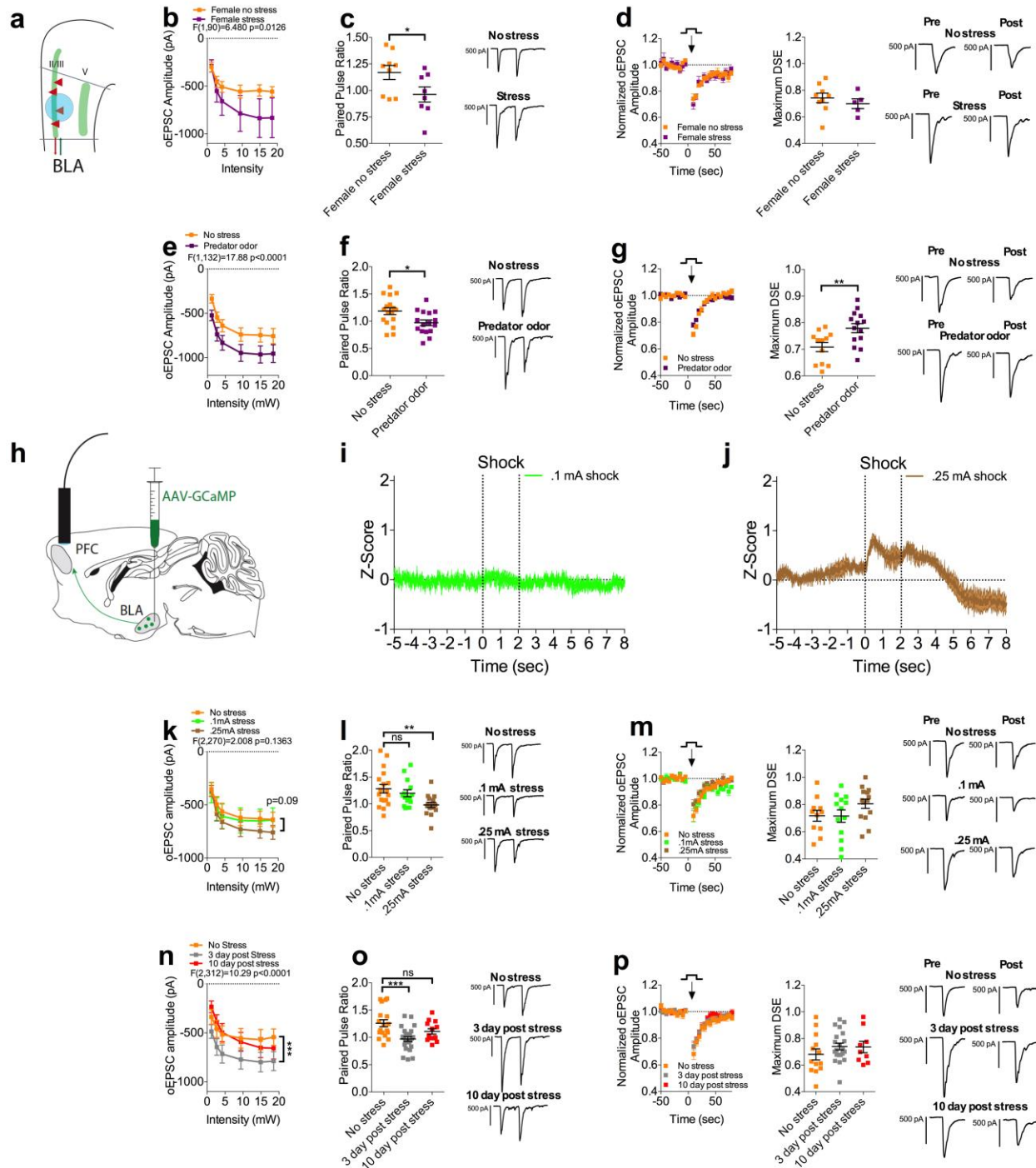
Figure S3: Dose response, time course, and generalizability of stress induced presynaptic strengthening at BLA-L2 rAAV positive synapses

(a) Schematic for voltage-clamp recordings of oEPSCs from L2/3 rAAV-positive neurons.

(b) Optically-evoked input/output curve from L2/3 rAAV-positive neurons from non-stressed (n=9; N=3) and stressed (n=8; N=3 mice) female mice. Stress exposure enhances excitatory input to L2/3 rAAV- positive neurons.

(c) Effect of stress on PPR at BLA-L2/3 rAAV-positive synapses (No Stress: n=9, N=3, Stress: n=8, N=3). Stress exposure decreases PPR (p=0.0499).

(d) Effect of stress on DSE in female mice (No stress: n=9, N=3; Stress: n=5, N=3). Stress does not alter DSE magnitude in female mice (p=0.4560)

(e) Optically-evoked input/output curve from L2/3 rAAV-positive neurons from mice receiving no stress (n=17, N=4) or 10 minutes exposure to the predator odorant, 2MT (n=16, N=4). Predator odor exposure significantly increases excitatory input to L2/3 rAAV-positive neurons.

(f) Effect of predator odor on PPR at BLA-L2/3 rAAV-positive synapses (No stress: n=16, N=4; Predator odor: n=17, N=4). Predator odor decreases the PPR (p=0.0152).

(g) Effect of predator odor on DSE at BLA-L2/3 rAAV-positive synapses (No stress: n=12, N=4; Stress: n=13, N=4). Stress decreases DSE magnitude (p=0.0078).

(h) Schematic for *in vivo* fiber photometry recordings of BLA projections to the plPFC

(i) Z-score of Δf/f signal recorded from GCaMP6s expressing BLA terminals in the plPFC in response to 2 second 0.1 mA foot shock (N=5).

(j) Z-score of Δf/f signal recorded from GCaMP6s expressing BLA terminals in the plPFC in response to 2 second 0.25 mA foot shock (N=5).

(k) Optically-evoked input/output curve from L2/3 rAAV-positive neurons from mice receiving no stress (n=19; N=4) .01 mA foot-shock stress (n=14; N=4), and 0.25 mA foot-shock stress (n=15, N=4). 0.25 mA stress exposure induces a trend toward increased excitatory input to L2/3 rAAV-positive neurons (p=0.0943).

(l) Effect of 0.1. and 0.25 mA foot-shock stress on PPR at BLA-L2/3 rAAV-positive synapses (No Stress: n=19, N=4, 0.1 mA stress: n=14, N=4, 0.25 mA stress: n=15, N=4). 0.25 mA stress exposure decreases PPR (p=0.0058).

(m) Effect of 0.1 and 0.25 mA foot-shock stress on DSE at BLA-L2/3 rAAV-positive synapses (No stress: n=11, N=4; 0.1 mA stress: n=13, N=4; 0.25 mA stress: n=14, N=4). Neither 0.1 mA (p=0.9697) nor 0.25 mA (p=0.2504) foot-shock stress alter DSE magnitude.

(n) Optically-evoked input/output curve from L2/3 rAAV-positive neurons from mice receiving no stress (n=18, N=4), and mice recorded 3 (n=24, N=4) and 10 days (n=13, N=4) following 0.5 mA foot shock stress. Stress exposure increases excitatory input to L2/3 rAAV-positive neurons at 3 days post exposure (p=0.0002)

(o) Effect of 0.5 mA stress on PPR at 3 and 10 days post exposure (no stress: n=18, N=4; 3 day: n=24, N=4; 10 day: n=13, N=4). PPR is decreased at 3 days post stress exposure (p=0.0003).

(p) Effect of 0.5 mA stress on DSE at 3 and 10 days post exposure (no stress: n=13, N=4; 3 day: n=21, N=4; 10 day: n=9, N=4). DSE magnitude is not altered at 3 (p=0.3689) or 10 (p=0.3689) days post stress exposure.

All error bars represent ± SEM. "n" represents number of neurons, "N" represents number of mice. P values reported from two-tailed unpaired t-test (c,d,f,g) and one-way ANOVA (l,m,o,p). F and P values from ANOVA shown in relevant panels.
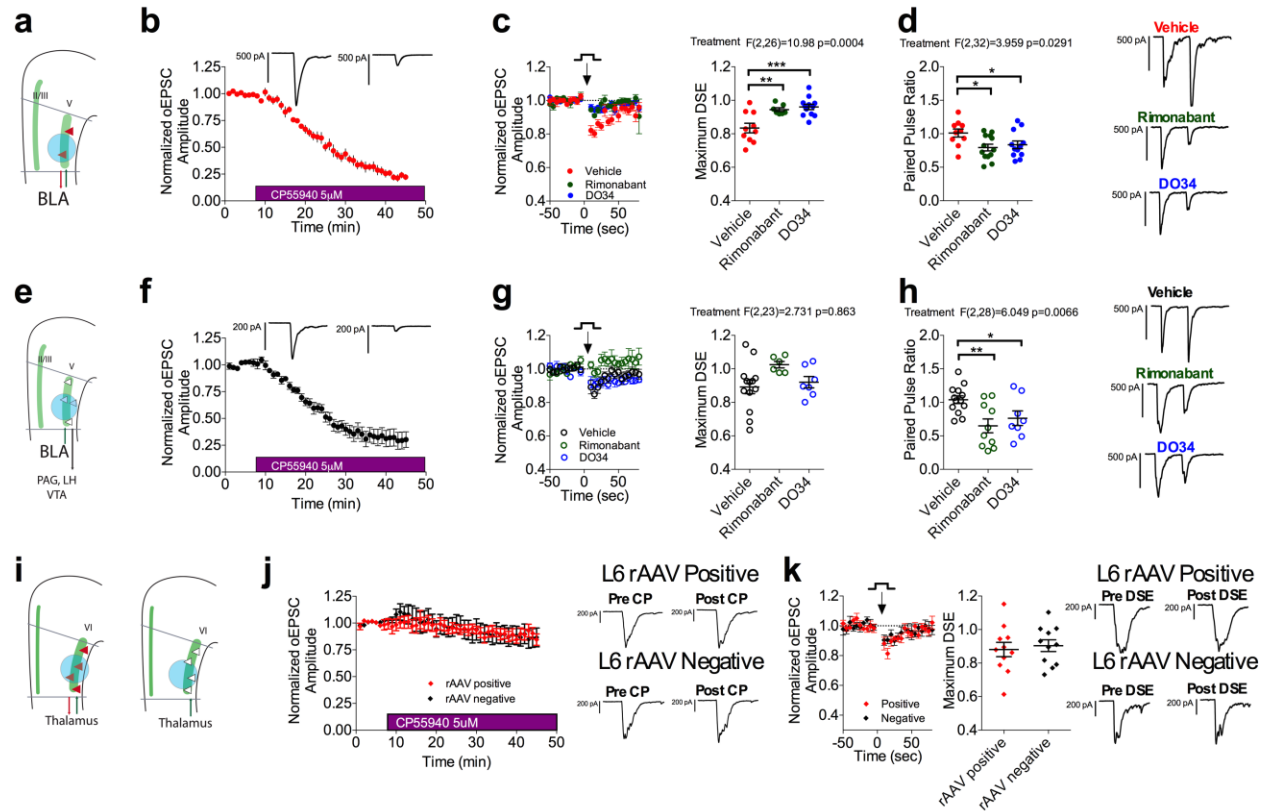
Figure S4: Phasic and tonic 2-AG signaling broadly regulate BLA-plPFC L5 glutamatergic synapses but not MDT-plPFC synapses

(a) Schematic for voltage-clamp recordings of oEPSCs from L5 rAAV-positive neurons at -70mV.

(b) Effect of 5 μM CP55,940 on oEPSC amplitude at BLA-L5 rAAV-positive synapses (n=8, N=6).

(c) Depolarization induced suppression of excitation (DSE) at BLA-L5 rAAV-positive synapses (n=11, N=5) is blocked by 10 μM rimonabant (n=7, N=4; One-way ANOVA with Holm-Sidak post-hoc correction, p=0.0023) and 2.5 μM DO34 (n=12, N=4; p=0.0003)

(d) PPR at BLA-L5 rAAV-positive synapses (n=10, N=5) is reduced by rimonabant (n=13, N=4; p=0.0217) and DO34 (n=10, N=4; p=0.0389).

(e) Schematic for voltage clamp-recordings of oEPSCs from L5 rAAV-negative neurons at -70mV.

(f) Effect of CP55,940 on oEPSC amplitude at BLA-L5 rAAV-negative synapses (n=7, N=5)

(g) Minimal depolarization induced suppression of excitation (DSE) is evoked at BLA-L5 rAAV-negative synapses (n=13, N=5). As such, there is no significant effect of rimonabant (n=6, N=6; One-way p=0.0580) or DO34 (n=7, N=4; p=0.6040)

(h) PPR at BLA-L5 rAAV-negative synapses (n=13, N=5) is reduced by rimonabant (n=12, N=5; p=0.0047) and DO34 (n=8 N=4; p=0.0347).

(i) Schematic for voltage-clamp recordings of oEPSCs from L6 rAAV-positive and negative neurons at -70mV.

(j) Effect of CP55,940 on oEPSC amplitude at MDT-L6 rAAV-positive (n=8, N=6) and negative (n=10, N=6) synapses. CP55,940 does not induce significant depression of oEPSC amplitude at MDT-L6 rAAV-positive or negative synapses.

(k) Minimal DSE was evoked at MDT-L6 rAAV positive (n=11, N=3) and rAAV negative (n=11, N=3) synapses.

All error bars represent $\pm$ SEM. "n" represents number of neurons, "N" represents number of mice. All post-hoc p values derived from one-way ANOVA with Holm-Sidak multiple comparisons (c,d,g,h) or two-tailed unpaired t-test (k). F and P values for ANOVA shown in relevant panels.

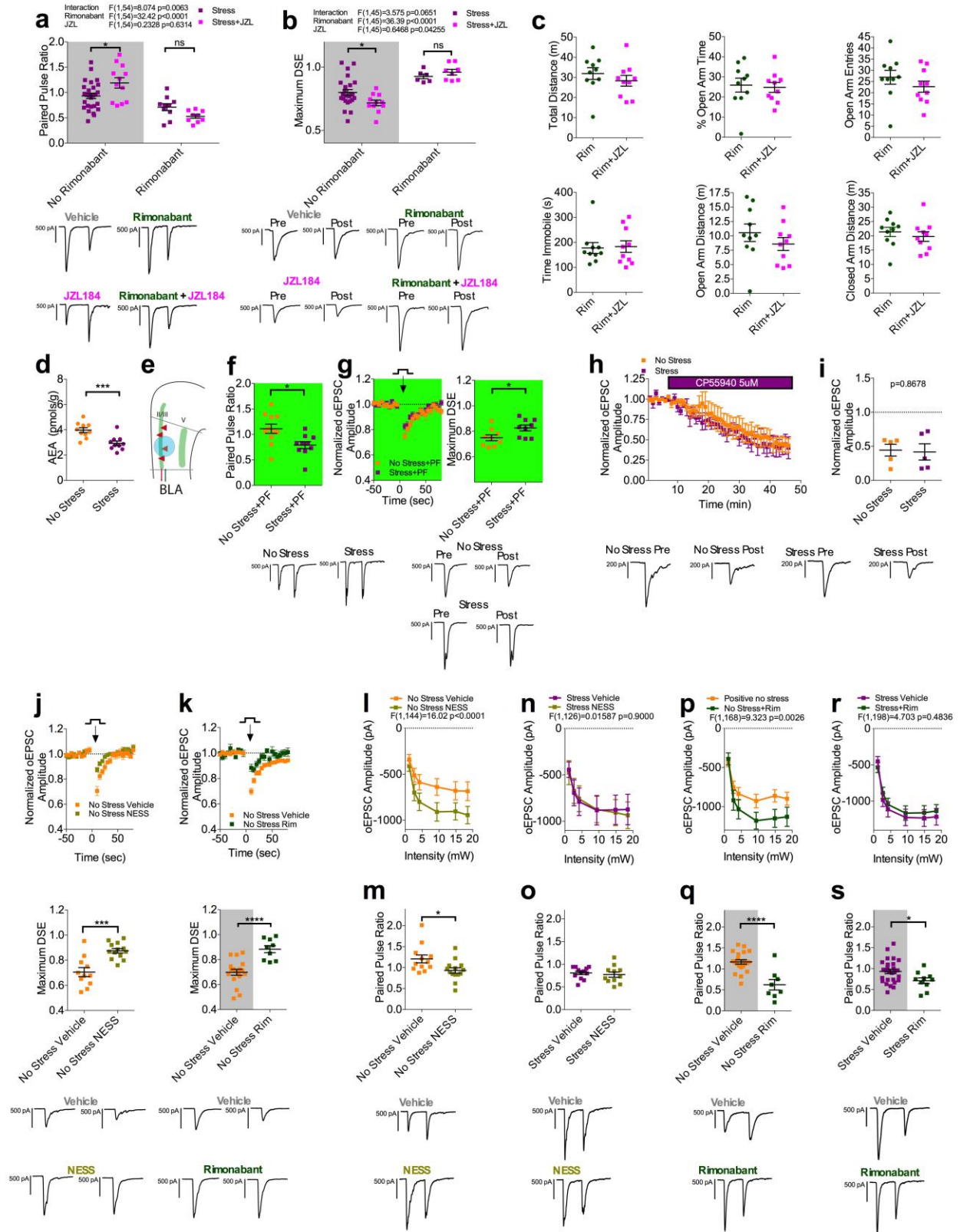**Figure S5: Rimonabant blocks the effects of JZL184, AEA augmentation does not rescue stress-induced changes in PPR or DSE, stress does not alter CB1 sensitivity, and stress occludes the effects of NESS and rimonabant at BLA-L2/3 rAAV positive synapses**

(a) (Stress and Stress+JZL without rimonabant from main text figure, grey shading) Effect of JZL and JZL+rimonabant on PPR in stressed mice. 1 µM JZL reverses the stress-induced decrease in PPR at BLA-L2/3 rAAV-positive synapses (Stress: n=27, N=11; Stress+JZL: n=13, N=4, Two-way ANOVA with Holm-Sidak post hoc correction, p=0.0158). JZL does not alter PPR in the presence of 10 µM rimonabant (Stress+rimonabant: n=10, N=5; Stress+rimonabant+JZL: n=9, N=2; p=0.1452).

(b) (Stress and Stress+JZL without rimonabant from main text figure, grey shading) Effect of JZL and JZL+rimonabant on PPR in stressed mice. JZL reverses the stress-induced attenuation of DSE magnitude at BLA-L2/3 rAAV-positive synapses (Stress: n=24, N=11; Stress+JZL: n=11, N=4). JZL does not alter DSE magnitude in the presence of rimonabant (p=0.5157).

(c) Effect of JZL in the presence of rimonabant in the EZM 24 hours after .5 mA foot-shock stress exposure. JZL has no behavioral effect in the presence of rimonabant. (Total Distance: p=0.3809)(Open Arm Time: p=0.7914)(Open Arm Entries: p=0.3042)(Time Immobile: p=0.8655)(Open Arm Distance: p=0.3127)(Closed Arm Distance: p=0.4981).

(d) Effect of stress on mPFC AEA levels. Stress exposure causes a decrease in mPFC AEA levels (No stress: N=10, Stress: N=10; p=0.0009).

(e) Schematic for voltage clamp-recordings of oEPSCs from L2 rAAV-positive neurons at -70mV.

(f) Effect of 10 µM PF3845 on PPR at BLA-L2 rAAV-positive synapses. PF3845 does not rescue the stress induced decrease in PPR at BLA-L2/3 rAAV positive synapses (No Stress: n=11, N=8; Stress: n=10, N=6; p=0.0121).

(g) Effect of PF3845 on DSE at BLA-L2 rAAV-positive synapses. PF3845 does not rescue the stress induced decrease in DSE magnitude at BLA-L2/3 rAAV positive synapses (No Stress: n=9, N=6; Stress: n=9, N=6; p=0.0299).

(h) Effect of 5 µM CP55,940 on oEPSC amplitude at BLA-L2/3 rAAV-positive synapses.

(i) Quantification of last 5 minutes of CP55,940 application on oEPSC amplitude at BLA-L2 rAAV-positive synapses. Stress does not cause a significant change in CP55,940 induced depression of oEPSC amplitude at BLA-L2/3 rAAV positive synapses (No Stress: n=5, N=3; Stress: n=5, N=2; p=0.8678).

(j) Effect of 1 µM NESS on DSE at BLA-L2/3 rAAV-positive synapses in non-stressed mice (vehicle: n=11, N=4; NESS: n=13, N=4). NESS blocks DSE (p=0.0002).

(k) (No Stress Vehicle from main text) Effect of 10 µM rimonabant on DSE at BLA-L2/3 rAAV-positive synapses in stress mice (vehicle: n=18, N=7; NESS: n=9, N=4). rimonabant blocks DSE (p<0.0001).

(l) Effect of NESS on optically-evoked input/output curve from L2/3 rAAV-positive neurons from non-stressed mice (vehicle: n=12, N=4; NESS: n=14, N=4). NESS enhances excitatory input.

(m) Effect of NESS on PPR at BLA-L2/3 rAAV-positive synapses from non-stressed mice (vehicle: n=12, N=4; NESS: n=14, N=4). NESS decreases the PPR (p=0.0209).

(n) Effect of NESS on optically-evoked input/output curve from L2/3 rAAV-positive neurons from stressed mice (vehicle: n=12, N=4; NESS: n=11, N=4). NESS does not affect excitatory input following stress.

(o) Effect of NESS on PPR at BLA-L2/3 rAAV-positive synapses from stressed mice (vehicle: n=12, N=4; NESS: n=11, N=4). NESS does not affect PPR following stress (p=0.5873).

(p) Effect of rimonabant on optically-evoked input/output curve from L2/3 rAAV-positive neurons from non-stressed mice (vehicle: n=21, N=8, rimonabant: n=8, N=4). Rimonabant enhances excitatory input.

(q) Effect of rimonabant on PPR at BLA-L2/3 rAAV-positive synapses from non-stressed mice (vehicle: n=21, N=8, rimonabant: n=8, N=4). Rimonabant decreases the PPR (p<0.0001).

(r) Effect of rimonabant on optically-evoked input/output curve from L2/3 rAAV-positive neurons from stressed mice (vehicle: n=27, N=10; rimonabant: n=10, N=4). Rimonabant does not affect excitatory input following stress.

(s) Effect of rimonabant on PPR at BLA-L2/3 rAAV-positive synapses from stressed mice (vehicle: n=27, N=10; rimonabant: n=10, N=4). Rimonabant decreases the PPR following stress (p=0.0297).

All error bars represent ± SEM. "n" represents number of neurons, "N" represents number of mice. P values reported from two-tailed unpaired t-test (c,d,f,g,i,j,k,m,o,q,s) and post-hoc p values reported from two-way ANOVA with Holm-Sidak multiple comparisons (a,b). F and P values for ANOVA shown in relevant panels.
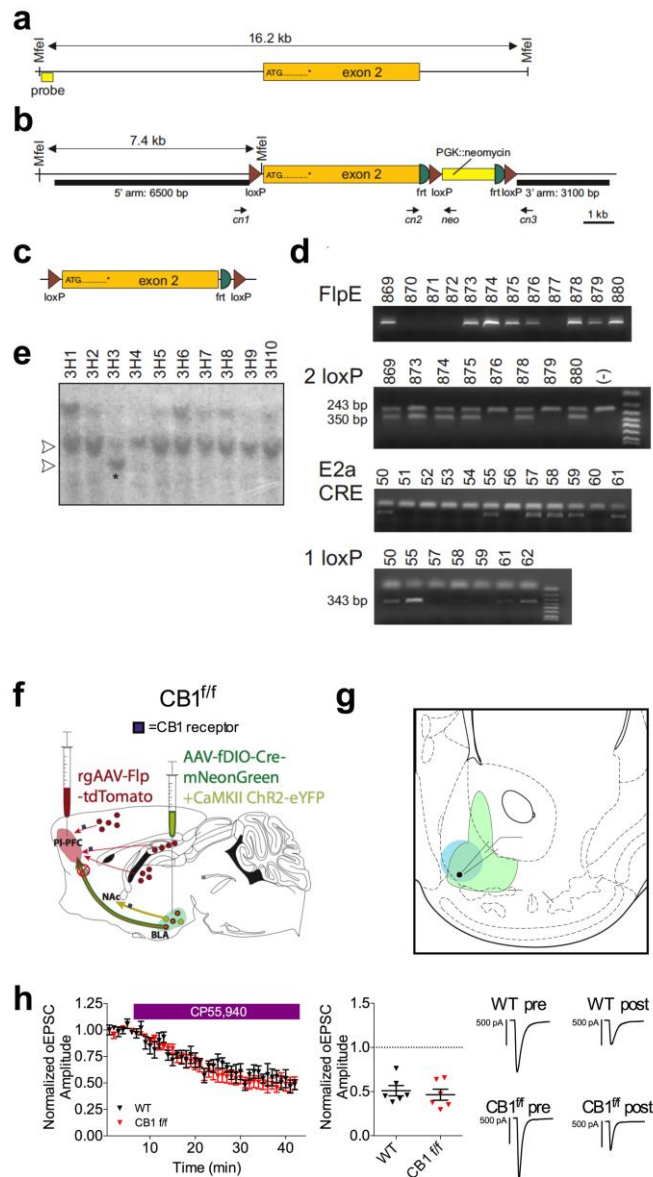
Figure S6: INTRSECT approach leads to selective deletion of the CB1 receptor from BLA neurons that project to the plPFC and not from BLA neurons that project to other brain regions

(a) Schematic representation of the cnr1 gene with exons 1 and 2 separated by large intron.

(b) Schematic representation of the cnr1 gene after homologous recombination. Three loxP and 2 FRT sites are highlighted around the coding exon. A PGK-driven neomycin resistance gene cassette is also included. The 5' and 3' arms of recombination are also highlighted. Note the location of PCR primers used to genotype the mice: Primers cn2 – neo were used to amplify a 389 bp fragment from the mutant allele only; primers cn2 and cn3 amplify a 342 and 350 bp fragments from wild-type allele and 2 loxP allele, respectively; primers cn1 and cn3 amplify a 343 bp fragment once exon 2 has been deleted.

(c) Structure of the mutant allele after Flpe-mediated recombination. This recombination eliminates the neomycin cassette and leaves exon 2 flanked by 2 loxP sites.

(d) Southern blot analysis of 10 ES cell clones showing the presence of a 16 kb band in all samples and a smaller 7.4 kb fragment in clone 3H3.

(e) PCR analysis of progeny of 3 loxP mice crossed with FlpE mice giving rise to mice demonstrating a 350 bp fragment originating from the 2 loxP allele. Also shown is a PCR analysis of progeny of 2 loxP mice crossed with E2a-CRE mice giving rise to mice demonstrating a 343 bp fragment originating from the 1 loxP allele.

(f) Schematic for deletion of CB1 from plPFC projecting BLA neurons and expression of CaMKII-ChR2-eYFP in BLA projection neurons.

(g) Schematic for recording of BLA evoked oEPSCs in the Nucleus Accumbens (NAc) Shell

(h) Effect of CP55,940 on oEPSC amplitude at BLA-NAc shell synapses. WT and CB1$^{f/f}$ INTRSECT mice have equal sensitivity to CP55,940 induced depression of BLA evoked oEPSCs in the NAc shell (WT: n=6, N=3; CB1$^{f/f}$ n=6, N=2; p=0.6048).

All error bars represent ± SEM. "n" represents number of neurons, "N" represents number of mice. P values reported from two-tailed unpaired t-test (h).

CHAPTER III

Conclusions, Caveats, and Future Directions

A conserved pathophysiological mechanism driving anxious states

The lack of a pathophysiological understanding of stress and anxiety related disorders has stymied the development of novel therapeutic treatments for these conditions. Indeed, the rational design of new drugs is precluded by the fact that there are no discernable molecular or biological targets for many affective illnesses. Over the past decade, multiple human fMRI studies have attempted to unravel the neural basis for these disorders. These studies have strongly supported the role of amygdala-dmPFC circuit in threat processing in stressful situations. Additionally, hyperactivity within this circuit has been purported to serve as a biomarker anxiety disorders (Kalisch and Gerlicher, 2014; Robinson et al., 2012). In collaboration with the lab of Jenni Blackford, we corroborated this data by showing that the BLA *specifically* couples to the dPFC during exposure to threatening stimuli, and that the degree of coupling within this circuit correlates with trait ratings of anxiety (Appendix Figure 1)

Here, we expand upon this data using a translational mouse model of traumatic stress exposure. To first validate this model, we demonstrated that this stress paradigm elicited a robust anxiety-like phenotype in the EZM assay, measured 24 hours after stress exposure. It is important to note that anxiety in and of itself is not necessarily deleterious, as it promotes harm avoidance. Indeed, experiencing anxiety directly after a stressful event is biologically normal part of the stress response, and is important for promoting avoidance of the stressor. However, anxiety becomes maladaptive when it persists for longer periods of time or in appropriate

situations, to ultimately lead to negative emotional, cognitive, or behavioral outcomes. Thus, we decided to examine whether exposure to a single stressor elicited an anxiety-like behavioral outcome in a neutral environment (EZM) 24 hours after stressor cessation. As mentioned, mice continued to express an anxiety-like behavioral phenotype at this 24 time point, suggesting maladaptive anxiety. In the future, we will expand our study to understand whether this behavior persists over longer time periods.

It is important to note here that there are several caveats and drawbacks to the EZM. Firstly, it is a relatively rudimentary assay in that it primarily analyzes a binary behavior: either the mouse is in the open arms or not. Thus it is possible that we are missing other more complex indices of anxiety-like behavior in rodents. Furthermore, as with many anxiety tests in rodents, the EZM weighs two competing innate drives: foraging behavior and the desire to explore novel environments against the desire to avoid bright open spaces where the animal could be subject to predation. Assays like these have thus been collectively been described as inducing approach-avoidance conflict. A caveat to these assays (e.g. EZM) is that it is difficult to interpret, for example, whether an increase in open arm time is indicative of decreased anxiety, or an increased desire to explore novel environments. In the future, we hope to expand our behavioral repertoire to include alternative tests of rodent anxiety including marble burying or testing parameters of autonomic arousal.

These caveats notwithstanding, stress strongly decreased open arm time, suggestive of an anxiety-like phenotype. As previously mentioned, recent human research has suggested that increased amygdalo-cortical coupling could represent an etiological biomarker that underlies stress and anxiety related disorders. To further validate our translational model, we tested whether similar indices of amygdalo-cortical strengthening were elicited by our stress paradigm.

Here, we initially demonstrate that BLA projections to the plPFC are indeed activated by stress exposure using *in vivo* fiber photometry. There are however, a number of caveats to this approach as well. Firstly, given the size of the lens, we are most likely picking up fluorescence signal from BLA terminals impinging on both L2/3 and L5. Therefore it is difficult to determine whether the fluorescence change we see with fiberphotometry is due to increased BLA terminal activity in L2/3 or 5. This is an important point, due to the fact that the persistent stress-induced increase in amygdalo-cortical strengthening is only observed in L2/3. In the future, it may be possible, using layer specific Cre driver lines and intersectional genetic strategies, to decipher whether there BLA input is being preferentially routed to distinct cortical lamina during stress exposure.

While these data demonstrate that BLA input to the plPFC is potentiated during stress, it does not necessarily show that the activity of plPFC neurons themselves are altered by stress exposure. To address this, we used a combination of fiber photometry and miniendoscopy to directly monitor the activity of these neurons during the stressor. These data demonstrate, that while the overall activity of the plPFC is enhanced by stress exposure, there is a significant population of neurons that are inhibited by stress exposure. Our investigation of the BLA-plPFC circuit focused primarily on the stress-activated neuronal population, and thus we admittedly understand that this may only represent a portion of the picture. Additionally, it is highly probable that the stress-induced activity of plPFC neurons is influenced by multiple extrinsic and intrinsic connections, not just by projections from the BLA. In the future, we hope to determine whether the stress-induced activation of plPFC neurons is directly driven by BLA input by using circuit specific inhibition of BLA-plPFC projections, combined with miniendoscopy. If the stress-induced activation of plPFC neurons is primarily driven by BLA excitatory input, we

would expect that inhibition of this input would decrease stress induced plPFC neuronal firing. However, the data that we have generated thus far does clearly demonstrate that stress increases the activity of a large proportion of plPFC neurons, and that the stress-induced excitatory neural responses outweigh the inhibitory responses. Our fiberphotometry and endoscopy data demonstrate that in rodents, similar to humans, stress exposure activates BLA projections to the PL (Robinson et al., 2012) as well as PL neurons themselves (Kalisch and Gerlicher, 2014), suggesting significant functional homology within this circuit between rodents and humans.

A drawback to the numerous human studies investigating this circuit is that most of these studies are unable to draw causal inferences between activity in the amygdala-dmPFC circuit and the behaviors it is purported linked to. Here, we used a chemogenetic strategy to specifically manipulate the activity of BLA neurons that project to the plPFC. We first demonstrated that this strategy led to activation not only of BLA neurons, but also plPFC neurons that receive excitatory input from these neurons. Furthermore, chemogenetic activation of these neurons induced a similar behavioral phenotype as stress exposure. Thus, our chemogenetic strategy phenocopied aspects of both the behavioral and neural effects of stress exposure, i.e. activation of the BLA-plPFC circuit. These data suggest that stress could be inducing its anxiogenic effects through activation of the BLA-plPFC circuit. As previously mentioned, in the future, we hope to conclusively test this by examining whether inhibition of this circuit can reverse the behavioral and physiological effects of stress exposure. Given that our data closely mirrors the human data investigating the role of this circuit in promoting and upholding the anxious state, we suggest that activity in this circuit could serve as an etiological biomarker for stress and anxiety related disorders. Furthermore, we suggest that monitoring activity in this circuit could represent a

diagnostic tool for probing the efficacy of pharmacological or cognitive behavioral interventions for anxiety disorders.

As we observed a significant anxiety-like phenotype at 24 hours post-stress exposure, we also used this time point to determine whether there were persistent changes in amygdalo-cortical functioning that tracked with the behavioral change. As previously mentioned, we saw an increase in presynaptic excitatory input from the BLA specifically to layer 2/3 neurons. We found this interesting for multiple reasons. Firstly, many studies examining projections mPFC remain agnostic to the cortical lamina they are recording from. It was well known that the different lamina have unique projecting targets and engage in unique functions. While layer 5 projects most strongly to subcortical and brainstem targets, L2/3 is primarily involved in cortico-cortical communication and communication with other forebrain structures. The fact that we observed an increase in excitatory input specifically to L2/3 suggests that the BLA is capable of routing different information to the different cortical lamina. Our data, in combination with previous studies, suggests that the BLA routes negatively valenced information specifically to the superficial cortical lamina (Kim et al., 2016); in our case this negatively valenced information relates to the stressor. In the future, it would be interesting to examine what information the BLA routes to the deeper cortical layers. For example, it is tempting to speculate that it could send information relating to environmental cues, such as tones that predict footshock stress in cued fear conditioning, as both the BLA and PL appear to be integral to this type of conditioned emotional learning.

We further demonstrate that this stress specifically enhances excitatory input from the BLA to L2/3 neurons that send reciprocal projections back to the BLA. We suggest that this amygdalo-cortical strengthening is involved in promoting and upholding anxious states,

96

conceptually similar to the fMRI data in humans (Robinson et al., 2012). One important caveat is that although we know the projection target of the rAAV positive neurons we recorded from, we can not make any definitive conclusions about the projection target of the rAAV negative neurons. To ameliorate this issue, we conducted another set of experiments in which a virus driving the expression of ChR2 was put in the BLA, but the rAAV was introduced into the contralateral plPFC. This allowed us to investigate whether BLA input to contralateral plPFC projecting L2/3 neurons was also modulated by stress exposure. Interestingly, we saw a significant reduction in excitatory input to these neurons, coupled with a significant increase in the PPR, suggesting a lower release probability (Appendix figure 2). These data suggest that while BLA input to plPFC neurons that project back to the BLA is strengthened, BLA input to plPFC neurons that project to other cortical areas is weakened. In the future, it will be interesting to follow up on these studies to determine what role this shift in input bias plays in driving stress-related behaviors.

One noted limitation of our study is that we focused primarily on excitatory responses in glutamatergic projection neurons. Indeed, stress exposure has been shown to dynamically modulate the activity of a variety of different GABAergic interneuron populations within the mPFC(Girgenti et al., 2019; Holland et al., 2014). Furthermore, stress susceptibility has been demonstrated to be associated with decreased excitatory input on the Parvalbumin expressing interneurons in the mPFC(Perova et al., 2015). This, coupled with prior studies and our data showing that excitatory input from the BLA drives feedforward inhibition onto excitatory neurons in the mPFC, suggests that stress exposure may similarly alter BLA input onto inhibitory interneurons(McGarry and Carter, 2016). In the future, we hope to investigate how

stress alters BLA input on both excitatory and inhibitory neurons in the mPFC, as this is an acknowledged drawback of our study.

Our investigation of BLA input the mPFC has primarily focused on projections to the plPFC. It should be noted, however, that the BLA also sends dense excitatory projections to the ilPFC. As previously discussed, the ilPFC appears to play an opposing role to the plPFC in many fear related and anxiety states in both rodents and humans. Thus, we expected that stress would induce opposite or divergent effects on BLA input to the ilPFC. To test this, we used a similar experimental paradigm as previously described, but recorded in the ilPFC instead of the plPFC. Contrary to what we expected, we found that stress exposure also significantly increased excitatory input to L2/3 ilPFC cells that project back to the BLA. This again corresponded with a significant reduction in the PPR (Appendix figure 3). However, we also observed a significant increase in excitatory input to L2/3 ilPFC neurons that do not project back to the BLA (rAAV negative). We additionally found the L5 rAAV positive neurons also exhibited significantly decreased PPR following stress. These data were quite surprising to us, as previous literature suggests that the ilPFC plays an opposing role to the plPFC, and we thus expected to see the opposite change. These data suggest that the boundary between the ilPFC and plPFC may not be as clearly defined in reference to stress-related physiological and behavioral changes. Instead, we posit that unique information regarding the stressor could be preferentially routed to the superficial layers of the mPFC as a whole (rather than being segregated to the ilPFC or plPFC), and that lasting strengthening of this input could promote anxious states following stress. However, these data are highly preliminary and future studies will be necessary to understand whether there are unique functional roles of BLA projections to the superficial and deeper cortical layers.

Input and cell type-specific eCB signaling in the plPFC

Given the stress-induced change in presynaptic release probability we observed (in both plPFC and ilPFC), we hypothesized this change could be due an attenuation of eCB regulation of BLA input. We first examined whether excitatory input from the BLA was regulated by eCB signaling using pharmacological approaches. As mentioned above, 2-AG-CB1 signaling strongly regulates BLA glutamatergic input. This appeared to occur in an input specific manner, as input from the MDT was not sensitive to application of CB1 agonist, nor did we observe significant DSE. We further examined excitatory input from the vHIPP, and observed that, much like input from the BLA, this input was highly regulated by CB1 signaling, as CP55,940 application strongly depressed oEPSC amplitude (Appendix figure 4). Interestingly, we were not able to evoke significant DSE at this input, which was quite surprising to us, given the potent regulation of this input by CB1 signaling. This suggests that there could be mechanistically distinct modes of eCB regulation of different excitatory inputs to the plPFC. For example, perhaps eCB regulation of input from the vHIPP may require concomitant GqGPCR receptor stimulation to induce 2-AG release. However, this is purely speculative, and further experiments will be required to test this hypothesis. Regardless, we observed three highly distinct modes of eCB regulation of excitatory signaling, depending on the source of the glutamatergic input: BLA: CP55,940 sensitive, robust DSE; vHIPP: CP55,940 sensitive, no DSE; DMT: CP55,940 insensitive, no DSE.

It should also be noted that even when solely examining BLA input to the plPFC, there are significant laminar differences as to 2-AG regulation of glutamatergic signaling. For example, although we observed DSE uniformly across the L2/3 neurons we recorded from, we

only observed DSE in L5 neurons that projected back to the BLA, and not in the rAAV-negative neurons. Similar to the lack of DSE we observed at vHIPP inputs to the plPFC, this suggests that 2-AG mobilization requires different stimuli and perhaps unique machinery depending on the neural population being recorded from.

2-AG signaling collapse as a translationally relevant mechanism driving stress-induced amygdalo-cortical strengthening

Given that stress induced a significant reduction in the PPR at L2/3 rAAV-positive neurons and that BLA input is highly regulated by 2-AG signaling, we tested whether this stress-induced change in presynaptic release was due to impaired 2-AG signaling. As previously mentioned above, using pharmacological and genetic tools, we demonstrated that stress induced a collapse of both tonic and phasic 2-AG regulation of excitatory input from the BLA. This effect did not seem to be stress modality-specific, as predator odor stress induced similar changes. However, tonic and phasic 2-AG signaling were not always perfectly correlated. For example, in female mice, stress exposure impaired tonic but not phasic 2-AG signaling. Similarly, 0.25 mA footshock stress impaired tonic but not phasic 2-AG signaling, and the phasic component of 2-AG signaling recovered more quickly than the tonic component following 0.5 mA footshock stress. These data suggest that there are most likely mechanistically distinct molecular pathways that drive tonic and phasic 2-AG signaling. Phasic 2-AG signaling in the form of DSE is well known to be driven primarily by calcium influx, while recent studies have suggested that tonic 2-AG signaling could be driven by GqGPCRs, such as the muscarinic acetylcholine receptor (MAchR) (Ramikie et al., 2014). Therefore, it is conceivable that calcium driven 2-AG release is less sensitive to stress-induced impairment than the tonic component

100

driven by GqGPCR signaling. In the future, it will be interesting to mechanistically dissect the machinery that drives tonic and phasic 2-AG signaling in the plPFC. Furthermore, we hope to probe whether tonic and phasic 2-AG signaling regulate distinct behaviors or affective states at the organismal level.

Although our physiology experiments clearly demonstrate that stress induces a collapse of 2-AG regulation of excitatory input from the BLA, it does not reveal whether 2-AG signaling collapse is causally related to stress-induced affective pathology. As previously mentioned, we first demonstrated that plPFC 2-AG depletion, accomplished through conditional DAGL deletion, phenocopied the synaptic and behavioral effects of stress exposure, strongly supporting a role for 2-AG signaling collapse in driving stress-induced affective pathology. However, this approach did come with multiple caveats. Firstly, to delete DAGL, we used a Cre virus driven by the CMV promoter. This will lead to deletion of DAGL not only in neurons, but also in astrocytes and microglia. It has been demonstrated that both astrocytes and microglia express components of the eCB system, and play an integral but unique role in eCB signaling (Navarrete et al., 2014). Therefore, knocking DAGL out of these populations could contribute the anxiety-like phenotype we observe. Furthermore, this approach will lead to removal of DAGL indiscriminately from plPFC neurons, both excitatory and inhibitory populations. Therefore, it is difficult to disentangle what neural populations are driving the behavioral effect we observe. In the future, we hope to ameliorate these concerns by using the INTRSECT approach to specifically delete DAGL from plPFC neurons that project to the BLA. This could be accomplished by using a DAGL f/f mouse and putting a retrograde Flp virus in the BLA, and a Flp dependent Cre virus in the plPFC, which should ostensibly lead to selective DAGL deletion from BLA projecting plPFC neurons. Despite our lack of cellular resolution, our data still

demonstrate a crucial role of prefrontocortical 2-AG signaling in regulating anxiety-like behavior, and suggest that stress could be eliciting its anxiogenic effects through impairing this signaling system.

To enhance our circuit level understanding of BLA-plPFC eCB signaling, we used the INTRSECT approach to determine whether CB1 deletion from plPFC projecting BLA neurons was similarly able to recapitulate the anxiogenic effects of stress exposure. As discussed above, this did not elicit any behavioral effects at baseline. This was surprising, given that we have previously demonstrated that activation of the BLA-plPFC circuit is anxiogenic, and that we have pharmacologically shown that impairing CB1 regulation of this projection increases excitatory input to the plPFC. However, we observed that following stress exposure, mice that had CB1 deleted from the BLA-plPFC projection were significantly more susceptible to the anxiogenic effects of stress exposure than their control littermates. One explanation for these results is that, under a basal non-stressed state, the BLA-plPFC circuit is relatively quiescent, and thus CB1 does not play a crucial role in attenuating its activity. However, we have shown that stress exposure directly leads to activation of the BLA-plPFC circuit. Thus, following stress induced activation of this circuit, CB1 plays a crucial role in regulating and dampening BLA input. Removal of this negative feedback system then results in enhanced stress-induced anxiety like behavior.

Translational potential and application for human studies

Although there have been a myriad of studies examining how stress can alter the physiology and function of numerous brain areas, how these changes are causally related to stress-induced affective pathology are still unclear. Overall, a primary goal of this work was to

gain a better understand of the pathophysiological link between stress exposure and the development of anxious states. Here we describe a mechanism by which circuit-specific eCB signaling collapse could represent a causative link driving anxiety-like behavior after stress. We hope that this data furthers the support for the development of drugs targeting the eCB system for the treatment of affective disorders. For example, a clinical MAGL inhibitor is in phase 2 trials for CNS disorders currently. Our data build on previous preclinical work to further support the therapeutic potential of MAGL inhibitors for stress and trauma-related disorders. Importantly, our central finding that MAGL inhibition reverses stress-induced anxiety-like behavior and synaptic strengthening in the BLA-dmPFC circuit, combined with previous studies demonstrating enhanced amygdala-dmPFC coupling in humans with anxiety disorders, provide a potential approach to test candidate circuit engagement by clinical MAGL inhibitors to facilitate clinical trials advancement and patient selection. For example, determining whether MAGL inhibition reduces BLA-dmPFC coupling in humans, as it does in mice, could support the advancement of MAGL inhibitors for anxiety and stress-related disorders. If confirmed, this could also allow for optimal patient selection or stratification based upon the degree of BLA-dmPFC coupling exhibited prior to study entry. Both would allow for intermediate, smaller scale de-risking trials, prior to large-scale clinical efficacy trials.

Appendix
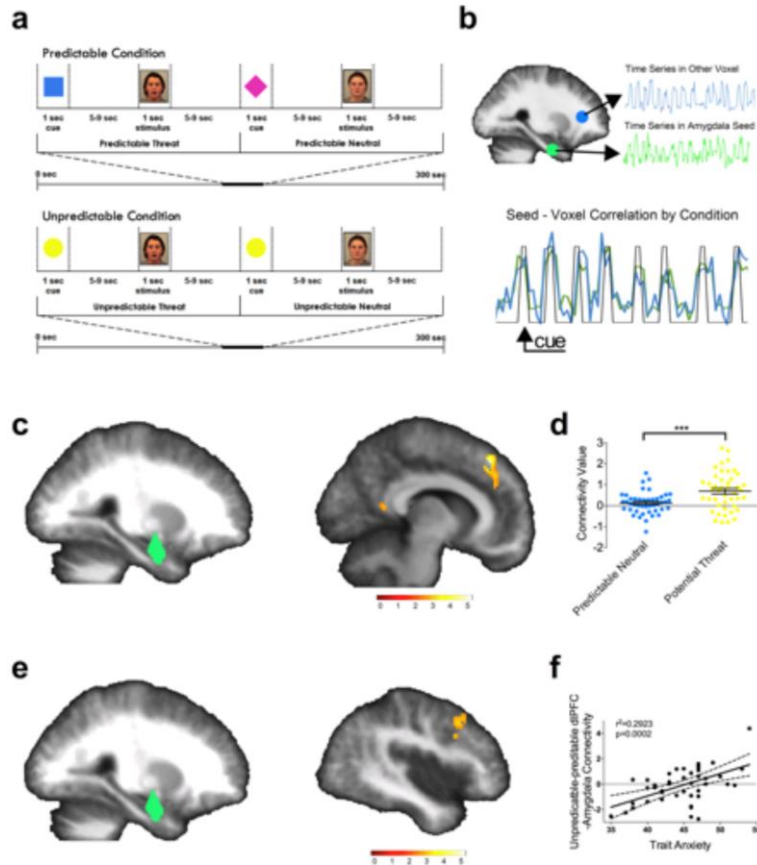
Figure A1. Threat and stress engage an amygdalo-cortical circuit in humans
(a) Schematic of fMRI cued anticipation task
(b) Schematic diagram showing task-based functional connectivity with an amygdala seed and an example of connectivity with a voxel in another brain region (top) modulated by condition (bottom). The color bar reflects t values.
(c) During unpredictable threat cues, the BLA seed (green) shows significant connectivity with the dmPFC (peak voxel x = -12, y = 32, z = 44, t = 5.48, k = 286, p < .05, cluster corrected). The color bar reflects t values.
(d) Dot plots illustrate significantly increased BLA-dmPFC connectivity for the unpredictable threat cue and predictable neutral cue conditions (Cohen's d = 1.38, p < .0001).
(e) Trait anxiety is correlated with enhanced BLA-dlPFC connectivity (peak voxel: x = 48, y = 16, z = 30, t = 3.85, k = 155; P < .05, cluster corrected). The color bar reflects t values.

(f) The scatterplot illustrates the correlation between trait anxiety and the connectivity values from the significant dlPFC cluster (r^2=0.2923, p=0.0002).

All error bars represent ± SEM.   "N" represents number of mice. P values reported from two-tailed unpaired t-tests (d,j,l)
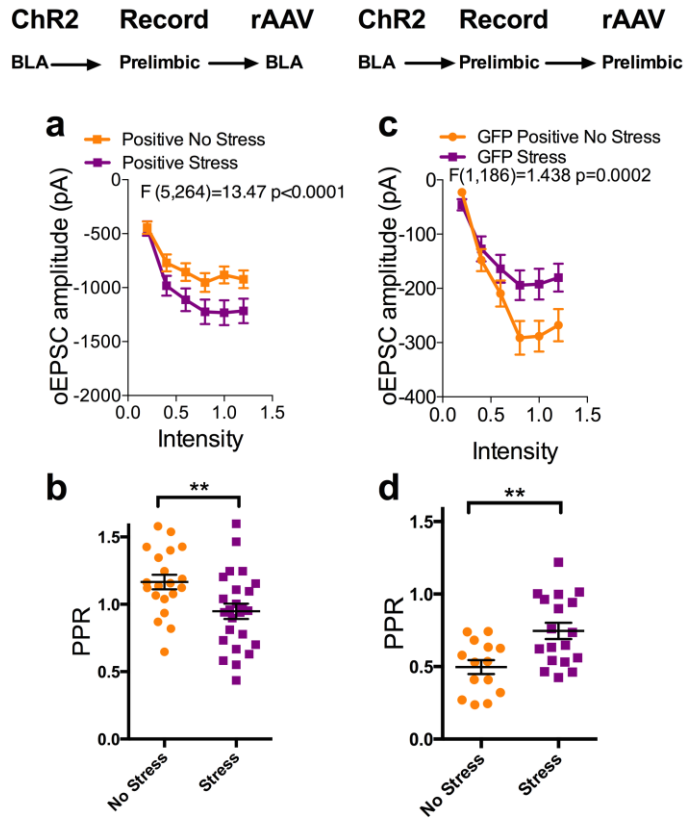
Figure A2: Effect of stress on BLA input to BLA projecting and contralateral plPFC projecting plPFC neurons

   (a) Optically-evoked input/output curve from L2/3 plPFC neurons that project back to the BLA from non-stressed (n=21; N=8) and stressed (n=27; N=10 mice) mice. Stress exposure enhances excitatory input to L2/3 plPFC neurons that project to the BLA.
   (b) Effects of stress on Paired Pulse Ratio (PPR) at BLA-L2/3 plPFC-BLA synapses (No Stress: n=21, N=8, Stress: n=27, N=10). Stress exposure decreases PPR at BLA-L2/3 plPFC-BLA synapses (p=0.0023).
   (c) Optically-evoked input/output curve from L2/3 plPFC neurons that project to the contralateral plPFC (n=15; N=4) and stressed (n=18; N=4 mice) mice. Stress exposure decreases excitatory input to L2/3 plPFC neurons that project to the contralateral plPFC.
   (d) Effects of stress on Paired Pulse Ratio (PPR) at BLA-L2/3 plPFC-plPFC synapses (No Stress: n=21, N=8, Stress: n=27, N=10). Stress exposure increases PPR at BLA-L2/3 plPFC-plPFC synapses (p=0.0041).

   All error bars represent ± SEM. "n" represents number of neurons, "N" represents number of mice. P values reported from two-tailed unpaired t-test (b,d). F and P values for two-way ANOVA shown in relevant panels.
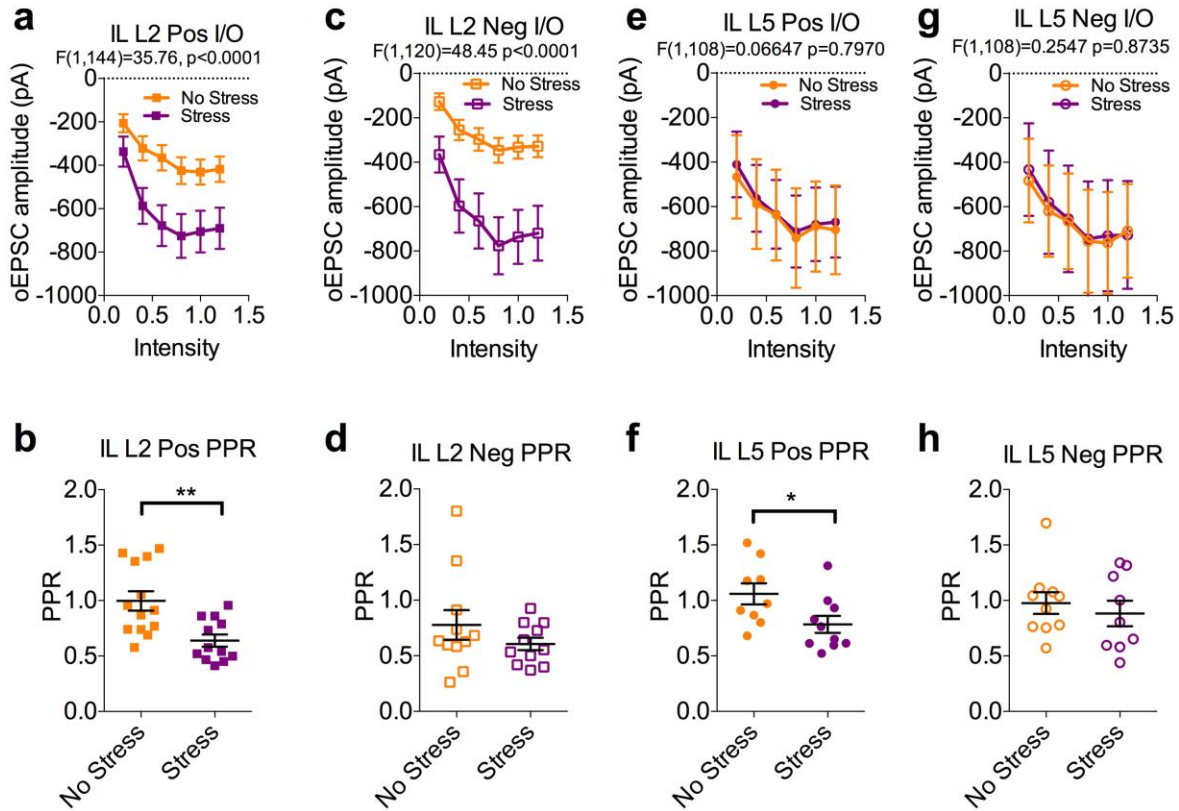
Figure A3: Stress exposure enhances excitatory input from the BLA to L2/3 ilPFC

    (a) Optically-evoked input/output curve from ilPFC L2/3 rAAV-positive neurons from non-stressed (n=13; N=4) and stressed (n=12; N=4 mice) mice. Stress exposure enhances excitatory input to ilPFC L2/3 rAAV- positive neurons.

    (b) Effects of stress on Paired Pulse Ratio (PPR) at BLA-L2/3 ilPFC rAAV-positive synapses (No Stress: n=13, N=4, Stress: n=12, N=4). Stress exposure decreases PPR at BLA-L2/3 ilPFC rAAV-positive synapses.

    (c) Optically-evoked input/output curve from ilPFC L2/3 rAAV-negative neurons from non-stressed (n=11, N=4) and stressed (n=11, N=4) mice. Stress exposure enhances excitatory input to ilPFC L2/3 rAAV-negative neurons.

    (d) Effects of stress on Paired Pulse Ratio (PPR) at BLA-L2/3 ilPFC rAAV-negative synapses (No Stress: n=11, N=4, Stress: n=11, N=4). Stress exposure does not alter PPR at BLA-L2/3 ilPFC rAAV-negative synapses.

    (e) Optically-evoked input/output curve from ilPFC L5 rAAV-positive neurons from non-stressed (n=9; N=4) and stressed (n=10; N=4 mice) mice. Stress exposure does not alter excitatory input to ilPFC L5 rAAV- positive neurons.

    (f) Effects of stress on Paired Pulse Ratio (PPR) at BLA-L5 ilPFC rAAV-positive synapses (No Stress: n=9, N=4, Stress: n=10, N=4). Stress exposure decreases PPR at BLA-L5 ilPFC rAAV-positive synapses.

    (g) Optically-evoked input/output curve from ilPFC L5 rAAV-negative neurons from non-stressed (n=10, N=4) and stressed (n=9, N=4) mice. Stress exposure does not alter excitatory input to ilPFC L5 rAAV-negative neurons.

(h) Effects of stress on Paired Pulse Ratio (PPR) at BLA-L5 ilPFC rAAV-negative synapses (No Stress: n=10, N=4, Stress: n=9, N=4). Stress exposure does not alter PPR at BLA-L5 ilPFC rAAV-negative synapses.

All error bars represent ± SEM. "n" represents number of neurons, "N" represents number of mice. P values reported from two-tailed unpaired t-test (b,d,f,h). F and P values for two-way ANOVA shown in relevant panels.
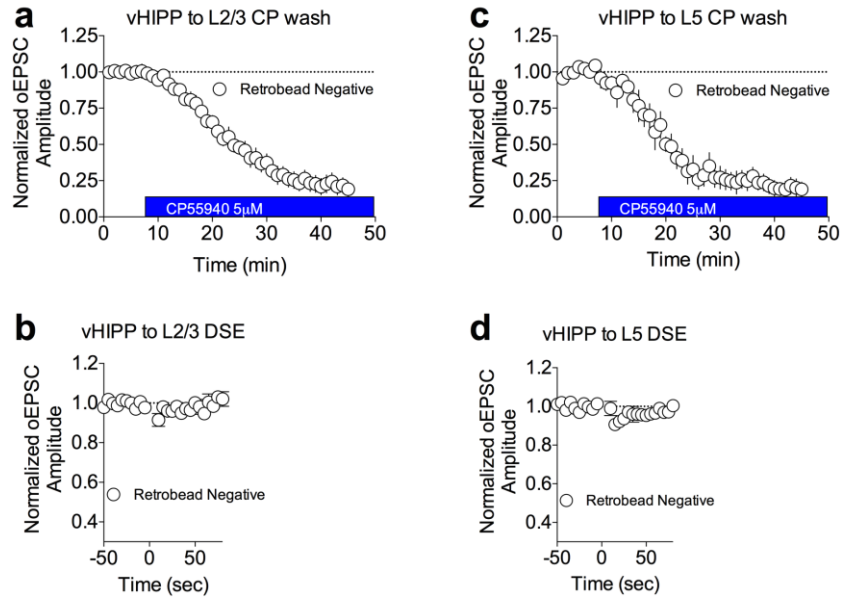
Excitatory input from the vHIPP to the plPFC is regulated by CB1 signaling

   (a) Effect of 5 μM CP55,940 on oEPSC amplitude at vHIPP-L2/3 plPFC retrobead-negative synapses (n=10, N=4).

   (b) DSE is not present at vHIPP-L2/3 plPFC retrobead-negative synapses (n=12, N=4).

   (c) Effect of 5 μM CP55,940 on oEPSC amplitude at vHIPP-L2/3 plPFC retrobead-negative synapses (n=5, N=3).

   (d) DSE is not present at vHIPP-L5 plPFC retrobead-negative synapses (n=11, N=4).

All error bars represent ± SEM. "n" represents number of neurons, "N" represents number of mice.

REFERENCES

(2017). In The Health Effects of Cannabis and Cannabinoids: The Current State of Evidence and Recommendations for Research (Washington (DC)).

Abbott, A. (2011). Novartis to shut brain research facility. Nature *480*, 161-162.

Adhikari, A., Lerner, T.N., Finkelstein, J., Pak, S., Jennings, J.H., Davidson, T.J., Ferenczi, E., Gunaydin, L.A., Mirzabekov, J.J., Ye, L.*, et al.* (2015). Basomedial amygdala mediates top-down control of anxiety and fear. Nature *527*, 179-185.

Ahn, K., Johnson, D.S., Mileni, M., Beidler, D., Long, J.Z., McKinney, M.K., Weerapana, E., Sadagopan, N., Liimatta, M., Smith, S.E.*, et al.* (2009). Discovery and characterization of a highly selective FAAH inhibitor that reduces inflammatory pain. Chem Biol *16*, 411-420.

Akana, S.F., Chu, A., Soriano, L., and Dallman, M.F. (2001). Corticosterone exerts site-specific and state-dependent effects in prefrontal cortex and amygdala on regulation of adrenocorticotropic hormone, insulin and fat depots. J Neuroendocrinol *13*, 625-637.

Aliczki, M., Barna, I., Till, I., Baranyi, M., Sperlagh, B., Goldberg, S.R., and Haller, J. (2016). The effects anandamide signaling in the prelimbic cortex and basolateral amygdala on coping with environmental stimuli in rats. Psychopharmacology (Berl) *233*, 1889-1899.

Amano, T., Duvarci, S., Popa, D., and Pare, D. (2011). The fear circuit revisited: contributions of the basal amygdala nuclei to conditioned fear. J Neurosci *31*, 15481-15489.

Anderson, A.K., and Phelps, E.A. (2001). Lesions of the human amygdala impair enhanced perception of emotionally salient events. Nature *411*, 305-309.

Anderson, G.R., Aoto, J., Tabuchi, K., Foldy, C., Covy, J., Yee, A.X., Wu, D., Lee, S.J., Chen, L., Malenka, R.C.*, et al.* (2015). beta-Neurexins Control Neural Circuits by Regulating Synaptic Endocannabinoid Signaling. Cell *162*, 593-606.

Antoni, F.A. (1986). Hypothalamic control of adrenocorticotropin secretion: advances since the discovery of 41-residue corticotropin-releasing factor. Endocr Rev *7*, 351-378.

Apps, R., and Strata, P. (2015). Neuronal circuits for fear and anxiety - the missing link. Nat Rev Neurosci *16*, 642.

Arnsten, A.F. (2009). Stress signalling pathways that impair prefrontal cortex structure and function. Nat Rev Neurosci *10*, 410-422.

Arnsten, A.F. (2015). Stress weakens prefrontal networks: molecular insults to higher cognition. Nat Neurosci *18*, 1376-1385.

Arnsten, A.F., Wang, M.J., and Paspalas, C.D. (2012). Neuromodulation of thought: flexibilities and vulnerabilities in prefrontal cortical network synapses. Neuron *76*, 223-239.

Baggelaar, M.P., Chameau, P.J., Kantae, V., Hummel, J., Hsu, K.L., Janssen, F., van der Wel, T., Soethoudt, M., Deng, H., den Dulk, H.*, et al.* (2015). Highly Selective, Reversible Inhibitor Identified by Comparative Chemoproteomics Modulates Diacylglycerol Lipase Activity in Neurons. J Am Chem Soc *137*, 8851-8857.

Ball, S.G., Kuhn, A., Wall, D., Shekhar, A., and Goddard, A.W. (2005). Selective serotonin reuptake inhibitor treatment for generalized anxiety disorder: a double-blind, prospective comparison between paroxetine and sertraline. J Clin Psychiatry *66*, 94-99.

Ballenger, J.C., Burrows, G.D., DuPont, R.L., Jr., Lesser, I.M., Noyes, R., Jr., Pecknold, J.C., Rifkin, A., and Swinson, R.P. (1988). Alprazolam in panic disorder and agoraphobia: results from a multicenter trial. I. Efficacy in short-term treatment. Arch Gen Psychiatry *45*, 413-422.

Bambico, F.R., Katz, N., Debonnel, G., and Gobbi, G. (2007). Cannabinoids elicit antidepressant-like behavior and activate serotonergic neurons through the medial prefrontal cortex. J Neurosci *27*, 11700-11711.

Battle, D.E. (2013). Diagnostic and Statistical Manual of Mental Disorders (DSM). Codas *25*, 191-192.

Bedse, G., Hartley, N.D., Neale, E., Gaulden, A.D., Patrick, T.A., Kingsley, P.J., Uddin, M.J., Plath, N., Marnett, L.J., and Patel, S. (2017). Functional Redundancy Between Canonical Endocannabinoid Signaling Systems in the Modulation of Anxiety. Biol Psychiatry *82*, 488-499.

Bereza, B.G., Machado, M., and Einarson, T.R. (2009). Systematic review and quality assessment of economic evaluations and quality-of-life studies related to generalized anxiety disorder. Clin Ther *31*, 1279-1308.

Beyeler, A., Chang, C.J., Silvestre, M., Leveque, C., Namburi, P., Wildes, C.P., and Tye, K.M. (2018). Organization of Valence-Encoding and Projection-Defined Neurons in the Basolateral Amygdala. Cell Rep *22*, 905-918.

Beyeler, A., Namburi, P., Glober, G.F., Simonnet, C., Calhoon, G.G., Conyers, G.F., Luck, R., Wildes, C.P., and Tye, K.M. (2016). Divergent Routing of Positive and Negative Information from the Amygdala during Memory Retrieval. Neuron *90*, 348-361.

Bhatnagar, S., Vining, C., and Denski, K. (2004). Regulation of chronic stress-induced changes in hypothalamic-pituitary-adrenal activity by the basolateral amygdala. Ann N Y Acad Sci *1032*, 315-319.

Blanco, C., Schneier, F.R., Schmidt, A., Blanco-Jerez, C.R., Marshall, R.D., Sanchez-Lacay, A., and Liebowitz, M.R. (2003). Pharmacological treatment of social anxiety disorder: a meta-analysis. Depress Anxiety *18*, 29-40.

Blankman, J.L., Simon, G.M., and Cravatt, B.F. (2007). A comprehensive profile of brain enzymes that hydrolyze the endocannabinoid 2-arachidonoylglycerol. Chem Biol *14*, 1347-1356.

Bluett, R.J., Baldi, R., Haymer, A., Gaulden, A.D., Hartley, N.D., Parrish, W.P., Baechle, J., Marcus, D.J., Mardam-Bey, R., Shonesy, B.C.*, et al.* (2017). Endocannabinoid signalling modulates susceptibility to traumatic stress exposure. Nat Commun *8*, 14782.

Bortolato, M., Mangieri, R.A., Fu, J., Kim, J.H., Arguello, O., Duranti, A., Tontini, A., Mor, M., Tarzia, G., and Piomelli, D. (2007). Antidepressant-like activity of the fatty acid amide hydrolase inhibitor URB597 in a rat model of chronic mild stress. Biol Psychiatry *62*, 1103-1110.

Bosch-Bouju, C., Larrieu, T., Linders, L., Manzoni, O.J., and Laye, S. (2016). Endocannabinoid-Mediated Plasticity in Nucleus Accumbens Controls Vulnerability to Anxiety after Social Defeat Stress. Cell Rep *16*, 1237-1242.

Burgos-Robles, A., Kimchi, E.Y., Izadmehr, E.M., Porzenheim, M.J., Ramos-Guasp, W.A., Nieh, E.H., Felix-Ortiz, A.C., Namburi, P., Leppla, C.A., Presbrey, K.N.*, et al.* (2017). Amygdala inputs to prefrontal cortex guide behavior amid conflicting cues of reward and punishment. Nat Neurosci *20*, 824-835.

Burgos-Robles, A., Vidal-Gonzalez, I., and Quirk, G.J. (2009). Sustained conditioned responses in prelimbic prefrontal neurons are correlated with fear expression and extinction failure. J Neurosci *29*, 8474-8482.

Burgos-Robles, A., Vidal-Gonzalez, I., Santini, E., and Quirk, G.J. (2007). Consolidation of fear extinction requires NMDA receptor-dependent bursting in the ventromedial prefrontal cortex. Neuron *53*, 871-880.

Busquets-Garcia, A., Puighermanal, E., Pastor, A., de la Torre, R., Maldonado, R., and Ozaita, A. (2011). Differential role of anandamide and 2-arachidonoylglycerol in memory and anxiety-like responses. Biol Psychiatry *70*, 479-486.

Cadas, H., di Tomaso, E., and Piomelli, D. (1997). Occurrence and biosynthesis of endogenous cannabinoid precursor, N-arachidonoyl phosphatidylethanolamine, in rat brain. J Neurosci *17*, 1226-1242.

Cadogan, A.K., Alexander, S.P., Boyd, E.A., and Kendall, D.A. (1997). Influence of cannabinoids on electrically evoked dopamine release and cyclic AMP generation in the rat striatum. J Neurochem *69*, 1131-1137.

Calhoon, G.G., and Tye, K.M. (2015). Resolving the neural circuits of anxiety. Nat Neurosci *18*, 1394-1404.

Carlisi, C.O., and Robinson, O.J. (2018). The role of prefrontal-subcortical circuitry in negative bias in anxiety: Translational, developmental and treatment perspectives. Brain Neurosci Adv *2*, 2398212818774223.

Cavener, V.S., Gaulden, A., Pennipede, D., Jagasia, P., Uddin, J., Marnett, L.J., and Patel, S. (2018). Inhibition of Diacylglycerol Lipase Impairs Fear Extinction in Mice. Front Neurosci *12*, 479.

Cerqueira, J.J., Mailliet, F., Almeida, O.F., Jay, T.M., and Sousa, N. (2007). The prefrontal cortex as a key target of the maladaptive response to stress. J Neurosci *27*, 2781-2787.

Chanda, D., Neumann, D., and Glatz, J.F.C. (2019). The endocannabinoid system: Overview of an emerging multi-faceted therapeutic target. Prostaglandins Leukot Essent Fatty Acids *140*, 51-56.

Ciocchi, S., Herry, C., Grenier, F., Wolff, S.B., Letzkus, J.J., Vlachos, I., Ehrlich, I., Sprengel, R., Deisseroth, K., Stadler, M.B., *et al.* (2010). Encoding of conditioned fear in central amygdala inhibitory circuits. Nature *468*, 277-282.

Cook, S.C., and Wellman, C.L. (2004). Chronic stress alters dendritic morphology in rat medial prefrontal cortex. J Neurobiol *60*, 236-248.

Corcoran, K.A., and Quirk, G.J. (2007). Activity in prelimbic cortex is necessary for the expression of learned, but not innate, fears. J Neurosci *27*, 840-844.

Coutts, A.A., and Pertwee, R.G. (1997). Inhibition by cannabinoid receptor agonists of acetylcholine release from the guinea-pig myenteric plexus. Br J Pharmacol *121*, 1557-1566.

Craske, M.G., Stein, M.B., Eley, T.C., Milad, M.R., Holmes, A., Rapee, R.M., and Wittchen, H.U. (2017). Anxiety disorders. Nat Rev Dis Primers *3*, 17024.

Cravatt, B.F., Giang, D.K., Mayfield, S.P., Boger, D.L., Lerner, R.A., and Gilula, N.B. (1996). Molecular characterization of an enzyme that degrades neuromodulatory fatty-acid amides. Nature *384*, 83-87.

Cremers, H.R., Demenescu, L.R., Aleman, A., Renken, R., van Tol, M.J., van der Wee, N.J., Veltman, D.J., and Roelofs, K. (2010). Neuroticism modulates amygdala-prefrontal connectivity in response to negative emotional facial expressions. Neuroimage *49*, 963-970.

Cui, G., Jun, S.B., Jin, X., Pham, M.D., Vogel, S.S., Lovinger, D.M., and Costa, R.M. (2013). Concurrent activation of striatal direct and indirect pathways during action initiation. Nature *494*, 238-242.

Cullinan, W.E., Herman, J.P., Battaglia, D.F., Akil, H., and Watson, S.J. (1995). Pattern and time course of immediate early gene expression in rat brain following acute stress. Neuroscience *64*, 477-505.

Cuthbert, B.N., and Insel, T.R. (2010). Toward new approaches to psychotic disorders: the NIMH Research Domain Criteria project. Schizophr Bull *36*, 1061-1062.

Cuthbert, B.N., and Insel, T.R. (2013). Toward the future of psychiatric diagnosis: the seven pillars of RDoC. BMC Med *11*, 126.

Dayas, C.V., Buller, K.M., Crane, J.W., Xu, Y., and Day, T.A. (2001). Stressor categorization: acute physical and psychological stressors elicit distinctive recruitment patterns in the amygdala and in medullary noradrenergic cell groups. Eur J Neurosci *14*, 1143-1152.

Devane, W.A., Hanus, L., Breuer, A., Pertwee, R.G., Stevenson, L.A., Griffin, G., Gibson, D., Mandelbaum, A., Etinger, A., and Mechoulam, R. (1992). Isolation and structure of a brain constituent that binds to the cannabinoid receptor. Science *258*, 1946-1949.

Di, S., Boudaba, C., Popescu, I.R., Weng, F.J., Harris, C., Marcheselli, V.L., Bazan, N.G., and Tasker, J.G. (2005). Activity-dependent release and actions of endocannabinoids in the rat hypothalamic supraoptic nucleus. J Physiol *569*, 751-760.

Dinh, T.P., Carpenter, D., Leslie, F.M., Freund, T.F., Katona, I., Sensi, S.L., Kathuria, S., and Piomelli, D. (2002). Brain monoglyceride lipase participating in endocannabinoid inactivation. Proc Natl Acad Sci U S A *99*, 10819-10824.

Dinh, T.P., Kathuria, S., and Piomelli, D. (2004). RNA interference suggests a primary role for monoacylglycerol lipase in the degradation of the endocannabinoid 2-arachidonoylglycerol. Mol Pharmacol *66*, 1260-1264.

Do-Monte, F.H., Quinones-Laracuente, K., and Quirk, G.J. (2015). A temporal shift in the circuits mediating retrieval of fear memory. Nature *519*, 460-463.

Duvarci, S., and Pare, D. (2014). Amygdala microcircuits controlling learned fear. Neuron *82*, 966-980.

Ehrlich, I., Humeau, Y., Grenier, F., Ciocchi, S., Herry, C., and Luthi, A. (2009). Amygdala inhibitory circuits and the control of fear memory. Neuron *62*, 757-771.

Fegley, D., Kathuria, S., Mercier, R., Li, C., Goutopoulos, A., Makriyannis, A., and Piomelli, D. (2004). Anandamide transport is independent of fatty-acid amide hydrolase activity and is blocked by the hydrolysis-resistant inhibitor AM1172. Proc Natl Acad Sci U S A *101*, 8756-8761.

Felix-Ortiz, A.C., Beyeler, A., Seo, C., Leppla, C.A., Wildes, C.P., and Tye, K.M. (2013). BLA to vHPC inputs modulate anxiety-related behaviors. Neuron *79*, 658-664.

Felix-Ortiz, A.C., Burgos-Robles, A., Bhagat, N.D., Leppla, C.A., and Tye, K.M. (2015). Bidirectional modulation of anxiety-related and social behaviors by amygdala projections to the medial prefrontal cortex. Neuroscience.

Fenno, L.E., Mattis, J., Ramakrishnan, C., and Deisseroth, K. (2017). A Guide to Creating and Testing New INTRSECT Constructs. Curr Protoc Neurosci *80*, 4 39 31-34 39 24.

Fenster, R.J., Lebois, L.A.M., Ressler, K.J., and Suh, J. (2018). Brain circuit dysfunction in post-traumatic stress disorder: from mouse to man. Nat Rev Neurosci *19*, 535-551.

Fogaca, M.V., Aguiar, D.C., Moreira, F.A., and Guimaraes, F.S. (2012). The endocannabinoid and endovanilloid systems interact in the rat prelimbic medial prefrontal cortex to control anxiety-like behavior. Neuropharmacology *63*, 202-210.

Franco, R., Reyes-Resina, I., Aguinaga, D., Lillo, A., Jimenez, J., Raich, I., Borroto-Escuela, D.O., Ferreiro-Vera, C., Canela, E.I., Sanchez de Medina, V.*, et al.* (2019). Potentiation of cannabinoid signaling in microglia by adenosine A2A receptor antagonists. Glia *67*, 2410-2423.

Gabbott, P.L., Warner, T.A., Jays, P.R., Salway, P., and Busby, S.J. (2005). Prefrontal cortex in the rat: projections to subcortical autonomic, motor, and limbic centers. J Comp Neurol *492*, 145-177.

Galante, M., and Diana, M.A. (2004). Group I metabotropic glutamate receptors inhibit GABA release at interneuron-Purkinje cell synapses through endocannabinoid production. J Neurosci *24*, 4865-4874.

Ganon-Elazar, E., and Akirav, I. (2009). Cannabinoid receptor activation in the basolateral amygdala blocks the effects of stress on the conditioning and extinction of inhibitory avoidance. J Neurosci *29*, 11078-11088.

Gifford, A.N., and Ashby, C.R., Jr. (1996). Electrically evoked acetylcholine release from hippocampal slices is inhibited by the cannabinoid receptor agonist, WIN 55212-2, and is potentiated by the cannabinoid antagonist, SR 141716A. J Pharmacol Exp Ther *277*, 1431-1436.

Gillespie, C.F., Phifer, J., Bradley, B., and Ressler, K.J. (2009). Risk and resilience: genetic and environmental influences on development of the stress response. Depress Anxiety *26*, 984-992.

Ginn, S., and Horder, J. (2012). "One in four" with a mental health problem: the anatomy of a statistic. BMJ *344*, e1302.

Girgenti, M.J., Wohleb, E.S., Mehta, S., Ghosal, S., Fogaca, M.V., and Duman, R.S. (2019). Prefrontal cortex interneurons display dynamic sex-specific stress-induced transcriptomes. Transl Psychiatry *9*, 292.

Glaser, S.T., Abumrad, N.A., Fatade, F., Kaczocha, M., Studholme, K.M., and Deutsch, D.G. (2003). Evidence against the presence of an anandamide transporter. Proc Natl Acad Sci U S A *100*, 4269-4274.

Gong, J.P., Onaivi, E.S., Ishiguro, H., Liu, Q.R., Tagliaferro, P.A., Brusco, A., and Uhl, G.R. (2006). Cannabinoid CB2 receptors: immunohistochemical localization in rat brain. Brain Res *1071*, 10-23.

Gourie-Devi, M. (2018). Relevance of Neuroepidemiology: Burden of Neurological Disorders and Public Health Issues. Ann Indian Acad Neurol *21*, 237-238.

Gray, J.M., Vecchiarelli, H.A., Morena, M., Lee, T.T., Hermanson, D.J., Kim, A.B., McLaughlin, R.J., Hassan, K.I., Kuhne, C., Wotjak, C.T.*, et al.* (2015). Corticotropin-releasing hormone drives anandamide hydrolysis in the amygdala to promote anxiety. J Neurosci *35*, 3879-3892.

Greenberg, P.E., Sisitsky, T., Kessler, R.C., Finkelstein, S.N., Berndt, E.R., Davidson, J.R., Ballenger, J.C., and Fyer, A.J. (1999). The economic burden of anxiety disorders in the 1990s. J Clin Psychiatry *60*, 427-435.

Gross, C., and Hen, R. (2004). The developmental origins of anxiety. Nat Rev Neurosci *5*, 545-552.

Grupe, D.W., and Nitschke, J.B. (2011). Uncertainty is associated with biased expectancies and heightened responses to aversion. Emotion *11*, 413-424.

Grupe, D.W., and Nitschke, J.B. (2013). Uncertainty and anticipation in anxiety: an integrated neurobiological and psychological perspective. Nat Rev Neurosci *14*, 488-501.

Gunaydin, L.A., Grosenick, L., Finkelstein, J.C., Kauvar, I.V., Fenno, L.E., Adhikari, A., Lammel, S., Mirzabekov, J.J., Airan, R.D., Zalocusky, K.A.*, et al.* (2014). Natural neural projection dynamics underlying social behavior. Cell *157*, 1535-1551.

Haj-Dahmane, S., Shen, R.Y., Elmes, M.W., Studholme, K., Kanjiya, M.P., Bogdan, D., Thanos, P.K., Miyauchi, J.T., Tsirka, S.E., Deutsch, D.G., *et al.* (2018). Fatty-acid-binding protein 5 controls retrograde endocannabinoid signaling at central glutamate synapses. Proc Natl Acad Sci U S A *115*, 3482-3487.

Hampson, R.E., Evans, G.J., Mu, J., Zhuang, S.Y., King, V.C., Childers, S.R., and Deadwyler, S.A. (1995). Role of cyclic AMP dependent protein kinase in cannabinoid receptor modulation of potassium "A-current" in cultured rat hippocampal neurons. Life Sci *56*, 2081-2088.

Hanus, L., Gopher, A., Almog, S., and Mechoulam, R. (1993). Two new unsaturated fatty acid ethanolamides in brain that bind to the cannabinoid receptor. J Med Chem *36*, 3032-3034.

Hashimotodani, Y., Ohno-Shosaku, T., and Kano, M. (2007). Presynaptic monoacylglycerol lipase activity determines basal endocannabinoid tone and terminates retrograde endocannabinoid signaling in the hippocampus. J Neurosci *27*, 1211-1219.

Hashimotodani, Y., Ohno-Shosaku, T., Maejima, T., Fukami, K., and Kano, M. (2008). Pharmacological evidence for the involvement of diacylglycerol lipase in depolarization-induced endocanabinoid release. Neuropharmacology *54*, 58-67.

Haubensak, W., Kunwar, P.S., Cai, H., Ciocchi, S., Wall, N.R., Ponnusamy, R., Biag, J., Dong, H.W., Deisseroth, K., Callaway, E.M., *et al.* (2010). Genetic dissection of an amygdala microcircuit that gates conditioned fear. Nature *468*, 270-276.

Henigsberg, N., Kalember, P., Petrovic, Z.K., and Secic, A. (2019). Neuroimaging research in posttraumatic stress disorder - Focus on amygdala, hippocampus and prefrontal cortex. Prog Neuropsychopharmacol Biol Psychiatry *90*, 37-42.

Hentges, S.T., Low, M.J., and Williams, J.T. (2005). Differential regulation of synaptic inputs by constitutively released endocannabinoids and exogenous cannabinoids. J Neurosci *25*, 9746-9751.

Herkenham, M., Lynn, A.B., Johnson, M.R., Melvin, L.S., de Costa, B.R., and Rice, K.C. (1991). Characterization and localization of cannabinoid receptors in rat brain: a quantitative in vitro autoradiographic study. J Neurosci *11*, 563-583.

Herkenham, M., Lynn, A.B., Little, M.D., Johnson, M.R., Melvin, L.S., de Costa, B.R., and Rice, K.C. (1990). Cannabinoid receptor localization in brain. Proc Natl Acad Sci U S A *87*, 1932-1936.

Herman, J.P., Figueiredo, H., Mueller, N.K., Ulrich-Lai, Y., Ostrander, M.M., Choi, D.C., and Cullinan, W.E. (2003). Central mechanisms of stress integration: hierarchical circuitry controlling hypothalamo-pituitary-adrenocortical responsiveness. Front Neuroendocrinol *24*, 151-180.

Herodotus, Rawlinson, G., and Blakeney, E.H. (1936). The history of Herodotus (London, New York,: J. M. Dent & sons. ltd.;
E. P. Dutton & co.).

Hill, M.N., Campolongo, P., Yehuda, R., and Patel, S. (2018). Integrating Endocannabinoid Signaling and Cannabinoids into the Biology and Treatment of Posttraumatic Stress Disorder. Neuropsychopharmacology *43*, 80-102.

Hill, M.N., Carrier, E.J., McLaughlin, R.J., Morrish, A.C., Meier, S.E., Hillard, C.J., and Gorzalka, B.B. (2008). Regional alterations in the endocannabinoid system in an animal model of depression: effects of concurrent antidepressant treatment. J Neurochem *106*, 2322-2336.

Hill, M.N., Hillard, C.J., and McEwen, B.S. (2011a). Alterations in corticolimbic dendritic morphology and emotional behavior in cannabinoid CB1 receptor-deficient mice parallel the effects of chronic stress. Cereb Cortex *21*, 2056-2064.

Hill, M.N., McLaughlin, R.J., Bingham, B., Shrestha, L., Lee, T.T., Gray, J.M., Hillard, C.J., Gorzalka, B.B., and Viau, V. (2010). Endogenous cannabinoid signaling is essential for stress adaptation. Proc Natl Acad Sci U S A *107*, 9406-9411.

Hill, M.N., McLaughlin, R.J., Morrish, A.C., Viau, V., Floresco, S.B., Hillard, C.J., and Gorzalka, B.B. (2009). Suppression of amygdalar endocannabinoid signaling by stress contributes to activation of the hypothalamic-pituitary-adrenal axis. Neuropsychopharmacology *34*, 2733-2745.

Hill, M.N., McLaughlin, R.J., Pan, B., Fitzgerald, M.L., Roberts, C.J., Lee, T.T., Karatsoreos, I.N., Mackie, K., Viau, V., Pickel, V.M.*, et al.* (2011b). Recruitment of prefrontal cortical endocannabinoid signaling by glucocorticoids contributes to termination of the stress response. J Neurosci *31*, 10506-10515.

Hill, M.N., and Patel, S. (2013). Translational evidence for the involvement of the endocannabinoid system in stress-related psychiatric illnesses. Biol Mood Anxiety Disord *3*, 19.

Hill, M.N., Patel, S., Carrier, E.J., Rademacher, D.J., Ormerod, B.K., Hillard, C.J., and Gorzalka, B.B. (2005). Downregulation of endocannabinoid signaling in the hippocampus following chronic unpredictable stress. Neuropsychopharmacology *30*, 508-515.

Hillard, C.J. (2014). Stress regulates endocannabinoid-CB1 receptor signaling. Semin Immunol *26*, 380-388.

Holland, F.H., Ganguly, P., Potter, D.N., Chartoff, E.H., and Brenhouse, H.C. (2014). Early life stress disrupts social behavior and prefrontal cortex parvalbumin interneurons at an earlier time-point in females than in males. Neurosci Lett *566*, 131-136.

Hsu, F.C., Zhang, G.J., Raol, Y.S., Valentino, R.J., Coulter, D.A., and Brooks-Kayal, A.R. (2003). Repeated neonatal handling with maternal separation permanently alters hippocampal GABAA receptors and behavioral stress responses. Proc Natl Acad Sci U S A *100*, 12213-12218.

Hyman, S.E. (2010). The diagnosis of mental disorders: the problem of reification. Annu Rev Clin Psychol *6*, 155-179.

Hyman, S.M., and Sinha, R. (2009). Stress-related factors in cannabis use and misuse: implications for prevention and treatment. J Subst Abuse Treat *36*, 400-413.

International Advisory Group for the Revision of, I.C.D.M., and Behavioural, D. (2011). A conceptual framework for the revision of the ICD-10 classification of mental and behavioural disorders. World Psychiatry *10*, 86-92.

Isokawa, M., and Alger, B.E. (2006). Ryanodine receptor regulates endogenous cannabinoid mobilization in the hippocampus. J Neurophysiol *95*, 3001-3011.

Janak, P.H., and Tye, K.M. (2015). From circuits to behaviour in the amygdala. Nature *517*, 284-292.

Jankord, R., and Herman, J.P. (2008). Limbic regulation of hypothalamo-pituitary-adrenocortical function during acute and chronic stress. Ann N Y Acad Sci *1148*, 64-73.

Johansen, J.P., Hamanaka, H., Monfils, M.H., Behnia, R., Deisseroth, K., Blair, H.T., and LeDoux, J.E. (2010). Optical activation of lateral amygdala pyramidal cells instructs associative fear learning. Proc Natl Acad Sci U S A *107*, 12692-12697.

Johnson, F.K., Delpech, J.C., Thompson, G.J., Wei, L., Hao, J., Herman, P., Hyder, F., and Kaffman, A. (2018). Amygdala hyper-connectivity in a mouse model of unpredictable early life stress. Transl Psychiatry *8*, 49.

Kaczocha, M., Glaser, S.T., and Deutsch, D.G. (2009). Identification of intracellular carriers for the endocannabinoid anandamide. Proc Natl Acad Sci U S A *106*, 6375-6380.

Kalisch, R., and Gerlicher, A.M. (2014). Making a mountain out of a molehill: on the role of the rostral dorsal anterior cingulate and dorsomedial prefrontal cortex in conscious threat appraisal, catastrophizing, and worrying. Neurosci Biobehav Rev *42*, 1-8.

Kano, M., Ohno-Shosaku, T., Hashimotodani, Y., Uchigashima, M., and Watanabe, M. (2009). Endocannabinoid-mediated control of synaptic transmission. Physiol Rev *89*, 309-380.

Kapp, B.S., Frysinger, R.C., Gallagher, M., and Haselton, J.R. (1979). Amygdala central nucleus lesions: effect on heart rate conditioning in the rabbit. Physiol Behav *23*, 1109-1117.

Karssen, A.M., Her, S., Li, J.Z., Patel, P.D., Meng, F., Bunney, W.E., Jr., Jones, E.G., Watson, S.J., Akil, H., Myers, R.M.*, et al.* (2007). Stress-induced changes in primate prefrontal profiles of gene expression. Mol Psychiatry *12*, 1089-1102.

Katona, I., and Freund, T.F. (2012). Multiple functions of endocannabinoid signaling in the brain. Annu Rev Neurosci *35*, 529-558.

Kessler, R.C., Berglund, P., Demler, O., Jin, R., Merikangas, K.R., and Walters, E.E. (2005a). Lifetime prevalence and age-of-onset distributions of DSM-IV disorders in the National Comorbidity Survey Replication. Arch Gen Psychiatry *62*, 593-602.

Kessler, R.C., Demler, O., Frank, R.G., Olfson, M., Pincus, H.A., Walters, E.E., Wang, P., Wells, K.B., and Zaslavsky, A.M. (2005b). Prevalence and treatment of mental disorders, 1990 to 2003. N Engl J Med *352*, 2515-2523.

Kessler, R.C., Petukhova, M., Sampson, N.A., Zaslavsky, A.M., and Wittchen, H.U. (2012). Twelve-month and lifetime prevalence and lifetime morbid risk of anxiety and mood disorders in the United States. Int J Methods Psychiatr Res *21*, 169-184.

Kim, J., and Alger, B.E. (2004). Inhibition of cyclooxygenase-2 potentiates retrograde endocannabinoid effects in hippocampus. Nat Neurosci *7*, 697-698.

Kim, J., and Alger, B.E. (2010). Reduction in endocannabinoid tone is a homeostatic mechanism for specific inhibitory synapses. Nat Neurosci *13*, 592-600.

Kim, J., Isokawa, M., Ledent, C., and Alger, B.E. (2002). Activation of muscarinic acetylcholine receptors enhances the release of endogenous cannabinoids in the hippocampus. J Neurosci *22*, 10182-10191.

Kim, J., Pignatelli, M., Xu, S., Itohara, S., and Tonegawa, S. (2016). Antagonistic negative and positive neurons of the basolateral amygdala. Nat Neurosci.

Kim, M.J., Gee, D.G., Loucks, R.A., Davis, F.C., and Whalen, P.J. (2011). Anxiety dissociates dorsal and ventral medial prefrontal cortex functional connectivity with the amygdala at rest. Cereb Cortex *21*, 1667-1673.

King, M.B. (1992). Is there still a role for benzodiazepines in general practice? Br J Gen Pract *42*, 202-205.

Klugmann, M., Goepfrich, A., Friemel, C.M., and Schneider, M. (2011). AAV-Mediated Overexpression of the CB1 Receptor in the mPFC of Adult Rats Alters Cognitive Flexibility, Social Behavior, and Emotional Reactivity. Front Behav Neurosci *5*, 37.

Kondo, S., Kondo, H., Nakane, S., Kodaka, T., Tokumura, A., Waku, K., and Sugiura, T. (1998). 2-Arachidonoylglycerol, an endogenous cannabinoid receptor agonist: identification as one of the major species of monoacylglycerols in various rat tissues, and evidence for its generation through CA2+-dependent and -independent mechanisms. FEBS Lett *429*, 152-156.

Kotov, R., Krueger, R.F., Watson, D., Achenbach, T.M., Althoff, R.R., Bagby, R.M., Brown, T.A., Carpenter, W.T., Caspi, A., Clark, L.A., *et al.* (2017). The Hierarchical Taxonomy of Psychopathology (HiTOP): A dimensional alternative to traditional nosologies. J Abnorm Psychol *126*, 454-477.

Kreitzer, A.C., and Malenka, R.C. (2005). Dopamine modulation of state-dependent endocannabinoid release and long-term depression in the striatum. J Neurosci *25*, 10537-10545.

Kreitzer, A.C., and Regehr, W.G. (2001). Retrograde inhibition of presynaptic calcium influx by endogenous cannabinoids at excitatory synapses onto Purkinje cells. Neuron *29*, 717-727.

Kyriazi, P., Headley, D.B., and Pare, D. (2018). Multi-dimensional Coding by Basolateral Amygdala Neurons. Neuron *99*, 1315-1328 e1315.

Lafourcade, M., Elezgarai, I., Mato, S., Bakiri, Y., Grandes, P., and Manzoni, O.J. (2007). Molecular components and functions of the endocannabinoid system in mouse prefrontal cortex. PLoS One *2*, e709.

Lange, J.H., and Kruse, C.G. (2004). Recent advances in CB1 cannabinoid receptor antagonists. Curr Opin Drug Discov Devel *7*, 498-506.

LeDoux, J.E., Cicchetti, P., Xagoraris, A., and Romanski, L.M. (1990a). The lateral amygdaloid nucleus: sensory interface of the amygdala in fear conditioning. J Neurosci *10*, 1062-1069.

LeDoux, J.E., Farb, C., and Ruggiero, D.A. (1990b). Topographic organization of neurons in the acoustic thalamus that project to the amygdala. J Neurosci *10*, 1043-1054.

Lee, S.H., Ledri, M., Toth, B., Marchionni, I., Henstridge, C.M., Dudok, B., Kenesei, K., Barna, L., Szabo, S.I., Renkecz, T*., et al.* (2015). Multiple Forms of Endocannabinoid and Endovanilloid Signaling Regulate the Tonic Control of GABA Release. J Neurosci *35*, 10039-10057.

Lenz, R.A., and Alger, B.E. (1999). Calcium dependence of depolarization-induced suppression of inhibition in rat hippocampal CA1 pyramidal neurons. J Physiol *521 Pt 1*, 147-157.

Levenes, C., Daniel, H., Soubrie, P., and Crepel, F. (1998). Cannabinoids decrease excitatory synaptic transmission and impair long-term depression in rat cerebellar Purkinje cells. J Physiol *510 (Pt 3)*, 867-879.

Li, H., Penzo, M.A., Taniguchi, H., Kopec, C.D., Huang, Z.J., and Li, B. (2013). Experience-dependent modification of a central amygdala fear circuit. Nat Neurosci *16*, 332-339.

Likhtik, E., Stujenske, J.M., Topiwala, M.A., Harris, A.Z., and Gordon, J.A. (2014). Prefrontal entrainment of amygdala activity signals safety in learned fear and innate anxiety. Nat Neurosci *17*, 106-113.

Linnman, C., Zeidan, M.A., Furtak, S.C., Pitman, R.K., Quirk, G.J., and Milad, M.R. (2012). Resting amygdala and medial prefrontal metabolism predicts functional activation of the fear extinction circuit. Am J Psychiatry *169*, 415-423.

Lisboa, S.F., Camargo, L.H., Magesto, A.C., Resstel, L.B., and Guimaraes, F.S. (2014). Cannabinoid modulation of predator fear: involvement of the dorsolateral periaqueductal gray. Int J Neuropsychopharmacol *17*, 1193-1206.

Lisboa, S.F., Gomes, F.V., Terzian, A.L., Aguiar, D.C., Moreira, F.A., Resstel, L.B., and Guimaraes, F.S. (2017). The Endocannabinoid System and Anxiety. Vitam Horm *103*, 193-279.

Little, J.P., and Carter, A.G. (2013). Synaptic mechanisms underlying strong reciprocal connectivity between the medial prefrontal cortex and basolateral amygdala. J Neurosci *33*, 15333-15342.

Liu, J., Wang, L., Harvey-White, J., Huang, B.X., Kim, H.Y., Luquet, S., Palmiter, R.D., Krystal, G., Rai, R., Mahadevan, A.*, et al.* (2008). Multiple pathways involved in the biosynthesis of anandamide. Neuropharmacology *54*, 1-7.

Llano, I., Leresche, N., and Marty, A. (1991). Calcium entry increases the sensitivity of cerebellar Purkinje cells to applied GABA and decreases inhibitory synaptic currents. Neuron *6*, 565-574.

Long, J.Z., Li, W., Booker, L., Burston, J.J., Kinsey, S.G., Schlosburg, J.E., Pavon, F.J., Serrano, A.M., Selley, D.E., Parsons, L.H.*, et al.* (2009). Selective blockade of 2-arachidonoylglycerol hydrolysis produces cannabinoid behavioral effects. Nat Chem Biol *5*, 37-44.

Lowe, D.J.E., Sasiadek, J.D., Coles, A.S., and George, T.P. (2018). Cannabis and mental illness: a review. Eur Arch Psychiatry Clin Neurosci.

Lowery-Gionta, E.G., Crowley, N.A., Bukalo, O., Silverstein, S., Holmes, A., and Kash, T.L. (2018). Chronic stress dysregulates amygdalar output to the prefrontal cortex. Neuropharmacology *139*, 68-75.

Lutz, B., Marsicano, G., Maldonado, R., and Hillard, C.J. (2015). The endocannabinoid system in guarding against fear, anxiety and stress. Nat Rev Neurosci *16*, 705-718.

Machado, C.J., and Bachevalier, J. (2008). Behavioral and hormonal reactivity to threat: effects of selective amygdala, hippocampal or orbital frontal lesions in monkeys. Psychoneuroendocrinology *33*, 926-941.

Mackie, K., Lai, Y., Westenbroek, R., and Mitchell, R. (1995). Cannabinoids activate an inwardly rectifying potassium conductance and inhibit Q-type calcium currents in AtT20 cells transfected with rat brain cannabinoid receptor. J Neurosci *15*, 6552-6561.

Maejima, T., Hashimoto, K., Yoshida, T., Aiba, A., and Kano, M. (2001). Presynaptic inhibition caused by retrograde signal from metabotropic glutamate to cannabinoid receptors. Neuron *31*, 463-475.

Makara, J.K., Mor, M., Fegley, D., Szabo, S.I., Kathuria, S., Astarita, G., Duranti, A., Tontini, A., Tarzia, G., Rivara, S.*, et al.* (2005). Selective inhibition of 2-AG hydrolysis enhances endocannabinoid signaling in hippocampus. Nat Neurosci *8*, 1139-1141.

Malenka, R.C., and Bear, M.F. (2004). LTP and LTD: an embarrassment of riches. Neuron *44*, 5-21.

Manduca, A., Bara, A., Larrieu, T., Lassalle, O., Joffre, C., Laye, S., and Manzoni, O.J. (2017). Amplification of mGlu5-Endocannabinoid Signaling Rescues Behavioral and Synaptic Deficits in a Mouse Model of Adolescent and Adult Dietary Polyunsaturated Fatty Acid Imbalance. J Neurosci *37*, 6851-6868.

Marek, R., Jin, J., Goode, T.D., Giustino, T.F., Wang, Q., Acca, G.M., Holehonnur, R., Ploski, J.E., Fitzgerald, P.J., Lynagh, T.*, et al.* (2018). Hippocampus-driven feed-forward inhibition of the prefrontal cortex mediates relapse of extinguished fear. Nat Neurosci *21*, 384-392.

Mark, K.M., Stevelink, S.A.M., Choi, J., and Fear, N.T. (2018). Post-traumatic growth in the military: a systematic review. Occup Environ Med *75*, 904-915.

Matsuda, L.A., Lolait, S.J., Brownstein, M.J., Young, A.C., and Bonner, T.I. (1990). Structure of a cannabinoid receptor and functional expression of the cloned cDNA. Nature *346*, 561-564.

Matyas, F., Lee, J., Shin, H.S., and Acsady, L. (2014). The fear circuit of the mouse forebrain: connections between the mediodorsal thalamus, frontal cortices and basolateral amygdala. Eur J Neurosci *39*, 1810-1823.

Matyas, F., Yanovsky, Y., Mackie, K., Kelsch, W., Misgeld, U., and Freund, T.F. (2006). Subcellular localization of type 1 cannabinoid receptors in the rat basal ganglia. Neuroscience *137*, 337-361.

McDonald, A.J. (1998). Cortical pathways to the mammalian amygdala. Prog Neurobiol *55*, 257-332.

McEwen, B.S. (2012). Brain on stress: how the social environment gets under the skin. Proc Natl Acad Sci U S A *109 Suppl 2*, 17180-17185.

McEwen, B.S., Bowles, N.P., Gray, J.D., Hill, M.N., Hunter, R.G., Karatsoreos, I.N., and Nasca, C. (2015). Mechanisms of stress in the brain. Nat Neurosci *18*, 1353-1363.

McEwen, B.S., and Morrison, J.H. (2013). The brain on stress: vulnerability and plasticity of the prefrontal cortex over the life course. Neuron *79*, 16-29.

McEwen, B.S., and Stellar, E. (1993). Stress and the individual. Mechanisms leading to disease. Arch Intern Med *153*, 2093-2101.

McGarry, L.M., and Carter, A.G. (2016). Inhibitory Gating of Basolateral Amygdala Inputs to the Prefrontal Cortex. J Neurosci *36*, 9391-9406.

McGarry, L.M., and Carter, A.G. (2017). Prefrontal Cortex Drives Distinct Projection Neurons in the Basolateral Amygdala. Cell Rep *21*, 1426-1433.

McKernan, M.G., and Shinnick-Gallagher, P. (1997). Fear conditioning induces a lasting potentiation of synaptic currents in vitro. Nature *390*, 607-611.

McLaughlin, R.J., Hill, M.N., Bambico, F.R., Stuhr, K.L., Gobbi, G., Hillard, C.J., and Gorzalka, B.B. (2012). Prefrontal cortical anandamide signaling coordinates coping responses to stress through a serotonergic pathway. Eur Neuropsychopharmacol *22*, 664-671.

McLaughlin, R.J., Hill, M.N., Dang, S.S., Wainwright, S.R., Galea, L.A., Hillard, C.J., and Gorzalka, B.B. (2013). Upregulation of CB(1) receptor binding in the ventromedial prefrontal cortex promotes proactive stress-coping strategies following chronic stress exposure. Behav Brain Res *237*, 333-337.

McLaughlin, R.J., Hill, M.N., and Gorzalka, B.B. (2014). A critical role for prefrontocortical endocannabinoid signaling in the regulation of stress and emotional behavior. Neurosci Biobehav Rev *42*, 116-131.

Mechoulam, R., Ben-Shabat, S., Hanus, L., Ligumsky, M., Kaminski, N.E., Schatz, A.R., Gopher, A., Almog, S., Martin, B.R., Compton, D.R., *et al.* (1995). Identification of an endogenous 2-monoglyceride, present in canine gut, that binds to cannabinoid receptors. Biochem Pharmacol *50*, 83-90.

Mechoulam, R., and Gaoni, Y. (1965). Hashish. IV. The isolation and structure of cannabinolic cannabidiolic and cannabigerolic acids. Tetrahedron *21*, 1223-1229.

Milad, M.R., Pitman, R.K., Ellis, C.B., Gold, A.L., Shin, L.M., Lasko, N.B., Zeidan, M.A., Handwerger, K., Orr, S.P., and Rauch, S.L. (2009). Neurobiological basis of failure to recall extinction memory in posttraumatic stress disorder. Biol Psychiatry *66*, 1075-1082.

Miller, G. (2010). Is pharma running out of brainy ideas? Science *329*, 502-504.

Miller, N.S., and Gold, M.S. (1990). Benzodiazepines: reconsidered. Adv Alcohol Subst Abuse *8*, 67-84.

Mitte, K., Noack, P., Steil, R., and Hautzinger, M. (2005). A meta-analytic review of the efficacy of drug treatment in generalized anxiety disorder. J Clin Psychopharmacol *25*, 141-150.

Mondin, T.C., Konradt, C.E., Cardoso Tde, A., Quevedo Lde, A., Jansen, K., Mattos, L.D., Pinheiro, R.T., and Silva, R.A. (2013). Anxiety disorders in young people: a population-based study. Braz J Psychiatry *35*, 347-352.

Munck, A., Guyre, P.M., and Holbrook, N.J. (1984). Physiological functions of glucocorticoids in stress and their relation to pharmacological actions. Endocr Rev *5*, 25-44.

Munjack, D.J., Baltazar, P.L., Bohn, P.B., Cabe, D.D., and Appleton, A.A. (1990). Clonazepam in the treatment of social phobia: a pilot study. J Clin Psychiatry *51 Suppl*, 35-40; discussion 50-33.

Munro, S., Thomas, K.L., and Abu-Shaar, M. (1993). Molecular characterization of a peripheral receptor for cannabinoids. Nature *365*, 61-65.

Murphy, B.L., Arnsten, A.F., Goldman-Rakic, P.S., and Roth, R.H. (1996). Increased dopamine turnover in the prefrontal cortex impairs spatial working memory performance in rats and monkeys. Proc Natl Acad Sci U S A *93*, 1325-1329.

Myers, K.M., and Davis, M. (2007). Mechanisms of fear extinction. Mol Psychiatry *12*, 120-150.

Nabavi, S., Fox, R., Proulx, C.D., Lin, J.Y., Tsien, R.Y., and Malinow, R. (2014). Engineering a memory with LTD and LTP. Nature *511*, 348-352.

Nakazi, M., Bauer, U., Nickel, T., Kathmann, M., and Schlicker, E. (2000). Inhibition of serotonin release in the mouse brain via presynaptic cannabinoid CB1 receptors. Naunyn Schmiedebergs Arch Pharmacol *361*, 19-24.

Namburi, P., Al-Hasani, R., Calhoon, G.G., Bruchas, M.R., and Tye, K.M. (2016). Architectural Representation of Valence in the Limbic System. Neuropsychopharmacology *41*, 1697-1715.

Navarrete, M., and Araque, A. (2010). Endocannabinoids potentiate synaptic transmission through stimulation of astrocytes. Neuron *68*, 113-126.

Navarrete, M., Diez, A., and Araque, A. (2014). Astrocytes in endocannabinoid signalling. Philos Trans R Soc Lond B Biol Sci *369*, 20130599.

Neu, A., Foldy, C., and Soltesz, I. (2007). Postsynaptic origin of CB1-dependent tonic inhibition of GABA release at cholecystokinin-positive basket cell to pyramidal cell synapses in the CA1 region of the rat hippocampus. J Physiol *578*, 233-247.

Ohno-Shosaku, T., Hashimotodani, Y., Ano, M., Takeda, S., Tsubokawa, H., and Kano, M. (2007). Endocannabinoid signalling triggered by NMDA receptor-mediated calcium entry into rat hippocampal neurons. J Physiol *584*, 407-418.

Ohno-Shosaku, T., Maejima, T., and Kano, M. (2001). Endogenous cannabinoids mediate retrograde signals from depolarized postsynaptic neurons to presynaptic terminals. Neuron *29*, 729-738.

Olfson, M., Marcus, S.C., and Shaffer, D. (2006). Antidepressant drug therapy and suicide in severely depressed children and adults: A case-control study. Arch Gen Psychiatry *63*, 865-872.

Ongur, D., and Price, J.L. (2000). The organization of networks within the orbital and medial prefrontal cortex of rats, monkeys and humans. Cereb Cortex *10*, 206-219.

Otto, M.W., Tuby, K.S., Gould, R.A., McLean, R.Y., and Pollack, M.H. (2001). An effect-size analysis of the relative efficacy and tolerability of serotonin selective reuptake inhibitors for panic disorder. Am J Psychiatry *158*, 1989-1992.

Pan, B., Wang, W., Long, J.Z., Sun, D., Hillard, C.J., Cravatt, B.F., and Liu, Q.S. (2009). Blockade of 2-arachidonoylglycerol hydrolysis by selective monoacylglycerol lipase inhibitor 4-nitrophenyl 4-(dibenzo[d][1,3]dioxol-5-yl(hydroxy)methyl)piperidine-1-carboxylate (JZL184) Enhances retrograde endocannabinoid signaling. J Pharmacol Exp Ther *331*, 591-597.

Pan, X., Ikeda, S.R., and Lewis, D.L. (1998). SR 141716A acts as an inverse agonist to increase neuronal voltage-dependent Ca2+ currents by reversal of tonic CB1 cannabinoid receptor activity. Mol Pharmacol *54*, 1064-1072.

Patel, S., Hill, M.N., Cheer, J.F., Wotjak, C.T., and Holmes, A. (2017). The endocannabinoid system as a target for novel anxiolytic drugs. Neurosci Biobehav Rev *76*, 56-66.

Patel, S., and Hillard, C.J. (2006). Pharmacological evaluation of cannabinoid receptor ligands in a mouse model of anxiety: further evidence for an anxiolytic role for endogenous cannabinoid signaling. J Pharmacol Exp Ther *318*, 304-311.

Patel, S., Kingsley, P.J., Mackie, K., Marnett, L.J., and Winder, D.G. (2009). Repeated homotypic stress elevates 2-arachidonoylglycerol levels and enhances short-term endocannabinoid signaling at inhibitory synapses in basolateral amygdala. Neuropsychopharmacology *34*, 2699-2709.

Patel, S., Roelke, C.T., Rademacher, D.J., Cullinan, W.E., and Hillard, C.J. (2004). Endocannabinoid signaling negatively modulates stress-induced activation of the hypothalamic-pituitary-adrenal axis. Endocrinology *145*, 5431-5438.

Perova, Z., Delevich, K., and Li, B. (2015). Depression of excitatory synapses onto parvalbumin interneurons in the medial prefrontal cortex in susceptibility to stress. J Neurosci *35*, 3201-3206.

Pertwee, R.G. (1997). Pharmacology of cannabinoid CB1 and CB2 receptors. Pharmacol Ther *74*, 129-180.

Pitler, T.A., and Alger, B.E. (1992). Postsynaptic spike firing reduces synaptic GABAA responses in hippocampal pyramidal cells. J Neurosci *12*, 4122-4132.

Ponomarev, I., Rau, V., Eger, E.I., Harris, R.A., and Fanselow, M.S. (2010). Amygdala transcriptome and cellular mechanisms underlying stress-enhanced fear learning in a rat model of posttraumatic stress disorder. Neuropsychopharmacology *35*, 1402-1411.

Preuss, T.M. (1995). Do rats have prefrontal cortex? The rose-woolsey-akert program reconsidered. J Cogn Neurosci *7*, 1-24.

Prewitt, C.M., and Herman, J.P. (1998). Anatomical interactions between the central amygdaloid nucleus and the hypothalamic paraventricular nucleus of the rat: a dual tract-tracing analysis. J Chem Neuroanat *15*, 173-185.

Puente, N., Cui, Y., Lassalle, O., Lafourcade, M., Georges, F., Venance, L., Grandes, P., and Manzoni, O.J. (2011). Polymodal activation of the endocannabinoid system in the extended amygdala. Nat Neurosci *14*, 1542-1547.

Qin, Z., Zhou, X., Pandey, N.R., Vecchiarelli, H.A., Stewart, C.A., Zhang, X., Lagace, D.C., Brunel, J.M., Beique, J.C., Stewart, A.F.*, et al.* (2015). Chronic stress induces anxiety via an amygdalar intracellular cascade that impairs endocannabinoid signaling. Neuron *85*, 1319-1331.

Quirk, G.J., Repa, C., and LeDoux, J.E. (1995). Fear conditioning enhances short-latency auditory responses of lateral amygdala neurons: parallel recordings in the freely behaving rat. Neuron *15*, 1029-1039.

Rademacher, D.J., Meier, S.E., Shi, L., Ho, W.S., Jarrahian, A., and Hillard, C.J. (2008). Effects of acute and repeated restraint stress on endocannabinoid content in the amygdala, ventral striatum, and medial prefrontal cortex in mice. Neuropharmacology *54*, 108-116.

Radley, J.J., Arias, C.M., and Sawchenko, P.E. (2006). Regional differentiation of the medial prefrontal cortex in regulating adaptive responses to acute emotional stress. J Neurosci *26*, 12967-12976.

Ramikie, T.S., Nyilas, R., Bluett, R.J., Gamble-George, J.C., Hartley, N.D., Mackie, K., Watanabe, M., Katona, I., and Patel, S. (2014). Multiple mechanistically distinct modes of endocannabinoid mobilization at central amygdala glutamatergic synapses. Neuron *81*, 1111-1125.

Ravindran, L.N., and Stein, M.B. (2010). The pharmacologic treatment of anxiety disorders: a review of progress. J Clin Psychiatry *71*, 839-854.

Rey, A.A., Purrio, M., Viveros, M.P., and Lutz, B. (2012). Biphasic effects of cannabinoids in anxiety responses: CB1 and GABA(B) receptors in the balance of GABAergic and glutamatergic neurotransmission. Neuropsychopharmacology *37*, 2624-2634.

Riga, D., Matos, M.R., Glas, A., Smit, A.B., Spijker, S., and Van den Oever, M.C. (2014). Optogenetic dissection of medial prefrontal cortex circuitry. Front Syst Neurosci *8*, 230.

Robinson, O.J., Charney, D.R., Overstreet, C., Vytal, K., and Grillon, C. (2012). The adaptive threat bias in anxiety: amygdala-dorsomedial prefrontal cortex coupling and aversive amplification. Neuroimage *60*, 523-529.

Robinson, O.J., Krimsky, M., Lieberman, L., Allen, P., Vytal, K., and Grillon, C. (2014). Towards a mechanistic understanding of pathological anxiety: the dorsal medial prefrontal-amygdala 'aversive amplification' circuit in unmedicated generalized and social anxiety disorders. Lancet Psychiatry *1*, 294-302.

Rodrigues, S.M., LeDoux, J.E., and Sapolsky, R.M. (2009). The influence of stress hormones on fear circuitry. Annu Rev Neurosci *32*, 289-313.

Rogan, M.T., Staubli, U.V., and LeDoux, J.E. (1997). Fear conditioning induces associative long-term potentiation in the amygdala. Nature *390*, 604-607.

Roitman, P., Mechoulam, R., Cooper-Kazaz, R., and Shalev, A. (2014). Preliminary, open-label, pilot study of add-on oral Delta9-tetrahydrocannabinol in chronic post-traumatic stress disorder. Clin Drug Investig *34*, 587-591.

Roozendaal, B., Koolhaas, J.M., and Bohus, B. (1990). Differential effect of lesioning of the central amygdala on the bradycardiac and behavioral response of the rat in relation to conditioned social and solitary stress. Behav Brain Res *41*, 39-48.

Rubino, T., Guidali, C., Vigano, D., Realini, N., Valenti, M., Massi, P., and Parolaro, D. (2008a). CB1 receptor stimulation in specific brain areas differently modulate anxiety-related behaviour. Neuropharmacology *54*, 151-160.

Rubino, T., Realini, N., Castiglioni, C., Guidali, C., Vigano, D., Marras, E., Petrosino, S., Perletti, G., Maccarrone, M., Di Marzo, V.*, et al.* (2008b). Role in anxiety behavior of the endocannabinoid system in the prefrontal cortex. Cereb Cortex *18*, 1292-1301.

Sawchenko, P.E., Brown, E.R., Chan, R.K., Ericsson, A., Li, H.Y., Roland, B.L., and Kovacs, K.J. (1996). The paraventricular nucleus of the hypothalamus and the functional neuroanatomy of visceromotor responses to stress. Prog Brain Res *107*, 201-222.

Schmid, P.C., Reddy, P.V., Natarajan, V., and Schmid, H.H. (1983). Metabolism of N-acylethanolamine phospholipids by a mammalian phosphodiesterase of the phospholipase D type. J Biol Chem *258*, 9302-9306.

Schmitt, L.I., Wimmer, R.D., Nakajima, M., Happ, M., Mofakham, S., and Halassa, M.M. (2017). Thalamic amplification of cortical connectivity sustains attentional control. Nature *545*, 219-223.

Sciolino, N.R., Zhou, W., and Hohmann, A.G. (2011). Enhancement of endocannabinoid signaling with JZL184, an inhibitor of the 2-arachidonoylglycerol hydrolyzing enzyme monoacylglycerol lipase, produces anxiolytic effects under conditions of high environmental aversiveness in rats. Pharmacol Res *64*, 226-234.

Segman, R.H., Shefi, N., Goltser-Dubner, T., Friedman, N., Kaminski, N., and Shalev, A.Y. (2005). Peripheral blood mononuclear cell gene expression profiles identify emergent post-traumatic stress disorder among trauma survivors. Mol Psychiatry *10*, 500-513, 425.

Senn, V., Wolff, S.B., Herry, C., Grenier, F., Ehrlich, I., Grundemann, J., Fadok, J.P., Muller, C., Letzkus, J.J., and Luthi, A. (2014). Long-range connectivity defines behavioral specificity of amygdala neurons. Neuron *81*, 428-437.

Shansky, R.M., Hamo, C., Hof, P.R., McEwen, B.S., and Morrison, J.H. (2009). Stress-induced dendritic remodeling in the prefrontal cortex is circuit specific. Cereb Cortex *19*, 2479-2484.

Sharma, S., Powers, A., Bradley, B., and Ressler, K.J. (2016). Gene x Environment Determinants of Stress- and Anxiety-Related Disorders. Annu Rev Psychol *67*, 239-261.

Shonesy, B.C., Bluett, R.J., Ramikie, T.S., Baldi, R., Hermanson, D.J., Kingsley, P.J., Marnett, L.J., Winder, D.G., Colbran, R.J., and Patel, S. (2014). Genetic disruption of 2-arachidonoylglycerol synthesis reveals a key role for endocannabinoid signaling in anxiety modulation. Cell Rep *9*, 1644-1653.

Sierra-Mercado, D., Padilla-Coreano, N., and Quirk, G.J. (2011). Dissociable roles of prelimbic and infralimbic cortices, ventral hippocampus, and basolateral amygdala in the expression and extinction of conditioned fear. Neuropsychopharmacology *36*, 529-538.

Sim-Selley, L.J., Brunk, L.K., and Selley, D.E. (2001). Inhibitory effects of SR141716A on G-protein activation in rat brain. Eur J Pharmacol *414*, 135-143.

Simon, G.M., and Cravatt, B.F. (2008). Anandamide biosynthesis catalyzed by the phosphodiesterase GDE1 and detection of glycerophospho-N-acyl ethanolamine precursors in mouse brain. J Biol Chem *283*, 9341-9349.

Sjostrom, P.J., Turrigiano, G.G., and Nelson, S.B. (2003). Neocortical LTD via coincident activation of presynaptic NMDA and cannabinoid receptors. Neuron *39*, 641-654.

Slattery, D.A., Neumann, I.D., and Cryan, J.F. (2011). Transient inactivation of the infralimbic cortex induces antidepressant-like effects in the rat. J Psychopharmacol *25*, 1295-1303.

Sotres-Bayon, F., and Quirk, G.J. (2010). Prefrontal control of fear: more than just extinction. Curr Opin Neurobiol *20*, 231-235.

Sotres-Bayon, F., Sierra-Mercado, D., Pardilla-Delgado, E., and Quirk, G.J. (2012). Gating of fear in prelimbic cortex by hippocampal and amygdala inputs. Neuron *76*, 804-812.

Steel, Z., Marnane, C., Iranpour, C., Chey, T., Jackson, J.W., Patel, V., and Silove, D. (2014). The global prevalence of common mental disorders: a systematic review and meta-analysis 1980-2013. Int J Epidemiol *43*, 476-493.

Stella, N., and Piomelli, D. (2001). Receptor-dependent formation of endogenous cannabinoids in cortical neurons. Eur J Pharmacol *425*, 189-196.

Stella, N., Schweitzer, P., and Piomelli, D. (1997). A second endogenous cannabinoid that modulates long-term potentiation. Nature *388*, 773-778.

Sternbach, L.H. (1978). The benzodiazepine story. Prog Drug Res *22*, 229-266.

Sumislawski, J.J., Ramikie, T.S., and Patel, S. (2011). Reversible gating of endocannabinoid plasticity in the amygdala by chronic stress: a potential role for monoacylglycerol lipase

inhibition in the prevention of stress-induced behavioral adaptation. Neuropsychopharmacology *36*, 2750-2761.

Sun, Y.X., Tsuboi, K., Okamoto, Y., Tonai, T., Murakami, M., Kudo, I., and Ueda, N. (2004). Biosynthesis of anandamide and N-palmitoylethanolamine by sequential actions of phospholipase A2 and lysophospholipase D. Biochem J *380*, 749-756.

Sung, K.W., Choi, S., and Lovinger, D.M. (2001). Activation of group I mGluRs is necessary for induction of long-term depression at striatal synapses. J Neurophysiol *86*, 2405-2412.

Suzuki, S., Saitoh, A., Ohashi, M., Yamada, M., Oka, J., and Yamada, M. (2016). The infralimbic and prelimbic medial prefrontal cortices have differential functions in the expression of anxiety-like behaviors in mice. Behav Brain Res *304*, 120-124.

Szabo, B., Dorner, L., Pfreundtner, C., Norenberg, W., and Starke, K. (1998). Inhibition of GABAergic inhibitory postsynaptic currents by cannabinoids in rat corpus striatum. Neuroscience *85*, 395-403.

Taylor, M.J., Rudkin, L., Bullemor-Day, P., Lubin, J., Chukwujekwu, C., and Hawton, K. (2013). Strategies for managing sexual dysfunction induced by antidepressant medication. Cochrane Database Syst Rev, CD003382.

Tovote, P., Fadok, J.P., and Luthi, A. (2015). Neuronal circuits for fear and anxiety. Nat Rev Neurosci *16*, 317-331.

Trivedi, M.H., Rush, A.J., Wisniewski, S.R., Nierenberg, A.A., Warden, D., Ritz, L., Norquist, G., Howland, R.H., Lebowitz, B., McGrath, P.J., *et al.* (2006). Evaluation of outcomes with citalopram for depression using measurement-based care in STAR*D: implications for clinical practice. Am J Psychiatry *163*, 28-40.

Truitt, W.A., Sajdyk, T.J., Dietrich, A.D., Oberlin, B., McDougle, C.J., and Shekhar, A. (2007). From anxiety to autism: spectrum of abnormal social behaviors modeled by progressive disruption of inhibitory neuronal function in the basolateral amygdala in Wistar rats. Psychopharmacology (Berl) *191*, 107-118.

Twitchell, W., Brown, S., and Mackie, K. (1997). Cannabinoids inhibit N- and P/Q-type calcium channels in cultured rat hippocampal neurons. J Neurophysiol *78*, 43-50.

Tye, K.M. (2018). Neural Circuit Motifs in Valence Processing. Neuron *100*, 436-452.

Ulrich-Lai, Y.M., and Herman, J.P. (2009). Neural regulation of endocrine and autonomic stress responses. Nat Rev Neurosci *10*, 397-409.

Vandevoorde, S., and Lambert, D.M. (2007). The multiple pathways of endocannabinoid metabolism: a zoom out. Chem Biodivers *4*, 1858-1881.

Vertes, R.P. (2004). Differential projections of the infralimbic and prelimbic cortex in the rat. Synapse *51*, 32-58.

Vigo, D., Thornicroft, G., and Atun, R. (2016). Estimating the true global burden of mental illness. Lancet Psychiatry *3*, 171-178.

Vijayraghavan, S., Wang, M., Birnbaum, S.G., Williams, G.V., and Arnsten, A.F. (2007). Inverted-U dopamine D1 receptor actions on prefrontal neurons engaged in working memory. Nat Neurosci *10*, 376-384.

Vytal, K.E., Overstreet, C., Charney, D.R., Robinson, O.J., and Grillon, C. (2014). Sustained anxiety increases amygdala-dorsomedial prefrontal coupling: a mechanism for maintaining an anxious state in healthy adults. J Psychiatry Neurosci *39*, 321-329.

Wamsteeker, J.I., Kuzmiski, J.B., and Bains, J.S. (2010). Repeated stress impairs endocannabinoid signaling in the paraventricular nucleus of the hypothalamus. J Neurosci *30*, 11188-11196.

Warden, D., Rush, A.J., Trivedi, M.H., Fava, M., and Wisniewski, S.R. (2007). The STAR*D Project results: a comprehensive review of findings. Curr Psychiatry Rep *9*, 449-459.

Weiskrantz, L. (1956). Behavioral changes associated with ablation of the amygdaloid complex in monkeys. J Comp Physiol Psychol *49*, 381-391.

Wilson, R.I., and Nicoll, R.A. (2001). Endogenous cannabinoids mediate retrograde signalling at hippocampal synapses. Nature *410*, 588-592.

Worley, N.B., Hill, M.N., and Christianson, J.P. (2018). Prefrontal endocannabinoids, stress controllability and resilience: A hypothesis. Prog Neuropsychopharmacol Biol Psychiatry *85*, 180-188.

Zhong, P., Wang, W., Pan, B., Liu, X., Zhang, Z., Long, J.Z., Zhang, H.T., Cravatt, B.F., and Liu, Q.S. (2014). Monoacylglycerol lipase inhibition blocks chronic stress-induced depressive-like behaviors via activation of mTOR signaling. Neuropsychopharmacology *39*, 1763-1776.

Zhou, P., Resendez, S.L., Rodriguez-Romaguera, J., Jimenez, J.C., Neufeld, S.Q., Giovannucci, A., Friedrich, J., Pnevmatikakis, E.A., Stuber, G.D., Hen, R*., et al.* (2018). Efficient and accurate extraction of in vivo calcium signals from microendoscopic video data. Elife *7*.

Zoppi, S., Perez Nievas, B.G., Madrigal, J.L., Manzanares, J., Leza, J.C., and Garcia-Bueno, B. (2011). Regulatory role of cannabinoid receptor 1 in stress-induced excitotoxicity and neuroinflammation. Neuropsychopharmacology *36*, 805-818.